The Analysis and Design of the Power Spectral Density for DC/DC Converters Using Randomized Switching Frequency Pulse Width Modulation

by

Jian Wang
B.S., Ocean University of Qingdao, 1997

A Thesis Submitted in Partial Fulfillment of the
Requirements for the Degree of

Master of Applied Science

in the Department of Electrical and Computer Engineering

We accept this thesis as conforming
to the required standard

[redacted]

Dr. R. L. Kirlin, Supervisor (Department of Electrical and Computer Engineering)

[redacted]

Dr. W. S. Lu, Departmental Member (Department of Electrical and Computer Engineering)

[redacted]

Dr. G. A. Beer, Outside Member (Department of Physics and Astronomy)

[redacted]

Dr. J. Zhou, External Examiner (Department of Mathematics and Statistics)

University of Victoria

Supervisor: Dr. R. L. Kirlin

ABSTRACT

In this thesis we study the analysis and design of the noise power spectral density for a randomized switching frequency pulse width modulation (RSFPWM) DC/DC converter based on the constant duty cycle scheme. We analyze the spectrum formulas of the controllable constant duty cycle scheme in order to control the power spectral density at a specified frequency. In some cases a null at the specified frequency is created. The effects of constraints on the switching frequencies are presented.

Further analysis considering the control of the power spectral density over a band of frequency is addressed under the assumption that the switching intervals are equally spaced and with symmetric probability distribution. Practical constraints on the switching frequencies are considered using optimization methods. Simulation results verify the theory and illustrate the effectiveness of our analysis and conclusions.

Examiners:

Dr. R. L. Kirlin, Supervisor (Department of Electrical and Computer Engineering)

Dr. W. S. Lu, Departmental Member (Department of Electrical and Computer Engineering)

Dr. G. A. Beer, Outside Member (Department of Physics and Astronomy)

Dr. J. Zhou, External Examiner (Department of Mathematics and Statistics)

Table of Contents

List of Tables

List of Figures

List of Symbols

$y_N^{(j)}(t)$: The j^{th} member of the truncated ensemble (stochastic process) containing exactly 2N+1 pulses in the principle interval $(-T_j/2, T_j/2)$

$u(t)$: The characteristic pulse shape with $u_{\max} = 1$

$y_n^{(j)}$: The amplitude of the *nth* pulse

$\tau_n^{(j)}$: The segment duration

$\phi_n^{(j)}$: The pulse duty cycle

$\varepsilon_n^{(j)}$: The epoch which marks the start of *nth* pulse

$Y_N^{(j)}(f)$: The Fourier transform of $y_N^{(j)}(t)$

$S_{u^{(j)}}(f)$: The Fourier transform of $u(t)$ in the j^{th} member of the truncated ensemble

$S_{Y_N}(f^*)$: The harmonic (f^*) power over the period T

$\overline{\tau}$: Mean duration

P_{s_i}: The probability density function (PDF) of switching

f_{LCM}: The least common multiple (LCM) of the switching frequencies

$R_{ys}^{(j)}(t)$: Auto-correlation function of the sampled pulse train

$W_{ys}^{(j)}(f)$: Sample spectrum (the Fourier transform of $R_{ys}^{(j)}(t)$)

$W_{ys}(f)$: The power spectrum density of pulse train

DC: The DC voltage component of the pulse train

P_{DC}: The power of DC component

τ_0: Constant duration

A_0: The constant pulse amplitude (initial DC level)

$\Psi_{s_i}(f)$: The characteristic function of the random segment variable τ

α: Constant duty cycle

f_s: Switching frequency

$\overline{f_s}$ or f_{ave}: Average switching frequency

T_k: The duration of the *kth* switching interval

ε_k: The delay time of the *kth* pulse within the *kth* interval

d_k: The on state duration of the *kth* pulse

α_k: The duty cycle of the *kth* interval

CDC: Constant Duty Cycle

CPW: Constant Pulse Width

EMI: Electromagnetic Interference

PDF: Probability Density Function

PSD: Power Spectral Density

PWM: Pulse Width Modulation

PPM: Pulse Position Modulation

RPPM: Random Pulse Position Modulation

RPWM: Random Pulse Width Modulation

RSFPWM: Randomized Switching Frequency Pulse Width Modulation

SRPWM: Standard Random Pulse Width Modulation

Acknowledgments

I would like to express my deepest gratitude to my supervisor, Dr. R. Lynn Kirlin, although I know only words are far away from enough. It has been my great pleasure to have met and worked with him, and from him I always get much more help than I expect. His kindness, generosity, patience and invaluable ideas help me out of every difficulty from my first day here. I respect him not only because of his specialty knowledge but because of also his personality. He definitely is a perfect supervisor.

I wish to express my special thanks respect to Dr. W. S. Lu for his kind discussion and encouragement. That is very important to me.

I also would like to thank Dr. J. Zhou and her important advice about my thesis work and enlightening idea about the further research. Also I should thank Dr. G. Beer for his kind help about the thesis revising.

Many thanks to Mrs. Vicky Smith since her help and advice keep me on the right track of graduation, also thanks to Mrs. Moneca for her help. Thank Mr. John Dorocicz and Steve Campbell for their in time technical help.

I would like to express my gratitude from deep my heart to my dear parents who are a big part of my life. They are always encouraging me towards my goals. I am greatly indebted to my wife, Xiaoli, for her continuous support and encouragement. Without her understanding and liberating me out of cooking work, I would not have finished my thesis. Also thanks her to feed me well.

To my dear parents,

and my dear wife

Chapter 1

Introduction and Thesis Outline

A typical power electronic system such as shown in Figure 1.1 is designed to process and control the electronic energy into a desired output [1], where the power converter is the basic component of the power processor. Switching mode converters are the most important systems in the power electronics fields. These have been accompanied with the fast development of silicon-based semiconductor switching devices and advances in microelectronics mainly due to the following reasons [1]-[4]:

1. They have very high efficiency.
2. They are cheaper to operate.
3. They have flexible implementation topologies to satisfy various requirements.

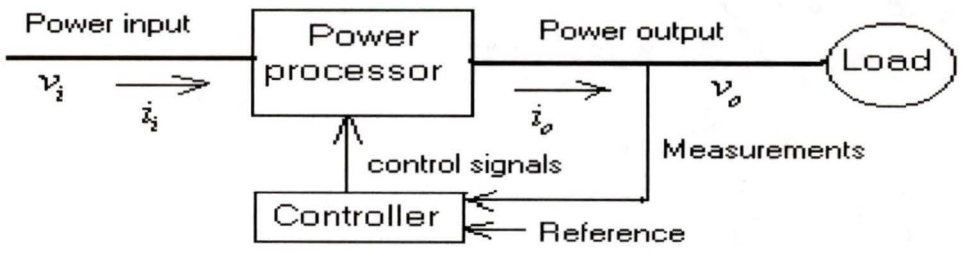

Figure 1.1. A typical power electronics system.

The control of switching converters has been an active area of research and development during the last several decades in power electronics. Among these different methods, pulse width modulation (PWM) techniques seem to receive the most consideration [2]-[4] [17] [18]. PWM controls the output voltage by employing switching at some frequency f_s and adjusting the on and off durations. The control signal, called the switching signal (switching function) [5], is a time function with value 1 during the on state and value 0 during the off state as shown in Figure 1.2. A simplified PWM DC/DC converter is described in Figure 1.2-(a), while Figure 1.2-(b) shows the corresponding switching signal, with T_s being the cycle duration. The start position of the on stage is considered to be the beginning of each cycle. The ratio of the duration of the on stage to the total cycle duration T_s is called the duty cycle (duty ratio):

$$D = \frac{t_{on}}{T_s} = \frac{t_{on}}{t_{on} + t_{off}}.$$

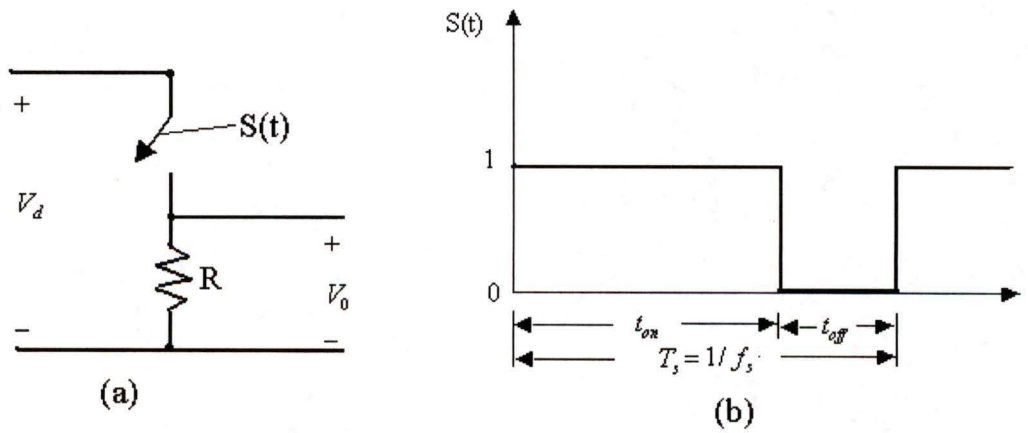

Figure 1.2. A simple example for PWM DC/DC converter (a) and its switching signal (b).

Regardless of the manner of operation, all the standard PWM techniques can be considered deterministic due to the uniqueness and invariability of the switching patterns over one cycle. The output is controlled by varying the duty cycle of the switching signal but the frequency of this signal is kept constant, so that the harmonic power of the output concentrates around a multiple of the switching frequency. This kind of switching-mode power conversion inherently causes unwanted harmonics and degrades reliability at the same time. The power spectrum content has been elaborated in [2] and it is clearly shown that there will be a harmonic spectrum at multiples of the switching frequency; these are known to be the main source of inverter acoustic noise and converter electromagnetic interference (EMI). There is also a risk of exciting a mechanical resonance due to the harmonics.

Various techniques have been explored in order to suppress the harmonic spectrum in PWM converters. Faster switching devices have been developed to reduce or eliminate the acoustic noise in power converters. As PWM techniques and microprocessors matured in the 1980's, most efforts were devoted toward the optimization of PWM waveforms ("programmed switching"). But this method is complex itself and needs a complicated control system. Alternative random switching schemes were then recognized and developed quickly due to their simplicity and effectiveness.

The principle of random modulation techniques can be traced back to 1960s in [6] from statistical communication theory. It is obvious that this kind of methodology did not receive appropriate attention in the power electronics field until references [19] [7] and [8] were published. Following these articles various random modulation schemes abound for both DC/DC converters and DC/AC inverters and these schemes, called random pulse

width modulation (RPWM), drew considerable attention. In RPWM schemes some parameters are subject to randomization. The motivation for RPWM schemes comes from the fact that they spread the harmonic content of the power spectrum into a broad continuous power spectrum of small magnitude since the switching pattern is not repetitive. The harmonics are significantly reduced or ideally eliminated. RPWM techniques for DC/DC conversion can be divided into four types [5] [6] [8] [9] [10] according to which parameters in the switching signal are randomized. The four types are as follows:

- Standard random pulse width modulation (SRPWM), which allows the pulse width to vary randomly within each cycle but holds the average duty cycle constant. The switching frequency is fixed.
- Random pulse position modulation (RPPM). The position of the on-state within each switching cycle is randomized. The switching frequency is fixed.
- Simplified aperiodic (randomized switching frequency) modulation, which is also called the constant duty cycle (CDC) scheme. CDC keeps duty cycle constant while randomizing the switching frequency.
- Aperiodic (randomized switching frequency) modulation, which is also called the constant pulse width (CPW) scheme. In CPW the pulse width is constant while the switching frequency is randomized such that average duty cycle is maintained.

In the existing technical literature tonal noise in inverter driven induction motors and EMI due to fast switching of semiconductors in DC/DC converters receive intensive attention. Although the implementation results are impressive and effective in practice, the existing theoretical analysis of RPWM literature is very limited and many aspects of

it need to be fully explored. Stankovic et al. presented the theoretical foundation and defined a unifying framework [5] [9], which is partly based on the results developed in communication theory [6] [16]. Also it gives a general formula for both discrete (harmonics) and continuous (noise) power spectra of the switching signal obtained by randomly dithering a nominally periodic switching signal. In fact some spectrum analysis efforts have been applied to this discipline, and they have received wide spread attention recently. It is now clear that it is necessary to study the theory behind randomization to produce efficient schemes.

Our task in this thesis focuses on the analysis and design of randomized switching frequency modulation in DC/DC conversion, especially the CDC method. We develop and apply methodology developed in [5], [6] in analysis and design of the power spectrum in DC/DC converters in order to better control the continuous noise power spectrum for specified objectives.

1.1 Statement of Problems

The problems addressed and studied in this thesis are listed and described in this section, which relates mostly to the signal processing aspects rather than specific circuits. Our emphases in this thesis focus on the theoretical analysis and design of spectral characteristics of DC/DC converters using randomized switching frequency modulation. The techniques can be extended to DC/AC inverters. The inverse problems in switching-mode conversion mainly include tonal noise, EMI and resonant vibration, which are all related to the frequency domain properties.

It has been shown that in RPWM it is easy to lower and disperse the harmonic power in output power spectra, but it is difficult to simultaneously control the continuous noise spectrum. It will be shown in a later section that the CDC scheme provides for specification of the shape of the continuous spectrum, localization of the switching harmonics and nulling the noise spectrum at given frequencies by designing the switching frequencies and their distribution. That is, we show that with certain segment widths or switching frequency source distributions the scheme produces a desired power spectrum, meeting specifications for the desired DC output, discrete components and various power spectral density criteria.

The analysis problems in random modulation relate to the spectral characteristic of the switching signal and other related waveforms and to the probability law that governs the switching. The design problem is to synthesize a random switching pattern that will optimize the power spectrum according to some given criteria.

We list the specific objectives studied in this thesis as follows:

Objective 1 To present and analyze the closed form equation of the power spectrum (both discrete and continuous) of DC/DC converters utilizing the randomized switching frequency PWM techniques, CDC and CPW. This is the analysis problem. In the CPW scheme, pulses (from ground to level A_0 volts) are fixed in duration while the switching rate has an average segment length which in turn yields the desired average DC level. In the CDC scheme segment lengths are randomized, but in each the duty cycle is constant. We will focus on studying the switching signal, a random pulse train, since all the other related waveforms in the conversion system can be obtained by simple relationships among random processes within linear systems.

Objective 2 To utilize the results of objective 1 to control the power spectral density at frequencies in a band or at discrete points. This is the design problem. Simultaneously the power that exists at the least common multiple f_{LCM} of the switching frequencies (discrete harmonics) should be determined and placed at satisfactory points in frequency. Because it is easy to select switching frequencies to produce an f_{LCM}, we concentrate instead on control of spectral density in this part of our study. Blind optimization methods are explored and studied under certain criteria. We utilize both conventional optimization methods and modern nonlinear methods.

In meeting objective 1 we will first present and study the formulation for a general probability density function. Then we will consider some specific continuous and discrete distributions as examples. In meeting objective 2, although formulation shows that the CPW scheme allows a spectral zero to be placed as desired within the constraints of the minimum, maximum and average switching frequency allowed, CPW does not provide control of the duty cycle within each segment and is deemed "uncontrollable". This is because with some non-zero probability a long string of pulses with low or high duty cycles may momentarily cause unacceptable deviations from the desired output DC level. Thus we will focus our study on the formula for the power spectral density using the CDC method. In meeting objective 2 we use blind optimization to deal with switching frequency constraints since in practice a switching frequency that is too low will lead to large ripple in the output, and a switching frequency that is too high will result in more energy loss.

Objective 1 is addressed in chapters 2 and 3. Objective 2 is addressed in chapters 3, 4, and 5, which deal with different specific objectives and methodologies.

1.2 Main Contributions

The main contributions of this thesis are:

- Presentation and study of the formulas of both the discrete and the continuous power spectra for the CPW modulation scheme.
- Presentation and study of the formulas of both the discrete and the continuous power spectra for the CDC modulation scheme.
- Design methods for nulling the power spectral density at one specified frequency and its harmonics. At the same time the least common multiple frequency f_{LCM} of the switching frequencies can be designed as needed and the powers of f_{LCM} and its harmonics are easily determined. Cases with constraints on switching frequencies are considered also, and examples explain how these constraints can limit the use of our methods.
- An analysis and design method for minimizing the power spectral density over a band of frequencies. Cases with constraints on switching frequencies are considered also.
- An optimization method for controlling the power spectral density. We first specify a suitable objective function and a set of constraints, and then we apply several optimization methods. Simulation results justify and demonstrate the effectiveness of the methods.

1.3 Outline and Contents

A literature survey on the development of RPWM is presented in chapter 2. Some basic knowledge about DC/DC converters utilizing RPWM is also presented in chapter 2. In chapter 2, we present the closed expression for power spectra for both the CDC scheme and the CPW scheme.

In chapter 3, we analyze the formulas obtained from chapter 2 for the CDC scheme and find the reasonable way to minimize the power spectral density at some specified frequencies. Also we study the situation when there are constraints on the switching frequencies. The design examples and Monte-Carlo simulation results verify the correctness and effectiveness of our methods.

Next we focus our analysis and simulations on the formulas for the spectral density using the CDC scheme in chapter 4. Since in many cases power suppression over a band of frequencies is desired, we develop our analysis and design accordingly.

In chapter 5 we formulate the power spectral density expression for the CDC scheme as an optimization objective function with corresponding constraints in closed form, and then we apply different optimization methods to this problem. Simulation results demonstrate the effectiveness.

Chapter 6 summarizes the thesis results and provides suggestions for future research work.

Appendix A presents the derivation of the denominator expression in chapter 3 for the formula of the CDC scheme under a uniform distribution. Appendices B and C contain the formulations of chapter 5 for optimizing the objective function with different constraints on the switching frequencies.

Chapter 2

Synopsis of RPWM in Power Conversion and Inversion

2.1 Fundamentals of Random Schemes in Converters

The classification of random modulation schemes depends mainly on which parameter in the switching function $s(t)$ is randomized, where the switching function can be defined as follows:

$$s(t) = \begin{cases} 1 & \textit{when switch is 'on'} \\ 0 & \textit{when switch is 'off'} \end{cases}$$

In random modulation schemes the switching function becomes a random pulse train. A general waveform of $s(t)$ is shown in Figure 2.1 with various parameters, where $s(t)$ has two discrete states 0 and 1. T_k is the k^{th} switching interval (the reciprocal of switching frequency) of the k^{th} cycle. ε_k is the delay time of the k^{th} pulse within the k^{th} cycle. d_k is the pulse duration (pulse width) within the k^{th} cycle. The duty cycle of the k^{th} cycle α_k is equal to the ratio of d_k to T_k. With the help of Figure 2.1, we can compare the

characteristics of different PWM schemes as follows. (note in any of the PWM schemes no overlap is allowed)

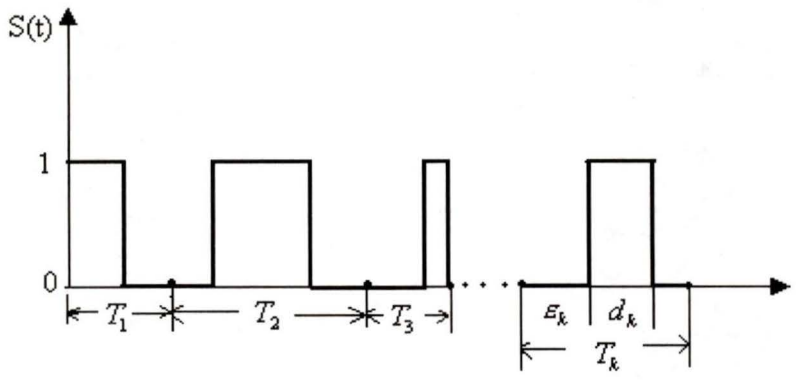

Figure 2.1 A general waveform of switching function $s(t)$.

Standard PWM

In this scheme, all the parameters are kept constant during the power conversion process.

Standard RPWM

The switching interval T_k and on state duration ε_k are fixed. d_k is randomized but holds the average duty cycle constant.

RPPM

RPPW is similar to the standard PWM with constant switching frequency except the position of each pulse within the interval is randomized.

Randomized Switching Frequency PWM (RSFPWM)

In this scheme, the switching intervals are not fixed and the waveform of the switching function is not periodic so it is also called aperiodic modulation. This scheme is subdivided:

- **The Constant Duty Cycle Modulation.**

  This scheme is also called random carrier-frequency modulation with fixed duty cycle (RCFMFD). Switching interval T_k and pulse width d_k are randomized but keep the duty cycle constant.

- **The Constant Pulse Width Modulation**

  This scheme is also called random carrier-frequency modulation with variable duty cycle (RCFMVD), which keeps the pulse width d_k constant but randomizes the switching intervals. This results in the randomization of duty cycle.

2.2 Literature Review

This section contains a survey of the existing literature on random modulation strategies for both converters (DC to DC) and inverters (DC to AC), although our study objective will concentrate on DC/DC converters. Understanding the evolution of the modulation methods in power electronics is necessary for directing our own work and establishing the merit of our results.

Some theoretical tools for analysis of random modulation schemes can be traced back to work on PWM in communication theory ([6] [16] [64]), but random modulation methods have been neglected by power electronics engineers until the recent 13 years. However it appears to have been mentioned for the first time in the power electronics field by Clarke in [12] in 1970, where the author studies a resonant type DC/DC converter. This paper is seldom cited in recent references except [5]. It suggests a series random dithering source which has a zero mean as the input of the analog comparator;

the experimental results show that the acoustic noise is attenuated and flat compared with random source shorted where some spikes are expected. It is also claimed that under the random operation the shielding problems become easier. No theoretical analysis is given. At that time people were interested in fast switching devices and then later soft-switching with the development of the microprocessor; so the random modulation idea was deserted in the power field until it resurged in 1987 [13], and became a world-wide research topic.

2.2.1 Development of RPWM in Modern Power Electronics

Early Developments of RPWM in Inverters

As an alternative method to the existing deterministic PWM techniques in the power field, randomized PWM was initially introduced in 1987 by Trzynadlowski, Legowski, and Kirlin [13], [7], in the context of voltage-controlled power inverters in modern power applications. These papers present a microprocessor-based method that utilizes a pseudo-random number sequence with a uniform probability density function to realize the randomization. The switching signal equals 1 or 0 according to the difference between the random number and the time varying (AC) value of the desired average switching function. A detailed theoretical analysis of the spectral density of the switching function is given, along with a block diagram and hardware implementation, and the experimental results are promising. These papers show that RPWM techniques prevent the generation of periodic ripple torque due to its non-repetitive switching patterns. A switching frequency of up to 240kHz results in a high quality output current with a simple hardware realization. However, the method requires a very high switching rate leading to losses, and the scheme allows undesired long sequences without switching.

In [20] the same random modulation scheme as in [13] is applied in a hypersonic MOSFET-based power inverter and a microprocessor is utilized. Simulation and experimental results verify the theory and give a high quality output current due to the high switching frequency. In addition, the output voltage spectrum is flatter than that produced in [13]. In [21] The same authors give more detail on the RPWM's operation and utilize an optimal harmonic modulation function, which increases the fundamental components by 20% compared to the pure sinusoidal modulating function. Other details and results are quite similar to those in [20]. Random modulation is extended to the control of a delta inverter in [11] where again a uniform distribution is employed. This paper reports on measurement of the acoustic spectrum and shows that RPWM can reduce the acoustic noise effectively because it can transfer harmonic power into a wide band continuous spectrum. It is reported by Kryter and Pearson in [27] [28] that the subjective annoyance of a sound is greater for narrow band (harmonics) than wide band having the same power. A non-sinusoidal modulation function that allows a significant improvement in the output is studied in [23].

Although the above random techniques show good performance in overcoming the shortcomings of the deterministic PWM, they have only limited frequency and magnitude control range and cannot work well under lower modulation index since that will lead to a large current and torque distortion. A so-called advanced random modulation technique is presented in [22], which modifies the technique in [13] in order to alleviate the former mentioned adverse problems. New trapezoidal modulating functions and chopper techniques are added in order to improve the quality of output when the modulation index

is low. The problems of resonant torsional vibrations in inverter-supplied AC drive systems are discussed and the hardware implementation problem is described in detail.

An application specific integrated circuit (ASIC) [33] [34] implements the RPWM scheme derived from [13]. A three-level inverter [33] supplying a small induction motor and a two-level inverter [34] has been presented. Experimental results are not straightforward since only time domain waveforms of outputs are shown.

All the papers we have documented up to this point adopt the so-called standard RPWM method that holds the switching frequency constant but varies the pulse duration randomly within each switching cycle.

Early Developments of RPWM in Converters

It appears that Tanaka, Ninomiya and Harada [8] provide the first paper which applies RPWM schemes in DC/DC converters. DC/DC converters are often operated at higher switching frequencies (beyond the audible band), and then the EMI problem is of more concern than the acoustic noise. The authors give an analysis under some plausible hypotheses. They appropriately use the power spectrum as the quality measure since it makes more sense with RPWM. They give more attention to the high frequency harmonics which contribute to the EMI problems. They also rightly point out that if the power of the switching noise is dispersed in the frequency domain, the peak level of the switching noise spectrum should be reduced. They present two control circuits for step-down (buck) DC/DC converters; one is the standard RPWM derived from communication theory [6] (the same as [7] [13]) and the other is so-called aperiodic modulation where the switching signal is no longer periodic. Block diagrams of the two strategies are shown in Figures 2.2 and 2.3 respectively.

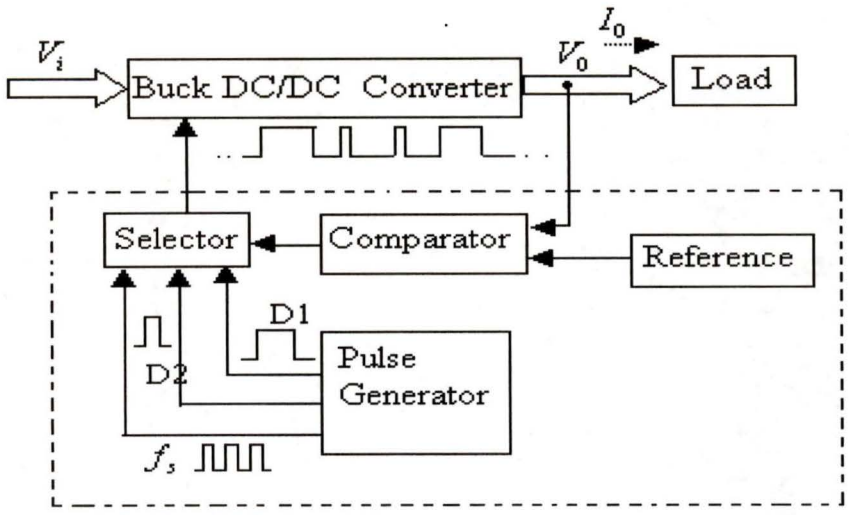

Figure 2.2. A simple block diagram for the standard RPWM DC/DC converter [8].

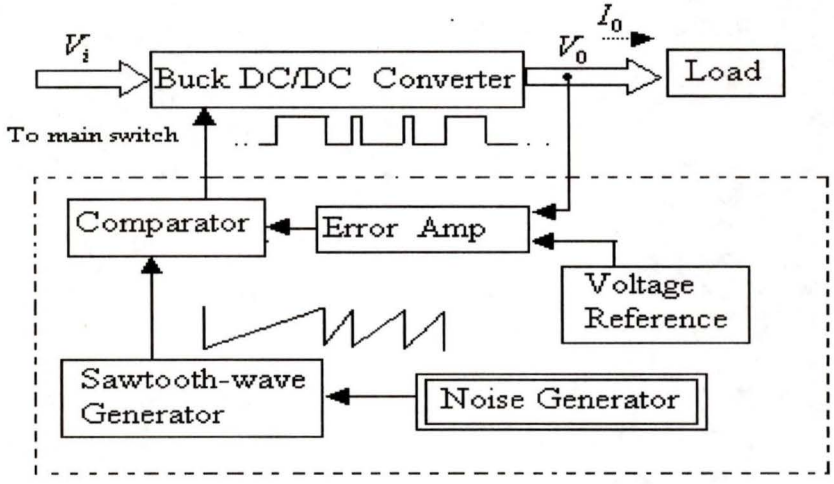

Figure 2.3. A simple block diagram for the aperiodic RPWM DC/DC converter [8].

There is no theoretical analysis given for these two methods, although experimental verification is provided. This paper also indicates that the second control circuit has advantages over the first since it is more effective at smoothing and reducing the

switching noise spectrum. In fact we will generalize the second circuit and give theoretical details in chapter 3, where it is called the CDC modulation scheme.

Papers [14] [15] also by the authors of [8] give some rudimentary theoretical analysis for the switching noise power spectrum of their earlier proposed strategies. A correct general formula is presented in [14] for the power spectrum of a randomly modulated impulse train but without the positive constraint on the time increment. The analysis is somewhat ad hoc, and the same results can be found in earlier communication literature [16], [6]. The authors use random switching with the normal distribution as an example and give a quantitative explanation about the relationship between the noise spectrum and the standard deviation of the distribution, but it is apparently not practical since it allows for both arbitrarily long switching intervals and negative intervals. However, the experiments show good accordance with theoretical analysis.

Developments in the RSFPWM Method

After introduction of random modulation into modern power electronics systems, different randomization schemes have been explored in both inverter and converter contexts. In this section, we survey these schemes but not in a strict chronological way.

Handley, Johnson and Boys, reference [24], present a randomization scheme for a chopper (DC/DC converter) supplying a DC motor system. Their approach differs from standard RPWM in that they dither (randomly vary) the switching frequency between a lower and an upper frequency bound while holding the average switching frequency and duty cycle constant. It means that the switching cycle duration is changing randomly from one cycle to the next cycle. Two distribution functions, uniform and square law, are considered. This appears to be the first paper which studies the effects of the probability

density function (PDF). The dithering scheme block diagram is shown in Figure 2.4. The authors give no theoretical analysis, but show experimental results and point out the difficulties of theoretical analysis. This method is similar to that of Figure 2.3 and has resulted in replacing tonal noise with wide-band noise.

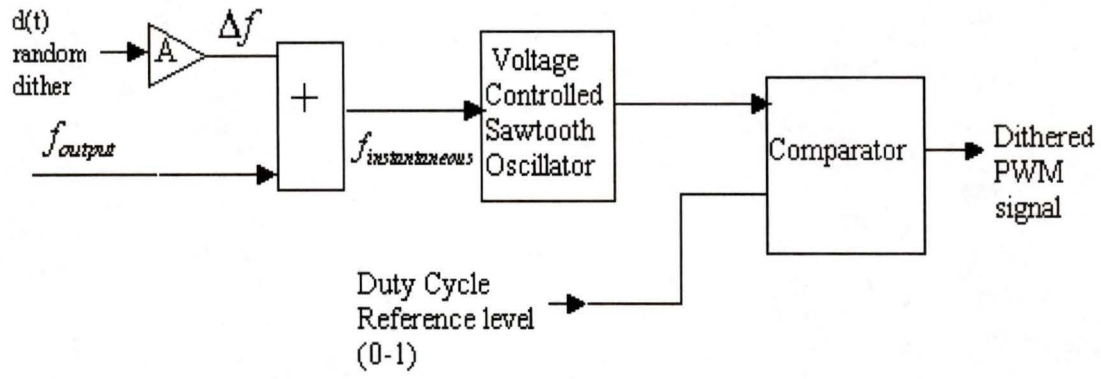

Figure 2.4. The block diagram for random switching function generation [24].

Reference [25] further develops the method presented in [24] and extends it into a three-phase inverter for AC drives. The implementation problems are elaborated, and the space vector modulation (SVM) with a dithering in switching frequency from one cycle to the next is used. Experimental results show that this technique reduces the noise annoyance in both converters and inverters even though the overall sound pressure level (SPL) is unchanged when compared to deterministic modulation. The authors conclude from the experimental results that a uniform distribution is the best choice for dithering.

An approximate theoretical analysis for the random modulation technique presented in [24] and [25] is developed by one of the same authors and others in [26] and [29], where the derivation of the voltage power spectral density is realized by dividing the

spectrum into different bands directly related to the harmonics present in the deterministic PWM waveform. But it is reported that the spectrum estimation theory deviates from experimental results, especially in the lower order bands. Paper [30] presents improvement for the above estimation methods by giving an improved auto-correlation function. Implementation and measurement problems for this random modulation strategy are presented in [31] and [32].

An important paper [35] by Habetler and Divan in random modulation considers a standard three-phase inverter with analog implementation of a triangular carrier-based modulator. This modulator maintains the advantage of standard PWM including real-time control and linear amplification. The authors assume the random modulation is band limited since a band limited noise is applied as dithering. Some inexact theoretical analysis is given. The experimental results are promising and the clear absence of tones in the spectrum of the acoustic noise generated by the machine can be observed. A study of similar random schemes in a specific boost (step-up) converter is found in [63] by Mihalic et al. The simulation and experimental set up are elaborated and results confirm the theory.

RPPM and Other RPWM Methods

A gray noise PWM randomizes the PWM pulse position in a DC/AC inverter within each switching interval while at the same time holding the switching frequency constant. In this paper only two positions are utilized (leading-edge or lagging-edge), which can be viewed as a specialized RPPM in terms of communication theory [6]. The authors apply random switching to the standard space-vector PWM for inverter control. The output spectrum contains both a continuous part and a pronounced discrete part (harmonics).

The power spectrum for this scheme is studied in [37] [38] and [39]. These papers build their analysis on theory from communications. Closed form formulas for both continuous and discrete spectra are presented. Experimental results confirm the theory very well.

In [40] Wang and Sanders present an application of a programmed random modulation technique combining programmed PWM with random dithering in a DC/DC converter which results in a good quality output in terms of spectral shaping. The optimization procedure is applied in the programmed switching sequence in the sense of minimizing the peak spectral components within the constant duty cycle. The same authors optimize the deterministic PWM scheme in [41].

Two types of microprocessor-based (mathematical and logical) random PWM schemes are presented and compared in a series of papers [42] [43] [44] by the same authors, Hui et al. It has been argued that for a logical approach, the number of bits is a crucial factor in determining the shape of the RPWM waveform and 10 bits is the lowest acceptable number. All the methods can be implemented in real time.

Interesting methods for converting the acoustic noise from a PWM inverter into music or useful information are considered by Ueda et al in [45], where the control is entirely digitized.

In [46] Shrivastva et al study a standard RPWM technique where a binomial distribution governs the randomization. The simulation results show that the harmonics can be almost entirely deleted. Reference [47] compares the continuous noise of the above random scheme with RPPM and finds that it is inherent in both schemes that continuous noise induces low-frequency voltage ripple. Kabu, Miyashita and Sone [62] revise the Standard RPWM in a similar way but use a normal distribution instead of the

binomial distribution. All these papers show the advantages over the conventional random scheme using a uniform distribution in the sense of suppressing the harmonics.

The output spectra (voltage, current and acoustic noise) of RPPM and RSFPWM are compared to experimental results in [57]. The authors also conclude that the latter scheme gives fewer discrete harmonics but increases the risk of exciting mechanical resonance. In [60] the same authors compare the fixed switching frequency random modulation schemes with a RSFPWM scheme and find that in lower frequencies they can get almost the same performance, although the latter achieves better results in the high frequency part.

2.2.2 Theoretical Analyses of RPWM

Before 1987 virtually all studies were mainly based on ad hoc methods and experimental confirmation with little theoretical analysis. Since then the situation has changed and many efforts include theoretical work. The emphasis has been the spectral characteristics of switching functions governing the power switch of a converter. Now we give an overview of the existing literature that develops theoretical analysis for both converters and inverters although our own work is with converters.

Apparently Trzynadlowski, Legowski and Kirlin [13] initiated in 1987 design and analysis research based on theoretical aspects of random modulation in DC/AC inverters. Papers [37] [38] [[39] present theoretical analyses of the power spectra of RPPM schemes with only two possible pulse positions in each switching cycle, the derivation being partly based on communication theory [6] [64]. Closed form equations are given and are verified by simulations and experiments. The authors also suggest a blind

optimization procedure which may be carried out using this formulation. The analysis of the RPPM scheme is considered in another series of papers [5] [9] [65] in a more general form.

A good review paper [49] covers the work on random modulation through 1994. It discusses RPWM strategies, power spectrum calculations and implementation issues on the converter-fed AC drive systems.

In [50] [52] the same authors of [37] have analyzed the random-width, minimum-loss space vector (RWMLSV) PWM strategy (introduced in [56]) when the switching frequency can vary randomly in a constrained range. An optimization procedure is presented to calculate the desired probability density function for the switching frequencies such that the continuous spectrum is maximized and the amplitude of the discrete harmonics is minimized. Although a large number of available switching frequencies can eliminate the harmonics in the output spectrum, in general only a limited-pool is applied in practical applications. A simulation example shows that only the minimum and maximum switching frequency should be used with equal probability from a limited pool of switching frequencies. In [51] the experimental results are addressed. However the authors realize the necessity of further studies on minimizing power in the discrete spectrum since the example also shows that the harmonic power is increased compared to the results using a uniform distribution of all the available switching frequencies.

References [54], [55] derive the harmonic components of the power spectrum for the RSFPWM scheme. Also the optimization procedure to eliminate the higher harmonics is

explored and the experimental results confirm the conclusion that two equiprobable widths with a non-integer ratio are the best choice.

Trzynadlowski et al [61] present a new optimization method for RSFRWM, the maximin optimization criterion, which is based on defining a common multiple deviation function. Compared to former methods this method effectively reduces the discrete harmonics. The experimental results verify the theory.

Another important theoretical analysis of random modulation techniques is a thesis [5] by Stankovic and a series of related papers [9] [65] etc. These references build a unified mathematical framework based on [6] for theoretical analyses of random modulation on which various DC/DC converters can be analyzed. A number of specific schemes have been studied on these general formulas and verified by experiments. The author in [5] also presents synthesis problems of random modulation (for DC/DC converters) with prescribed spectral criteria.

Based on the works mentioned above, the authors in [10] set their focus on the effects of the continuous noise spectrum in DC/DC converter performance. They give analyses on the standard RPWM and RPPM power spectra and conclude that for DC/DC converters the RPPM method offers much better output-voltage performance than the standard RPWM method since it has smaller output-voltage ripple.

A comparative investigation on the use of random modulation for DC/DC converters is given in [48] [53]. In these papers four schemes, RPPM, standard RPWM, RCFMFD and RCFMVD are analyzed, and expressions for their power spectra are verified by experiments, but the authors only consider a uniform distribution in these modulation schemes.

More general formulas are derived for a RSFPWM modulation scheme for DC/DC converters in a technical report [66], and our own analysis will base on that report. We will summarize the methods and conclusions of [66] in section 2.3.

A methodology for true comparison of analytical and measured frequency spectra in RPWM is addressed in [58] [59].

2.2.3 Summary

The review of relevant literature has shown that random modulation techniques can extend some power from harmonics to a wide band spectrum and reduce the amplitude of harmonic power. After much effort was put to the development of various randomization schemes, researchers realized the importance of theoretical analysis of RPWM. Some papers have been published in this area since 1987 and analytical expressions have been derived to explain and design the frequency characteristics, but those results are far from exhaustive. There is still an urgent need for fully developing and exploring the spectral theory.

2.3 The Power Spectrum of the RSFPWM Technique for DC/DC Converters

In this section we summarize the results of [66] which follows Middleton [6] and gives power spectrum formulas for two specific schemes: CPW and CDC, which are based on the formulations for the harmonic powers and the power spectral density of the aperiodic modulation scheme developed in [6].

In the CPW scheme, the pulses (from ground to level A_0 volts) are fixed in duration while the switching rate has an average segment length which in turn yields the desired average DC level. In the CDC scheme, segment lengths are randomized, but in each the duty cycle is constant.

Section 2.3.1 gives general spectral formulations for the randomized switching frequency modulation strategy. Section 2.3.2 gives a formulation for the CPW switching scheme. Section 2.3.3 gives a formulation for the CDC switching scheme.

2.3.1 Methodologies and General Formulas for RSFPWM

In the general aperiodic non-overlapping random pulse train with random amplitudes, the termination of one pulse segment (or switching interval) or pulse group segment is the beginning of the next, while their durations and amplitudes are randomized. This stochastic process has its j^{th} member shown in Figure 2.5 where one pulse per segment is assumed.

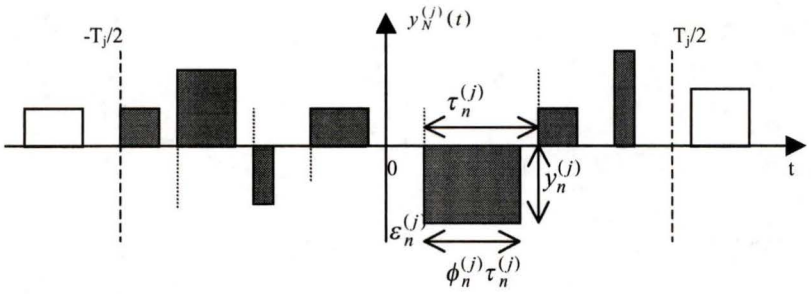

Figure 2.5. The general aperiodic non-overlapping random pulse trains.

To find the intensity spectrum and discrete tones of the pulse trains we begin by considering a member of the truncated ensemble containing exactly 2N+1 pulses in the principle interval $(-T_j/2, T_j/2)$, as defined below:

$$y_N^{(j)}(t) = \sum_{n=-N}^{N} y_n^{(j)} u\left(t - \varepsilon_n^{(j)}; \tau_n^{(j)}, \phi_n^{(j)}\right) \tag{2.1}$$

where $u(t)$ is the characteristic pulse shape with $u_{\max} = 1$, $y_n^{(j)}$ is the amplitude of the *nth* pulse, $\tau_n^{(j)}$ is the segment duration, $\phi_n^{(j)}$ is the pulse duty cycle and $\varepsilon_n^{(j)}$ is an epoch which marks the start of *nth* pulse. Both $\tau_n^{(j)}$ and $\varepsilon_n^{(j)}$ are randomly selected from their respective independent identical distributions (iid). Also $y_n^{(j)}$ and $\phi_n^{(j)}$ can be either deterministic values or selected from an iid distribution.

After some algebraic manipulations, the general formulation for power spectral density is

$$W_{ys}(f) = \frac{1}{\bar{\tau}}\left(E\left(y^2 \left|S_u(f;\tau,\phi)\right|^2\right) + 2\,\mathrm{Re}\left[\frac{E(yS_u(f;\tau,\phi)e^{j2\pi f\tau})E(y^*S_u^*(f;\tau,\phi))}{1 - E(e^{j2\pi f\tau})}\right]\right) \tag{2.2}$$

where $S_u(f;\tau,\phi) = e^{-j\pi f\tau\phi}\dfrac{\sin(\pi f\tau\phi)}{\pi f}$.

The DC voltage component of the pulse train is obtained from the following equation, wherein random variables τ_n, y_n *and* ϕ_n are statistically independent from sequence to sequence.

$$DC = \frac{E\left(yS_u(0;\tau,\phi)\right)}{\bar{\tau}} \tag{2.3}$$

2.3.2 Formulation of the CPW Scheme

For this switching scheme the switching pulses are rectangular, of constant duration, τ_0, while the spacing $\tau - \tau_0$ between pulses varies randomly and independently from pulse to pulse according to the switching frequency, which is selected from the set $\{f_{s_1}, f_{s_1}, ..., f_{s_M}\}$ based on a known PDF, P_{s_i}. The pulse amplitude (initial DC level) is assumed to be a constant equal to A_0. A sample of the j^{th} member of the ensemble is shown in Figure 2.6.

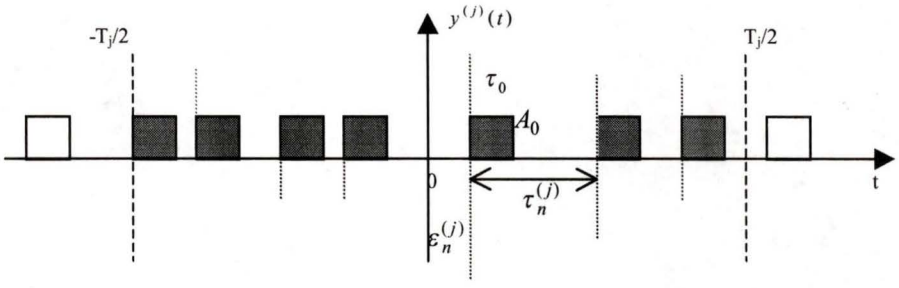

Figure 2.6. Constant pulse width switching scheme.

The resulting power spectral formulas are shown to be:

<u>One-sided spectral density (watts/Hz)</u>

$$W_{ys}(f) = \frac{\varepsilon A_0^2 \sin^2(\pi f \tau_0)}{\bar{\tau}\pi^2 f^2}\left(1 + 2\,\mathrm{Re}\left[\frac{E(e^{j2\pi f\tau})}{1 - E(e^{j2\pi f\tau})}\right]\right), \quad \varepsilon = \begin{cases} 1, & f = 0 \\ 2, & f > 0 \end{cases} \tag{2.4}$$

<u>Power at discrete frequencies (watts)</u>

$$P(f^*) = \begin{cases} P_{DC} = \left(\dfrac{A_0\tau_0}{\bar{\tau}}\right)^2, f^* = 0 \\ \dfrac{2A_0^2}{\left(\bar{\tau}\pi f^*\right)^2}\sin^2(\pi f^*\tau_0),\ f^* > 0 \end{cases} \tag{2.5}$$

2.3.3 Formulation of the CDC Scheme

This second technique represents a switching scheme with random pulse duration and constant duty cycle $\phi = \alpha$ = constant . The random variable τ is statistically independent from pulse to pulse and the switching frequency is selected from the set $\{f_{s_1}, f_{s_2}, ..., f_{s_M}\}$ having a given PDF. The pulse amplitude (initial DC level) is assumed to be constant and equal to A_0. A sample of the switching scheme is shown in Figure 2.7. The parameter *j* stands for the sample number.

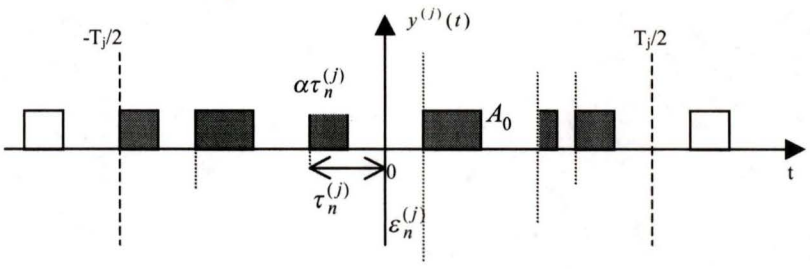

Figure 2.7. Constant duty cycle switching scheme.

The resulting power spectral formulas are shown to be:

Power at discrete frequencies (watts)

$$P(f^*)=\begin{cases}\left(A_0\alpha\right)^2, & f^*=0\\ S_y(f^*)=\dfrac{2A_0^2}{\left(\pi f^*\bar{\tau}\right)^2}\left|E\left\{\sin(\pi\alpha f^*\tau)e^{-j\pi\alpha f^*\tau}\right\}\right|^2 & \\ \quad=\dfrac{2A_0^2}{\left(2\pi f^*\bar{\tau}\right)^2}\left|E\left\{1-e^{-j2\pi\alpha f^*\tau}\right\}\right|^2, & f^*>0\end{cases} \tag{2.6}$$

One-sided spectral density (watts/Hz)

$$W_{ys}(f)=\frac{\varepsilon A_0^2}{\bar{\tau}\pi^2 f^2}\left(E\left\{\sin^2(\pi\alpha f\tau)\right\}+2\,\mathrm{Re}\left[\frac{\left(E\left\{\sin(\pi\alpha f\tau)e^{j\pi f\tau}\right\}\right)^2}{1-E\left\{e^{j2\pi f\tau}\right\}}\right]\right), \tag{2.7}$$

where $\varepsilon=\begin{cases}1, & f=0\\ 2, & f>0\end{cases}$.

2.4 Summary

Although various random modulation schemes are documented and theoretical analyses are studied by different researchers and the results are promising, we must notice some adverse aspects of these schemes such as the risk of resonance being increased accompanying the use of randomization. For example, if we know the drive's natural frequency at which there will exist a large mechanical vibration, we need to minimize the power at this frequency. This requires a tight control of the continuous noise spectrum and a careful choice of probability density function governing the random switching. Research in this area is important. This is the motivation of this thesis.

Since the importance and necessity of the synthesis problems are realized by researchers, which means to design and construct a switching function with desired properties, our purpose in this thesis is to study the synthesis problems in DC/DC converters based on the analysis of the power spectra formulas. We therefore in the next chapter analyze the formulas for the CDC scheme.

Chapter 3

Single Frequency Spectrum Design Problems

3.1 Introduction

The problems addressed in this chapter are the analysis and design of power spectra for RSFPWM DC/DC converters. In chapter 2 we have already summarized the formulas of power spectra for two kinds of RSFPWM: CPW and CDC. Several papers have argued the inherent advantages of these schemes such as efficiently reducing acoustic noise and EMI, but it becomes more and more important to tightly control the continuous noise spectrum. For instance we should put nulls at frequencies at which the load has resonance. Proper design of the switching frequencies and their PDF includes some control over the converter's output noise power spectral density at a specified frequency or a band of frequencies whose value we want to minimize.

Stankovic, Verghese, and Perrault [67] were the first to address the DC/DC converter problem of random switching design for spectral control of harmonic powers and cumulative power in specified bands, which is also our eventual intention. They used 2

switching frequencies selected at random, but with Markov statistics such that long sequences of one switching frequency were discouraged. They found the method ineffective for wide-band (a band of frequencies) control but successful for narrow-band (one specified frequency or harmonics). Our approach is quite different, designing only a stationary multiple switching frequency distribution, and entirely working from the formulation in the frequency rather than the time (auto-correlation) domain. We will also consider specification of a minimum switching frequency to control worst case ripple for the low probability case of continual selection of the same switching frequency, and we consider specification of a maximum switching frequency to control switching inefficiency and other circuit losses. In addition we give new and powerful analysis and design results for the powers of the harmonics related to the distribution of the switching frequencies.

This chapter is concerned with utilizing the results of analysis to attempt to control the power spectral density (PSD) at one specified frequency. Also the power that exists at the least common multiple f_{LCM} of the switching frequencies should be determined and f_{LCM} should be placed at satisfactory points in frequency. Because it is easy to select switching frequencies to produce a desired f_{LCM}, in this chapter we concentrate on the spectral density.

Although formulation shows that the CPW scheme allows a spectral zero to be placed as desired within specific constraints on switching frequency [66], CPW cannot control the duty cycle within each segment. It is deemed "uncontrollable" since it is possible that a long string of pulses with low or high duty cycles may momentarily cause

unacceptable ripples on the output voltage. Thus we further restrict our study here to the formula for the spectral density using the CDC method.

This chapter consists of 3 parts. Part 1 deals with the theoretical analysis of the formulas for the CDC scheme. Part 2 compares results of simulation experiments with prediction from spectral designs. Part 3 summarizes the findings.

3.2 Analysis of the Formulas for CDC RSFPWM

In this section we discuss issues involved in choosing the proper switching frequencies and their probabilities for control of the discrete frequencies having non-zero power and for minimization of the power spectrum at a desired null frequency f_0. Both design goals are oriented toward keeping spectral power away from frequencies known to be harmful to either the environment or to the loads on the converter. It is assumed that the designs can be updated in an adaptive fashion by monitoring the load dynamics.

We first concentrate on the expression in equation (2.7) which is rewritten here:

$$W_{ys}(f) = \frac{\varepsilon A_0^2}{\tau \pi^2 f^2}\left(E\left\{\sin^2(\pi\alpha f\tau)\right\} + 2\,\mathrm{Re}\left[\frac{\left(E\left\{\sin(\pi\alpha f\tau)e^{j\pi f\tau}\right\}\right)^2}{1-E\left\{e^{j2\pi f\tau}\right\}}\right]\right) \tag{3.1}$$

where $\varepsilon = \begin{cases} 1, & f = 0 \\ 2, & f > 0 \end{cases}$, α is duty cycle and τ is the reciprocal of switching frequency.

Because of the complexity we first consider each term in (3.1) separately for minimizing or avoiding peak. Later we will determine if both terms might simultaneously be manipulated. Blind minimization will be considered as a last resort in chapter 5, but we hope to find reasoning behind our approaches.

3.2.1 Method 1: Nulling $E\{\sin^2(\pi\alpha f\tau)\}$ and $E\{\sin(\pi\alpha f\tau)e^{j\pi f\tau}\}$ at f_0

Because a null can generally be repeated periodically on the frequency axis, we direct our attention to the lowest possible frequency that can be nulled given the constraints on the range of switching frequencies. Therefore we begin by noting that the first term $E\{\sin^2(\pi\alpha f\tau)\}$ in (3.1) is always non-negative, but it may have nulls if for the given α the random variables τ_i are selected such that the values of $\sin(\pi\alpha f\tau_i)$ are always zero at the lowest $f = f_0$. The numerator of the second term in (3.1) is nulled if $\left(E\{\sin(\pi\alpha f\tau)e^{j\pi f\tau}\}\right)^2$ is nulled. Although this term is generally complex, it nulls simultaneously with the first term if the argument of the sine function is a multiple of π other than zero. Thus writing $f_0 = \beta\bar{f}_s$, where $\bar{f}_s$ is the average switching frequency and β is a positive scale factor, we can see that for a null at f_0 (and all its harmonics) the relationship that the switching frequencies $f_{s_i} = 1/\tau_i$ must have to $\bar{f}_s$ is

$$\alpha\beta\bar{f}_s / f_{s_i} = k,\ k = 1,2,\ldots,N_s \tag{3.2}$$

or

$$f_{s_i} = \frac{\alpha\beta\bar{f}_s}{k} = \frac{\alpha f_0}{k},\ k = 1,\ 2,\ldots,N_s, \tag{3.3}$$

assuming N_s is the maximum number of switching frequencies used. (Note that the indexes i or k are denoting the rank order of the switching frequencies rather than their progression from small to large.) Because the f_{s_i} are also constrained to lie in

$[f_{s\min}, f_{s\max}]$ and the largest must be greater than the average, the largest $f_{s_i} = f_{s_1}$ in (3.3) is constrained by

$$\bar{f}_s \le f_{s_1} = \alpha\beta\bar{f}_s \le f_{s\max} \tag{3.4}$$

Similarly, the smallest $f_{s_i} = f_{s_{N_s}}$ is constrained by

$$f_{s\min} \le f_{s_{N_s}} = \alpha\beta\bar{f}_s / N_s \le \bar{f}_s \tag{3.5}$$

Limitations on f_0, the Null Frequency for $E\{\sin^2(\pi\alpha f\tau)\}$ and $\left(E\{\sin(\pi\alpha f\tau)e^{j\pi f\tau}\}\right)^2$

If the constraints (3.4) - (3.5) cannot be met, then no design can give a pure null in both terms of (3.1). In fact, (3.4) - (3.5) jointly give limits on the lowest frequency of null $f_0 = \beta\bar{f}_s$:

$$f_{s\min} \le f_{s_{N_s}} = \alpha f_0 / N_s \le \bar{f}_s \le f_{s_1} = \alpha f_0 \le f_{s\max}$$

or

$$\frac{f_{s\min}}{\alpha} \le \frac{f_{s_{N_s}}}{\alpha} = \frac{f_0}{N_s} \le \frac{\bar{f}_s}{\alpha} \le \frac{f_{s_1}}{\alpha} = f_0 \le \frac{f_{s\max}}{\alpha} \tag{3.6}$$

The relative locations of these frequencies are shown in Figure 3.1.

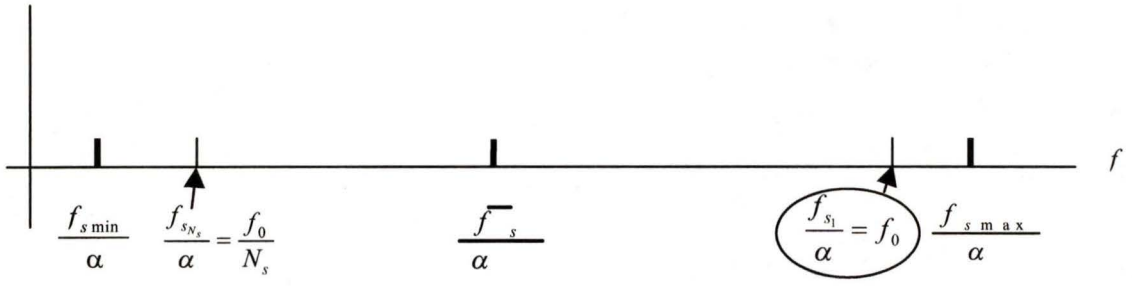

Figure 3.1. Relative placement of practical minimum $f_{s\min}$ and maximum $f_{s\max}$ switching frequencies and constrained minimum $f_{s_{N_s}}$ and maximum f_{s_1} switching frequencies such that a null appears at $f = f_0$.

So there are combinations of null frequency and duty cycle for which the lowest null cannot be placed at a frequency as low as desired for some given acceptable switching frequency range. Placing nulls at higher frequencies is not as difficult, because the frequencies of nulls are periodic, and we may choose any frequency kf_0 to null as long as f_0 satisfies the above expressions. The lowest switching frequency can easily satisfy (3.6) if $f_{s\min}$ is far away from $f_{s\max}$.

3.2.2 Method 2: Maximizing $1-E\{e^{j2\pi f\tau}\}$

The magnitude of the second term in (3.1) at frequencies other than those nulled by (3.6) is dominated by the denominator expression, $1-E\{e^{j2\pi f\tau}\}$, which can approach zero and cause the density not only to become large but perhaps to become infinite. To preclude that, we can force $1-E\{e^{j2\pi f\tau}\}$ to have maximum magnitude at a desired frequency $f_0' = \beta\bar{f}_s$ as above, except that we are denoting f_0' as the frequency at which we would like to maximize $1-E\{e^{j2\pi f\tau}\}$. (It remains to be determined whether or not we can have $f_0' = f_0$.) This maximization will minimize the maximum of the term because the magnitude of the numerator of this term is bounded by unity except the constant scalar; although the numerator may null, there are constraints preventing doing that.

We will now investigate the conditions for which the maximum $1-E\{e^{j2\pi f\tau}\}=2$ occurs. Note that the maximum magnitude of this expression is reached when it is also real, and that occurs when (for a disctete distribution of τ)

$$E\{e^{j2\pi f\tau}\} = \sum_{i=1}^{N_s} p_i e^{j2\pi f\tau_i} = -1.$$

Every exponential in the distribution can equal -1 if

$$2\pi f_0'/f_{s_i} = (2k+1)\pi,\ k = 0,1,2,\ldots,N_s$$

Thus we have that

$$f_{s_i} = \frac{2\beta\bar{f}_s}{2k-1} = \frac{2f_0'}{2k-1},\ k = 1,2,\ldots,N_s \tag{3.7}$$

where again the indices k and i indicate rank order of the switching frquencies rather than progression to higher frequencies. As before the minimum and maximum swithing frequencies are constrained according to

$$\bar{f}_s \le f_{s_1} = 2\beta\bar{f}_s \le f_{s\max} \tag{3.8}$$

$$f_{s\min} \le f_{s_{N_s}} = 2\beta\bar{f}_s/(2N_s - 1) \le \bar{f}_s \tag{3.9}$$

Now we remark that equations (3.3) - (3.5) are similar to equations (3.7) - (3.9) except that the factor α in (3.3) - (3.5) has been replaced by 2 in (3.7) - (3.9), and k and N_s in (3.3) - (3.5) have been respectively replaced by $2k$-1 and $2N_s$-1 in (3.7) - (3.9). Further we note that apparently (3.3) - (3.5) are most important for minimizing the maximum value of (3.1). Although the numerator of the second term in (3.1) may null, in practice there is no straightforward visible means of effecting that when the maximum and minimum constraints are set on the swtiching frequencies, as we show in the later design examples. If there is a choice to be made between the first term minimization and constraining the magnitude of the second term (and indeed the whole density), sometime minimizing the maximum of the second term is the most important due to practical considerations. That is because the second term is the source of strong peaks in the PSD.

Limitations on f_0', the Maximizing Frequency for $1-E\{e^{j2\pi f\tau}\}$

The constraints imposed by minimum, maximum and average switching frequencies on the frequency of the maximum of the denominator factor $1-E\{e^{j2\pi f\tau}\}$ are similar to those imposed by the term $E\{\sin^2(\pi\alpha f\tau)\}$. By rewriting (3.6) while replacing α with 2 and N_s by $2N_s$-1 we have

$$\frac{f_{s\min}}{2} \le \frac{f_{s_{N_s}}}{2} = \frac{f_0'}{(2N_s-1)} \le \frac{\bar{f}_s}{2} \le \frac{f_{s_1}}{2} = f_0' \le \frac{f_{s\max}}{2} \tag{3.10}$$

These bounds, together with those of Figure 3.1 for equation (3.6), are marked on the frequency axis in Figure 3.2.

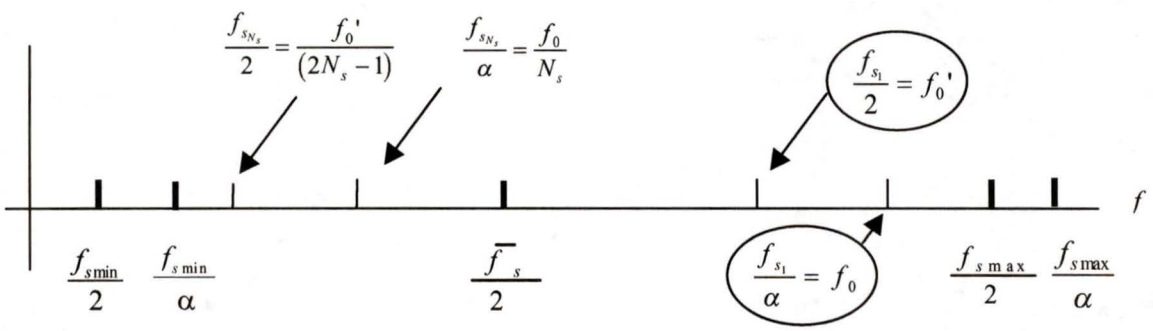

Figure 3.2. Relative placement of practical minimum $f_{s\min}$ and maximum $f_{s\max}$ switching frequencies and constrained minimum $f_{s_{N_s}}$ and maximum f_{s_1} switching frequencies such that $1-E\{e^{j2\pi f\tau}\}$ is maximized at $f = f_0'$ while also $E\{\sin^2(\pi\alpha f\tau)\}$ and $\left(E\{\sin(\pi\alpha f\tau)e^{j\pi f\tau}\}\right)^2$ are nulled at $f = f_0$.

Note that to meet the criterion of maximizing $1-E\{e^{j2\pi f\tau}\}$, $\frac{\bar{f}_s}{2} \le \frac{f_{s_1}}{2} = f_0' \le \frac{f_{s\max}}{2}$ bounds the lowest possible f_0' both above and below, and $\frac{f_{s\min}}{2} \le \frac{f_{s_{N_s}}}{2} = \frac{f_0'}{(2N_s-1)}$ limits

the number of switching frequencies that can be used. These findings are quite limiting. Almost certainly in practice, sub-optimality is going to result.

3.2.3 Comparison and Conclusion of the Methods for Controlling the Two Terms

If we combine the inequalities of (3.6) with those of (3.10) we have as shown in Figure 3.2 ($N_s \geq 2$),

$$\frac{f_{s\min}}{2} \leq \left(\frac{f_{s_{N_s}}}{2} = \frac{f_0'}{(2N_s - 1)} \right) \leq \left(\frac{f_{s_1}}{2} = f_0' \right) \leq \left(\frac{f_{s_1}}{\alpha} = f_0 \right) \leq \frac{f_{s\max}}{\alpha} \tag{3.11}$$

It is clear that both objectives cannot be met simultaneously because for $0 \leq \alpha \leq 1$ we cannot have $\frac{f_{s_1}}{\alpha} = f_0$ and $\frac{f_{s_1}}{2} = f_0'$ equal to each other. By our forgoing arguments, we must minimize the magnitude of the second term in (3.1), and this is accomplished through the equations (3.7) - (3.9). Clearly an overall or global optimum might be found, and that is the another approach, functional minimization to constraints, which we shall subsequently consider in chapter 5.

However it is easily shown analytically that when harmonics of the lowest nulling frequency of $E\{\sin^2(\pi\alpha f\tau)\}$ and $\left(E\{\sin(\pi\alpha f\tau)e^{j\pi f\tau}\}\right)^2$ fall on harmonics of the frequency of non-zero discrete power, that the result is a null in the PSD. That is, $1 - E\{e^{j2\pi f\tau}\}$ is zero when $f = kf_{LCM}$, causing frequencies of infinite power density, but the zero in the numerator at harmonics of $\frac{f_{s_1}}{\alpha} = f_0$ may fall exactly on $f = kf_{LCM}$. At such frequencies,

a spectral null results. But at such frequendies we must consider the effects of disctete power, it is not desirable.

From Figure 3.2 we may clearly observe that method 1 is suitable for controlling the PSD at higher frequencies but method 2 is suitable for controlling the PSD at lower frequencies, assuming the same switching frequency constraints.

3.2.4 Further Analysis of $1-E\{e^{j2\pi f\tau}\}$ and a Design Procedure

In this subsection we investigate the behavior of the denominator expression $1-E\{e^{j2\pi f\tau}\}$ as a function of f. We note that for discrete distributions of τ that the expectation $E\{e^{j2\pi f\tau}\}$ can be written

$$E\{e^{j2\pi f\tau}\}\Big|_{f=f_{sk}} = \sum_{i=1}^{N_s} p_i e^{j2\pi f_{sk}\tau_i} \tag{3.12}$$

The term for $i = k$ gives the positive real value p_i since the exponential is unity then. If the p_i is near unity, $1 - E\{e^{j2\pi f_{sk}\tau}\} \cong 0$ and a large spectral magnitude results. Further, when the switching frequencies are all in a narrow band $1-E\{e^{j2\pi f\tau}\} \cong 0$ for frequencies near $\bar{f}_s$ and its multiples. This phenomenon has been seen clearly in experimental work, and it is obvious that this factor is responsible.

Arbitrarily we now investigate the expression $1 - E\{e^{j2\pi f\tau}\}$ as a function of f, $f_{s\min}$ and $f_{s\max}$ for a continuous uniform distribution of τ. The algebra for this case, shown in appendix A, results in

$$E\left\{e^{j2\pi f\tau}\right\}=\frac{f_{s\min}f_{s\max}}{j\sqrt{2}\pi f\left(f_{s\max}-f_{s\min}\right)}\left(1-\cos\left(2\pi f\frac{f_{s\max}-f_{s\min}}{f_{s\min}f_{s\max}}\right)\right)^{1/2}e^{j\theta} \tag{3.13}$$

The reason for the $1/f$–scaled root-sinusoidal magnitude with period $\frac{f_{s\max}-f_{s\min}}{f_{s\min}f_{s\max}}$ Hz is that the spread of the argument in $e^{j2\pi f\tau}$ is in the range $\left[\frac{2\pi f}{f_{s\max}},\frac{2\pi f}{f_{s\min}}\right]$. For any particular f this range may be small or large with respect to a cycle (2π). If the range is small, $E\left\{e^{j2\pi f\tau}\right\}$ is approximately a constant with nearly unity magnitude. This situation may be favorable or unfavorable in the expression $1-E\left\{e^{j2\pi f\tau}\right\}$ depending on the angle θ, whose expression is shown in appendix A. If the range $\left[\frac{2\pi f}{f_{s\max}},\frac{2\pi f}{f_{s\min}}\right]$ is large (many cycles), $E\left\{e^{j2\pi f\tau}\right\}$ is approximately a constant with nearly zero magnitude, and this is a satisfactory value, because $1-E\left\{e^{j2\pi f\tau}\right\}\cong 1$, but this is not optimal for that f. For ranges not small but not an integer number of cycles, $E\left\{e^{j2\pi f\tau}\right\}$ will oscillate with f. Laboratory results have shown that for larger f the peakiness in the spectral density diminishes considerably except near f_{LCM} and its harmonics. The design implications are that to keep the spectral density from peaking near some $f=f_0$ it is sufficient that the uniform distribution of τ must be such that the argument range R_a is a whole number of cycles, an integer multiple of 2π rad:

$$\left[\frac{2\pi f}{f_{s\max}},\frac{2\pi f}{f_{s\min}}\right]=\left[\varphi-(2k-1)\pi,\varphi+(2k-1)\pi\right],\ k=1,2,\ldots \tag{3.14}$$

for some average principal angle φ, resulting in a zero mean for the exponential. An alternative is as previously, when we wanted $E\{e^{j2\pi f\tau}\}$ to equal –1, i.e., it would be desirable if

$$\left[\frac{2\pi f}{f_{s\max}}, \frac{2\pi f}{f_{s\min}}\right] = [\pi - \vartheta, \pi + \vartheta] \tag{3.15}$$

where ϑ is small so that $E\{e^{j2\pi f\tau}\} \cong -1$. For some f this may be possible, and in fact for any $f_{s\min}$ and $f_{s\max}$ there are f such that (3.15) is realized, although f may be small. In Figure 3.3 is a general set of plots for the cycle-normalized angle range $\mathrm{R_a} = \left[\frac{2\pi f}{f_{s\min}} - \frac{2\pi f}{f_{s\max}}\right] / (2\pi)$ *cycles* indicated in (3.15), but rewritten so that $\frac{f}{f_{s\max}}$ is a function of R_a:

$$\frac{f_{s\max}}{f_{s\min}} = \frac{\mathrm{R_a} + \frac{f}{f_{s\max}}}{\frac{f}{f_{s\max}}} \tag{3.16}$$

Figure 3.3 allows design of $f_{s\min}$ and $f_{s\max}$ to give an argument range that is either a small part of a cycle or a whole number of cycles at some particular frequency f. Suppose we want $f_{s\max} / f_{s\min}$ to be smaller than 2. Then looking at Figure 3.3 (b), we are confined to a small region near the bottom of the plots.

If further, we want spectral flattening near a small $f / f_{s\max}$, the solution point is further confined to the lower curves, say curves for 1 or 2 whole cycles of argument range.

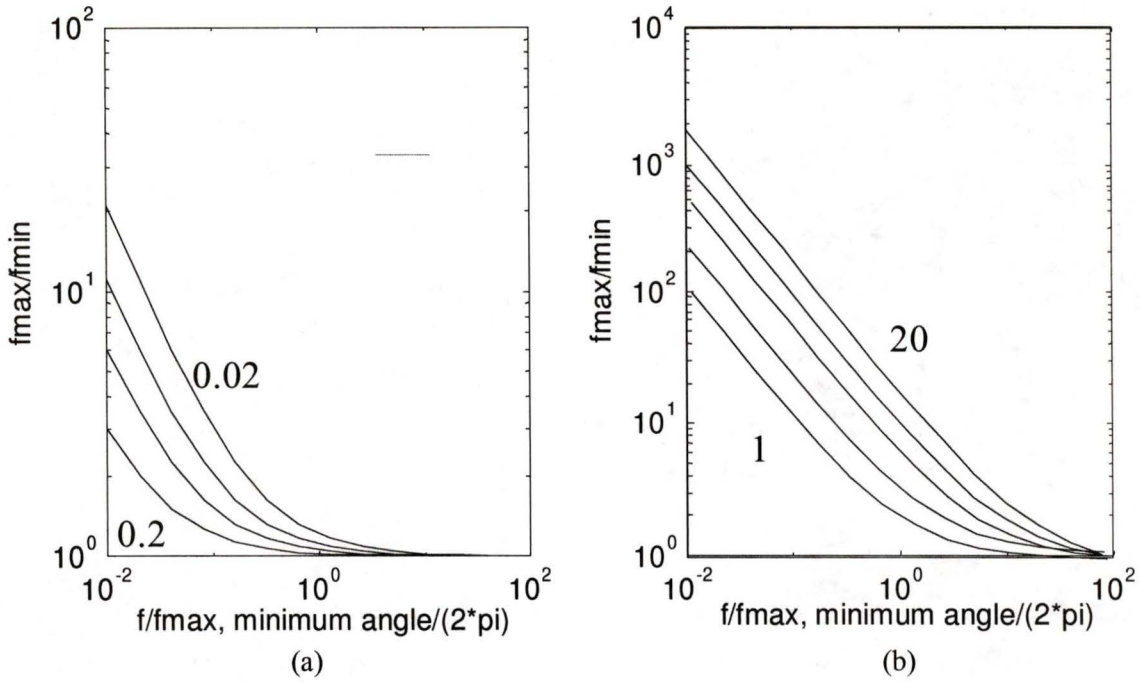

Figure 3.3. $f_{s\max} / f_{\min}$ for continuous uniformly distributed f_s in $[f_{s\min}, f_{s\max}]$ *vs* $f / f_{s\max}$, plotted for several a) fractional (0.02, 0.05, 0.1, 0.2) and b) integer (1, 2, 5, 10, 20) cylcles of argument range R_a.

Also for a given $f_{s\min}$ there is an f below which even one whole cycle of argument can not be obtained. For that situation the spectral density near that f may get quite large because the angle span of $e^{j2\pi f\tau}$ is no longer uniform over a cycle. Directing our attention to the curves in Figure 3.3 (a) we see that the minimum angle $2\pi f / f_{\max}$ rad (horizontal axis) is approaching zero as f gets smaller. The joint effect of both the small minimum angle and the narrow angle range is that the average exponential $E\{e^{j2\pi f\tau}\}$ will have magnitude near +1 causing 1- $E\{e^{j2\pi f\tau}\}$ to approach zero and W(f) to approach infinity. Of course the solution to the problem is to allow lower switching frequencies so that we can have a uniformly distributed argument of $e^{j2\pi f\tau}$ at the desired f.

It is also desirable to yield a spectral density with magnitude constrained to some least upper bound, over a band of frequencies. A design to this effect might be implemented with numerical optimization techniques.

3.3 Design Experiments and Simulation Results

The equation analyses of the last section and the experiments of this section show clearly that when we want to null a frequency's power the most effective term to utilize is $E\{\sin^2(\pi f\alpha\tau)\}$. When this term is zeroed, both terms in equation (3.1) are set to zero. That is to say, a sharp null appears in the PSD at frequencies for which this term is zero.

On the other hand when a singularity of the PSD (a frequency having real power) appears in the spectrum, the cause is the denominator factor $1-E\{e^{j2\pi f\tau}\}$. At frequencies for which $1-E\{e^{j2\pi f\tau}\}$ becomes zero, the PSD becomes infinite. Further there are other frequencies where $\left[1-E\{e^{j2\pi f\tau}\}\right]^{-1}$ becomes unacceptably large and causes a peak in the PSD. When we want to minimize the PSD within the constraints of the average and finite range of switching frequencies, the most important factor is $1-E\{e^{j2\pi f\tau}\}$. This is because we cannot null $E\{\sin^2(\pi f\alpha\tau)\}$ at an arbitrary frequency when we limit switching frequencies to range such as from 55 kHz to 75 kHz, which are the practical constraints used in our examples.

We have also found that even without the limitation on switching frequencies sometimes the term $E\{\sin^2(\pi f\alpha\tau)\}$ cannot be simply nulled if the frequency of desired null coincides with a harmonic of the least common multiple f_{LCM} of the set of discrete

random switching frequencies since then we need to consider the discrete power. This can be seen clearly in Figure 3.11 and the analysis can be found in experiment 1.3.

Thus in our following experiments we give most attention to the term $1-E\{e^{j2\pi f\tau}\}$. Through maximizing $1-E\{e^{j2\pi f\tau}\}$ we can shift the PSD maximum away from a specified frequency. Although we cannot eliminate the peak, we will see in chapter 5 that we may well minimize it by choosing the switching frequencies and their distribution. In this section we only study the switching frequencies with uniform distribution.

3.3.1 General Description of Experiments in This Section

Experiment 1 consists of three parts. Experiment 1.1 demonstrates that when we choose the switching frequencies freely, but with caution, such that the constraints are satisfied, there will be a peak appearing at frequency $f_0 = 62.5$ kHz. The result is shown in Figure 3.4. In addition, in experiment 1.1 we try different constant duty cycles and verify that the reason for the peak is that the denominator term $1-E\{e^{j2\pi f\tau}\}$ tends to zero. The plot of the analytical result is in Figure 3.7, where we can find the composed vector lies near the positive real axis. That is to say, the numerator of equation (3.1) tends to zero, so a significant peak appears at 62.5 kHz.

In experiment 1.2 we maximize the term $1-E\{e^{j2\pi f\tau}\}$ within the constraint that switching frequencies range within 55 kHz to 75 kHz. Maximization of $1-E\{e^{j2\pi f\tau}\}$ minimizes the peak at the desired frequency. The peak has been reduced by almost 50dB. The result is shown in Figures 3.9 and 3.10.

In experiment 1.3 we null the term $E\{\sin^2(\pi f\alpha\tau)\}$ at the specified frequency but demonstrate a conflict in design. In theory there should be a sharp null appearing at the desired f_0 = 62.5 kHz, but in fact there is a narrow peak appearing as shown in Figure 3.11. This peak is due to the fact that f_0 is a harmonic of the f_{LCM}. We analyze this phenomenon in detail and give a general conclusion.

In experiment 2 we try to maximize the term $1-E\{e^{j2\pi f\tau}\}$ without any constraints on the switching frequencies. The result in Figure 3.13 shows that the peak has been reduced to –37 dB.

In experiments 3.1-3.5 we null or minimize the PSD at the desired frequency f_0=62.5kHz while satisfying the constraint that the average switching frequency equals 62.5 kHz. We use two, three and four switching frequencies respectively.

In experiment 3.1 we illustrate an interesting method of producing a sharp null at the desired frequency, although the switching frequencies are outside the specified band. In experiment 3.2 we maximize $1-E\{e^{j2\pi f\tau}\}$ with 2 frequencies considerably outside the specified band. In experiment 3.3 we maximize $1-E\{e^{j2\pi f\tau}\}$ with 2 other frequencies. In experiments 3.4 and 3.5 we maximize $1-E\left\{e^{j2\pi f\tau}\right\}$ at f_0=62.5 kHz with 3 and 4 frequencies respectively, using a numerical search method to find multiple solutions.

All of the methods yield positive results, verifying that we have considerable control over the PSD at a specified frequency, particularly if the switching frequency band constraint is not too narrow and if a null is not desired at a frequency too low.

The following are our experiments and results with and without the constraints on the switching frequencies. Note that in all our experiments we have only tried to minimize or null the spectral power at a single specified frequency, $f_0 = 62.5$ kHz. This frequency, the average f_s, is the one most difficult to null within the constraints provided by Xantrex[1]. In these experiments we have used a constant 50% duty cycle to illustrate the method, but the method accommodates any arbitrary constant duty cycle.

3.3.2 Experiment 1: Comparison With and Without Constraints

This experiment includes three cases:

a) Constrained maximum and minimum switching frequencies.

b) Constrained switching frequency range and mean.

c) No design constraints on the switching frequencies.

The experiment switching scheme's parameters are given in Table 3.1.

Experiment 1.1. Constrained maximum and minimum switching frequencies

In addition to the parameters shown in Table 3.1, we demonstrate the effect of duty cycle in three different figures. We do this because we want to verify that the peak appearing is due to the denominator of the second term of equation (3.1); we will verify that the frequency of peak does not correlate to changes in duty cycle.

[1] the constraints of Xantrex are as follows: the switching frequency ranges from 55kHz to 75kHz, and the average switching frequency is 62.5kHz.

From Figure 3.4 we can see that the first major peak of the PSD is –21.7dB at f = 62.5 kHz. Keeping the other parameters the same as above while changing only the constant duty cycle from 50% to 80% and then 30% gives the results shown in Figures 3.5 and 3.6 respectively. We find that the peak still appears at f = 62.5kHz, verifying that the frequency of peak is not affected by the duty cycle.

Experiment 1	1.1	1.2	1.3
Switching frequencies kHz (uniform)	55, 75	74.9, 75 or 55, 55.1	15.6, 31.3
Average switching frequency kHz	65	74.95 or 55.05	23.4
Initial DC voltage	1	1	1
Sampling frequency kHz	1000	1000	1000
Bandwidth	500	500	500
Constant duty cycle, %	50	50	50
Periodogram characteristics	Hamming window, 30 averages 10 samples overlap	Hamming window, 30 averages 10 samples overlap	Hamming window, 30 averages 10 samples overlap

Table 3.1. Experiments 1.1, 1.2 and 1.3 parameters, duty cycle 50%.

Examining the PSD of equation (3.1) we find that the peak is due to the denominator of the second term, whose value does not change with duty cycle α. Thus the analytical and experimental findings agree and we can now direct attention to the second term's denominator.

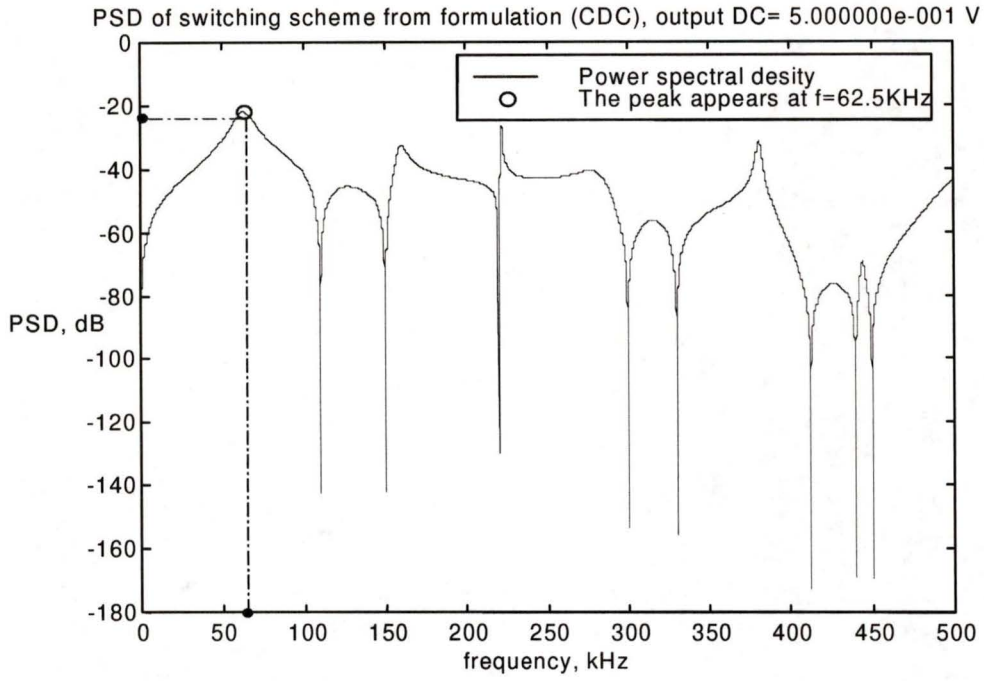

Figure 3.4. Result of experiment 1.1, frequencies [55, 75] kHz, and 50% duty cycle.

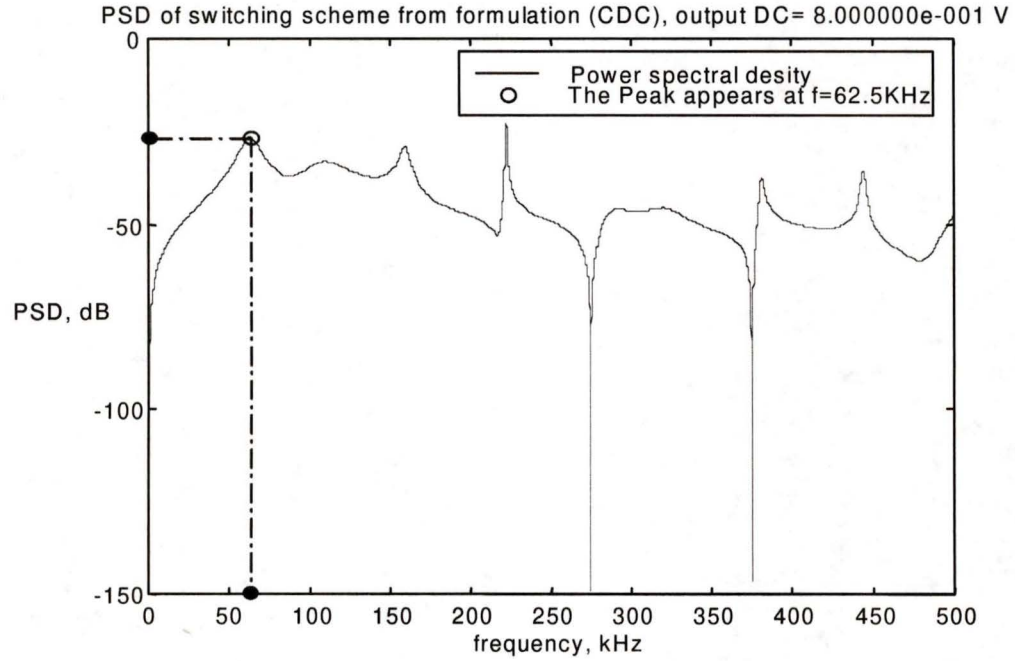

Figure 3.5. Result of Experiment 1.1 with 80% duty cycle.

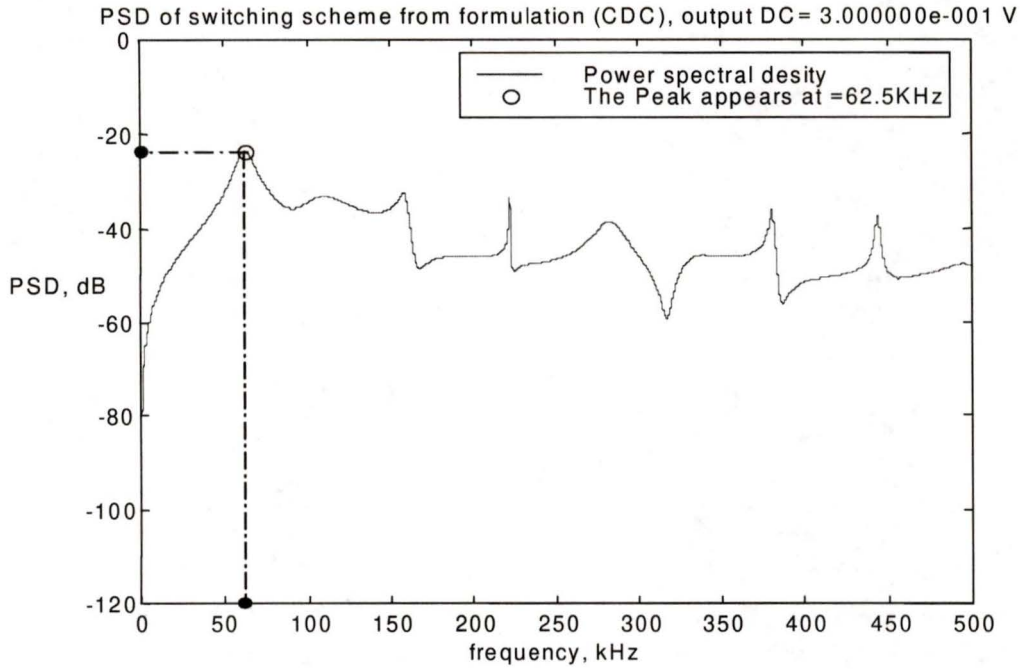

Figure 3.6. Experiment 1.1, 30% duty cycle.

General analysis of the term $1-E\{e^{j2\pi f\tau}\}$ for two switching frequencies

We begin analysis and experimentation considering just two randomly selected switching frequencies. Only 2 are considered so as to simply present the method of design. We can calculate the two angles of the exponential terms in the expectation at peak frequency. These angles are

$$\theta_{\max} = \frac{2f\pi}{f_{s\min}} = \frac{2\times 62.5\pi}{55} = 2.27\pi \approx 49^\circ + 360^\circ$$

$$\theta_{\min} = \frac{2f\pi}{f_{s\max}} = \frac{2\times 62.5\pi}{75} = 1.67\pi = 300^\circ$$

The complex vectors at these two angles are shown in Figure 3.7.

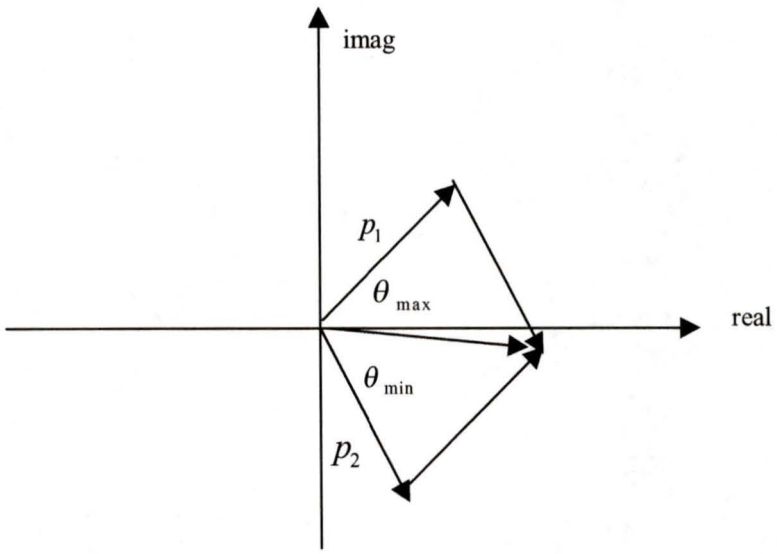

Figure 3.7. Complex exponential vectors for the two switching frequencies.

We can see that the vector composed of the two vectors lies near the positive real axis. That is to say, the numerator of equation (3.1) tends to zero, so a significant peak appears at 62.5 kHz.

Experiment 1.2: Two frequencies near the maximum.

If we want to flatten the spectral peak at $f_0 = 62.5$kHz, we will let the expected vector of the denominator $E\left\{e^{j2\pi f\tau}\right\}$ at $f = f_0$ lie far away from the positive real axis, becoming as close to negative real as possible. Within the limitations of the switching frequencies we can only choose frequencies between the extremes. If we choose two frequencies near the maximum, that is [74.9, 75] kHz, the exponential terms are as shown in the first quadrant in Figure 3.8. The spectral plot, shown in Figure 3.9, shows that the value at f =

62.5 kHz has power density –76.8dB, a great reduction from –22dB of experiment 1.1, but the spectral peak has shifted to about 75 kHz.

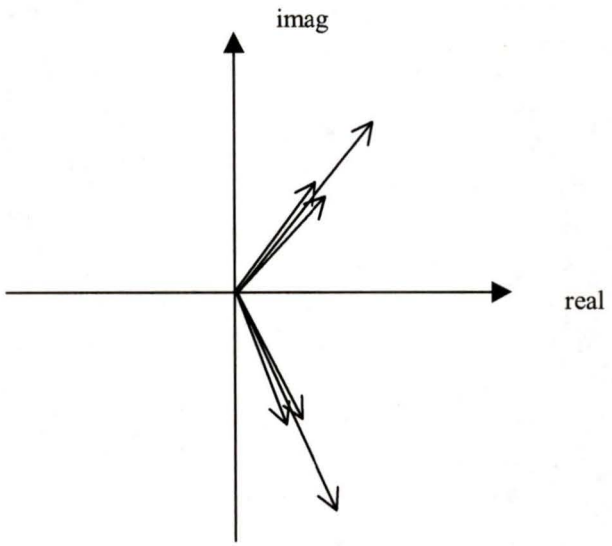

Figure 3.8. Complex exponential vectors for experiment 1.2 for frequency 62.5 kHz.

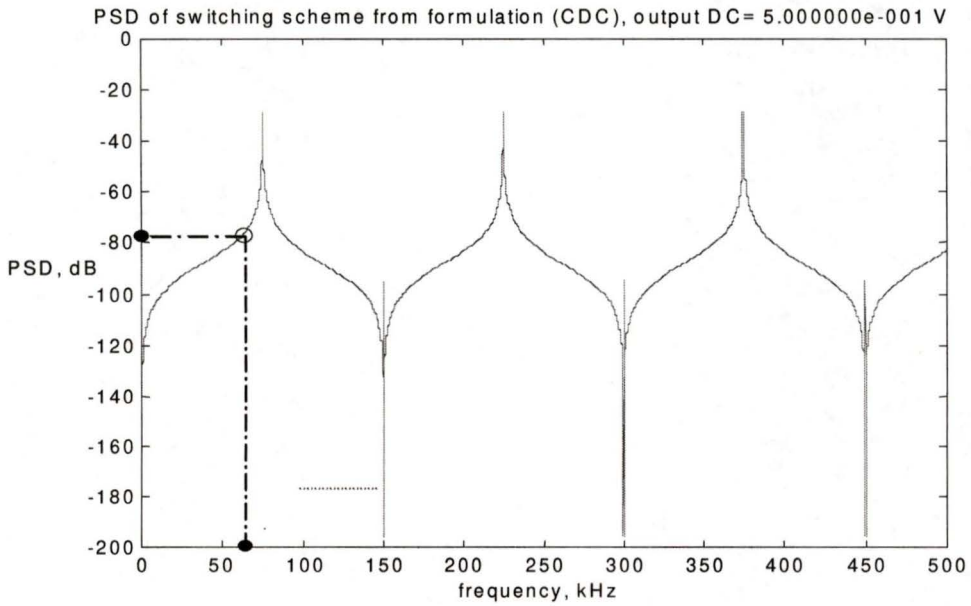

Figure 3.9. Experiment 1.2, switching frequencies [74.9,75] kHz, to reduce the PSD at 62.5 kHz, without f_{ave} constraints.

Next we change the switching frequencies to [55 55.1] kHz. The exponential terms are in the 4th quadrant of Figure 3.8, and the spectral result is shown in Figure 3.10. The value at f = 62.5 kHz is –71dB. So this experiment has clearly shown that we can control the spectral magnitude at a desired frequency by locating the switching frequency within the band constraints. However we have not yet satisfied the average frequency constraint.

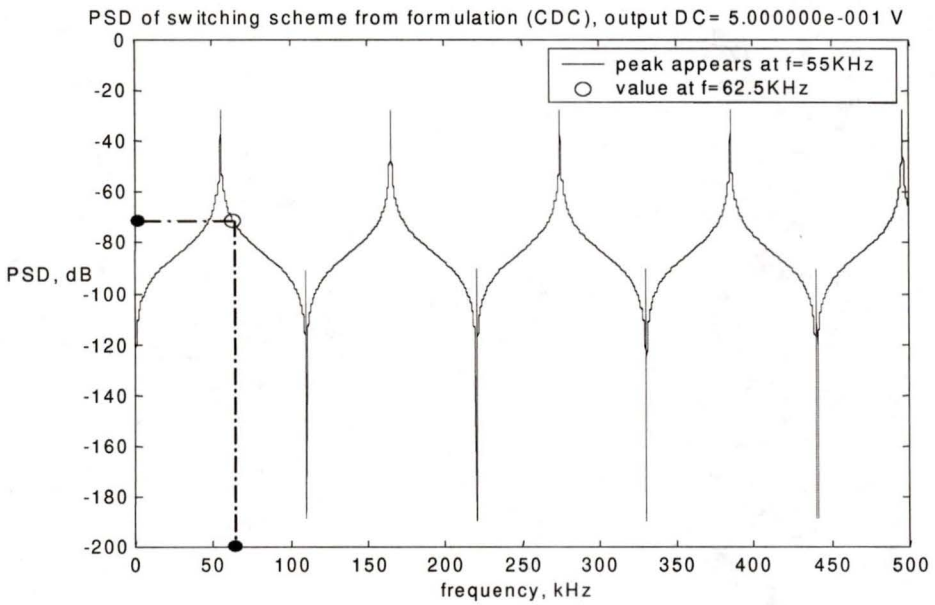

Figure 3.10. Experiment 1.2, switching frequencies [55, 55.1] kHz, to reduce the PSD at 62.5 kHz without f_{ave} constraints.

Experiment 1.3 Conflicting design for nulls and harmonics of the f_{LCM}:

If we have no limitation on switching frequencies then we can null $E\{\sin^2(\pi f\alpha\tau)\}$ at f_0 = 62.5 kHz to give a PSD null at f_0 by selecting switching frequencies

$$f_{s_k} = \frac{\alpha\beta\bar{f}_s}{k} = \frac{\alpha f_0}{k},\ k = 1,\ 2,\ldots, N_s \tag{3.17}$$

For the special case of 50% duty cycle we can choose k = 1 and k = 2 and obtain the switching frequencies 31.3 kHz and 15.6 kHz. Note that in this case that f_{LCM} = 62.5 kHz,

which would be counter to our desire to null at 62.5 kHz. The simulation proves that actually there is a peak appearing at the desired frequency because of the coincidence of the f_{LCM} which is half of f_0. The theoretical PSD value at f_0 = 62.5 kHz is –172.6dB, but the simulation value is about – 45dB. The experimental result is shown in Figure 3.11. In fact this conflict will always occur when duty cycle $\alpha = \frac{1}{2}, \frac{1}{3}, \cdots, \frac{1}{k}$, since then we must add the discrete power to the PSD according to equation (2.6). Thus for this coincidental case we cannot use the nulling of $E\{\sin^2(\pi f \alpha \tau)\}$ to get a sharp null at the desired frequency. This fact indicates that the method that ideally nulls the spectral power at a desired frequency, but, will be limited in some very unlikely cases. Considering the above limitation on null placement, in experiment 2 we will verify the use of $1 - E\{e^{j2\pi f\tau}\}$ for minimizing (but not nulling) the PSD at a specified frequency. First we conclude experiment 1.

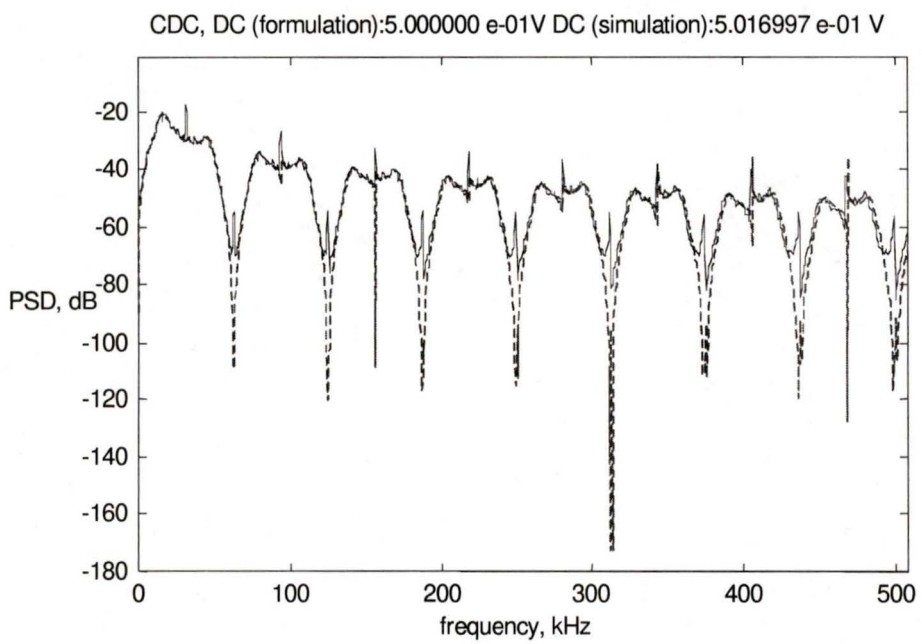

Figure 3.11. Experiment 1.3, switching frequencies [15.6, 31.3] kHz. Dotted plot represents the result from equation. Solid plot represents the result from simulation.

The above design conflict arose due to our use of 50% duty cycle (or 1/3 or 1/4 ...). However for another duty cycle we can still produce a sharp null at the desired frequency (62.5 kHz). We demonstrate this by changing the parameters shown as Table 3.2. With a duty cycle of 80%, the resulting PSD value at $f_0 = 62.5$ is –140.1 dB. The spectral result is shown in Figure 3.12.

Switching frequencies	25, 50 kHz with equal probabilities
The Average of switching frequencies	37.5 kHz
Initial Dc voltage value	1 volt
Sampling frequency	1000 kHz
Bandwidth	500 kHz
Constant duty cycle	80%
Periodogram characteristics	Hamming window, 30 averages 10 samples overlap

Table 3.2. Experiment parameters, duty cycle 80%.

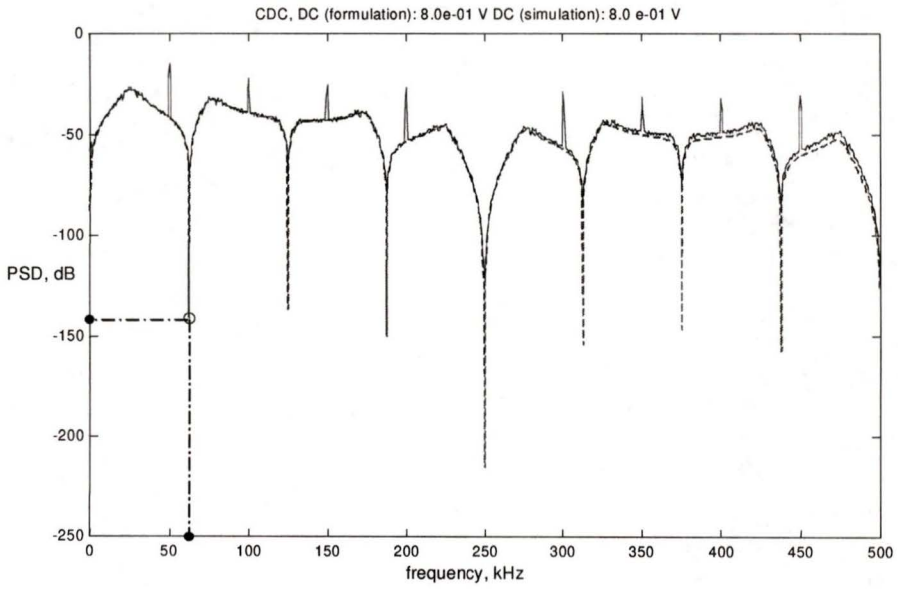

Figure 3.12. Results for parameters as given in Table 3.2, duty cycle 80%. The dotted plot represents the theoretical result. The solid plot represents the result from simulation. Since the duty cycle is not 1/2, 1/3,..., we have a perfect null at 62.5 kHz.

3.3.3 Experiment 2: Design for Avoiding Harmonics of the f_{LCM}

When we maximize $1 - E\{e^{j2\pi f\tau}\}$ to minimize the peak at $f_0 =$ 62.5 kHz according to equation (3.7), the switching frequencies for maximization are ideally

$$f_{s_k} = \frac{2\beta\bar{f}_s}{2k-1} = \frac{2f_0'}{2k-1}, \quad k = 1,2,\ldots,N_s.$$

We thus calculate that the set of possible switching frequencies is $\{125, 41.7, 25, \ldots\}$ kHz. From this set we choose 25 kHz and 41.7 kHz as our switching frequencies. The parameters shown in Table 3.3 give the spectrum in Figure 3.13. The resulting PSD value at $f_0 =$ 62.5kHz is about –37dB, a reduction of about 15dB from Figure 3.4.

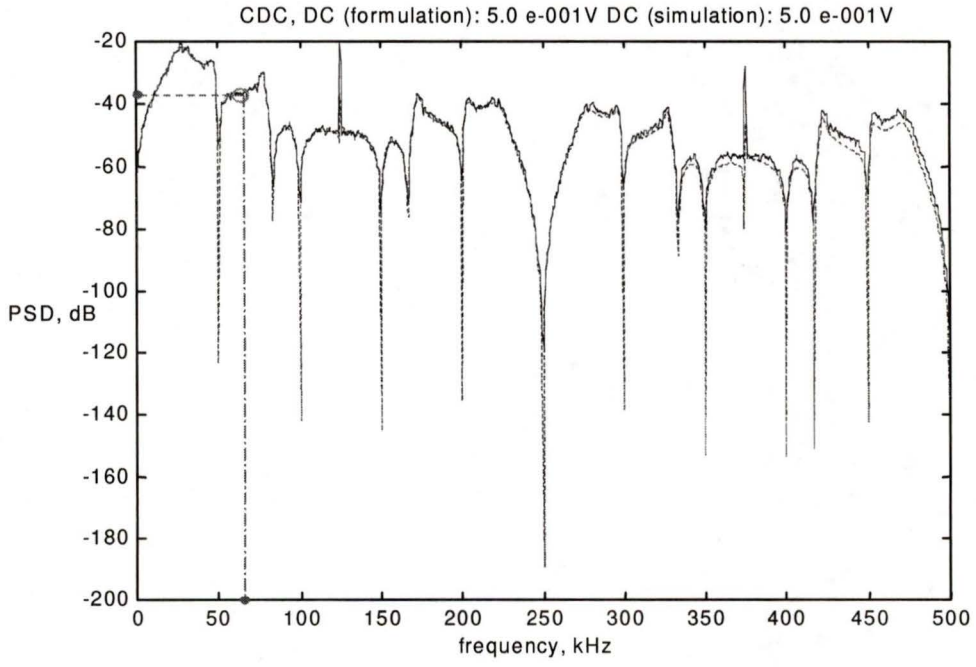

Figure 3.13. Results for parameters as given in Table 3.3, duty cycle 50%. Dotted plot represents the result from equation. Solid plot represents the result from simulation.

Switching frequencies	25, 41.7 kHz, equal probabilities
The Average of switching frequencies	33.4 kHz
Initial Dc voltage value	1 volt
Sampling frequency	1000 kHz
Bandwidth	500 kHz
Constant duty cycle	50%
Periodogram characteristics	Hamming window, 30 averages 10 samples overlap

Table 3.3. Experiment 2, for nulling while avoiding harmonics of the f_{LCM}.

The three PSD plots from experiments 1.1, 1.2 and 2 are shown together in Figure 3.14. The solid plot represents the switching scheme using $f_{switch} = 55$, 75 kHz, the dashed plot represents the switching scheme using $f_{switch} = 74.9$, 75 kHz and the long dash dotted plot represents the switching scheme using $f_{switch} = 25$, 41.7 kHz. We also use '+', '*', and 'o' to mark the PSD values at f_0=62.5 kHz respectively for the three methods.

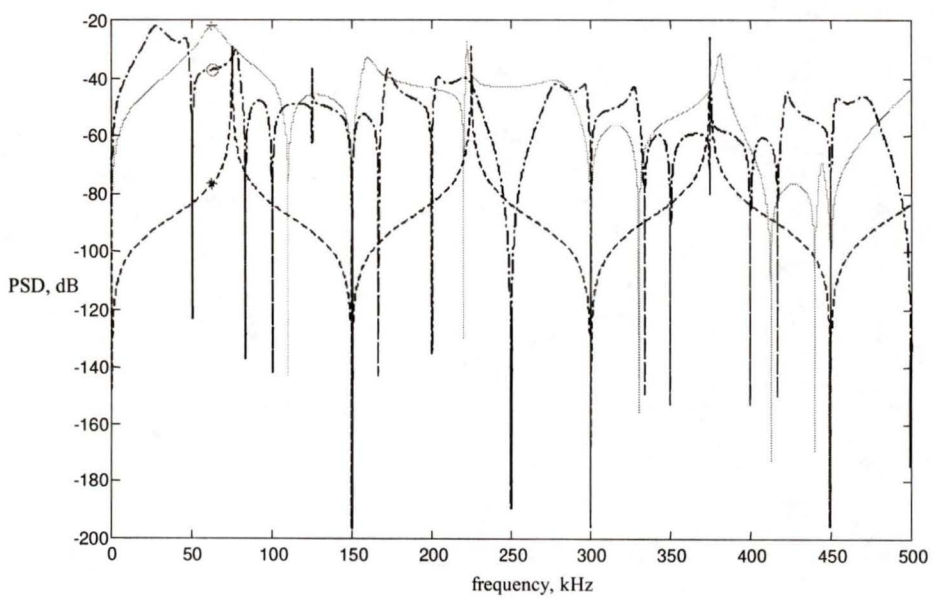

Figure 3.14. Overlaid plots of the three cases. Solid: f_s = 55,75 kHz;: dashed f_s = 74.9,75 kHz, long dash-dotted: f_s = 25,41.7 kHz. Note the values at the "design" frequency of 62.5 kHz.

The above experiments have not enforced the constraint that the average switching frequency $\overline{f}_s$ is 62.5 kHz. In the following experiments, we shall find the cost due to the $\overline{f}_s$ constraint for minimizing the PSD power at the selected frequency.

3.3.4 Experiments 3: Design for Minimization Under the Constraint of Average Switching Frequency f_{ave} = 62.5 kHz

Without trying to null, we now try to minimize the PSD at f_0 = 62.5 kHz with the constraint that average switching frequency is 62.5kHz. This f_0 is a reasonable frequency to select for minimization because if there were no randomization, there would clearly be an infinite PSD peak at the average and only switching frequency. Also if the band of switching frequencies is narrow around the mean, we would expect the average frequency to have a large PSD value. In any case, we may consider f_0 = 62.5 kHz as a typical frequency to minimize.

For simplicity we will experiment with only two switching frequencies, choosing them to have the desired mean, but also choosing in such a way that a null is placed at the mean. The two frequencies are related to each other due to the constraint on their mean, and this constrains the phases of the two terms in the expectation. We are able to satisfy the $\overline{f}_s$ constraint and place a null at the mean if we do not also have a max and min f_s constraint. Analysis of the effect of this choice on the denominator's expectation in $1 - E\{e^{j2\pi f\tau}\}$ is shown in Figure 3.15.

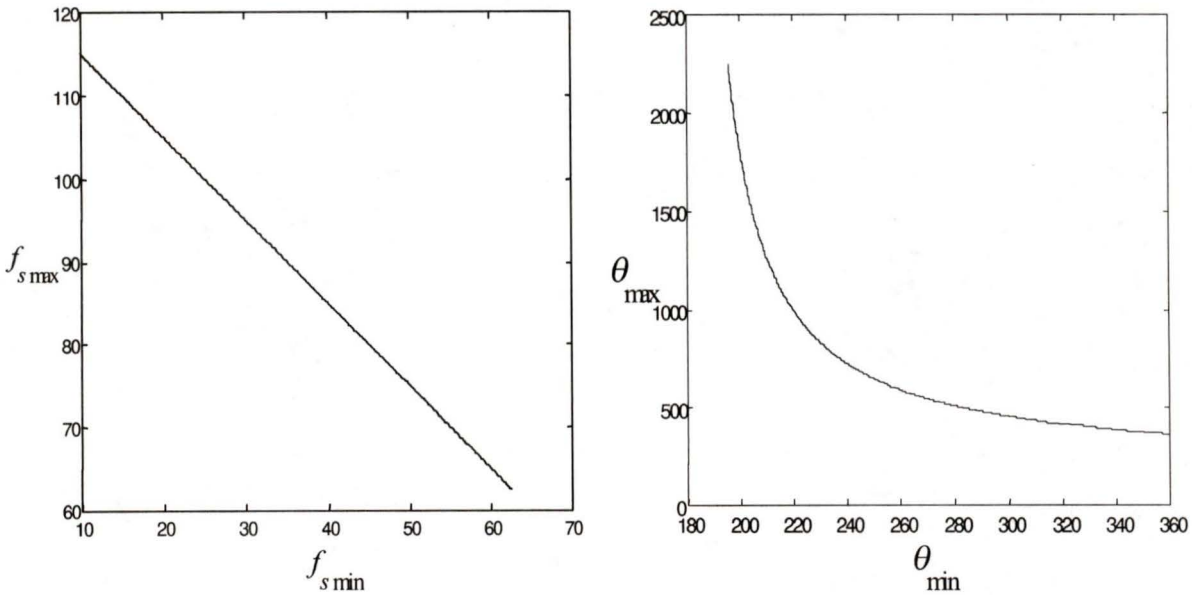

Figure 3.15. (a) The average-constrained relation between the low and the high switching frequencies (kHz) (b) the corresponding relation of the two angles (degrees).

Experiment 3.1 Moderately spread frequencies with a specified null.

The parameters for experiment 3.1 are as in Table 3.4. The frequencies chosen are a factor of 3 apart, both outside the Xantrex-specified band of [55, 75] kHz.

Switching frequencies	31.3, 93.7 kHz, equal probabilities
The Average of switching frequencies	62.5 kHz
Initial Dc voltage value	1 volt
Sampling frequency	1000 kHz
Bandwidth	500 kHz
Constant duty cycle	50%
Periodogram characteristics	Hamming window, 30 averages 10 samples overlap

Table 3.4. Experiment 3.1.

The theoretical and simulation results are shown together in Figure 3.16. The spectral plot shows that the value at f = 62.5 kHz has measured power density –60.4dB, a great reduction from –22dB of experiment 1.1 (shown in Figure3.4) where the two frequencies were arbitrarily chosen to be the maximum and minimum allowed.

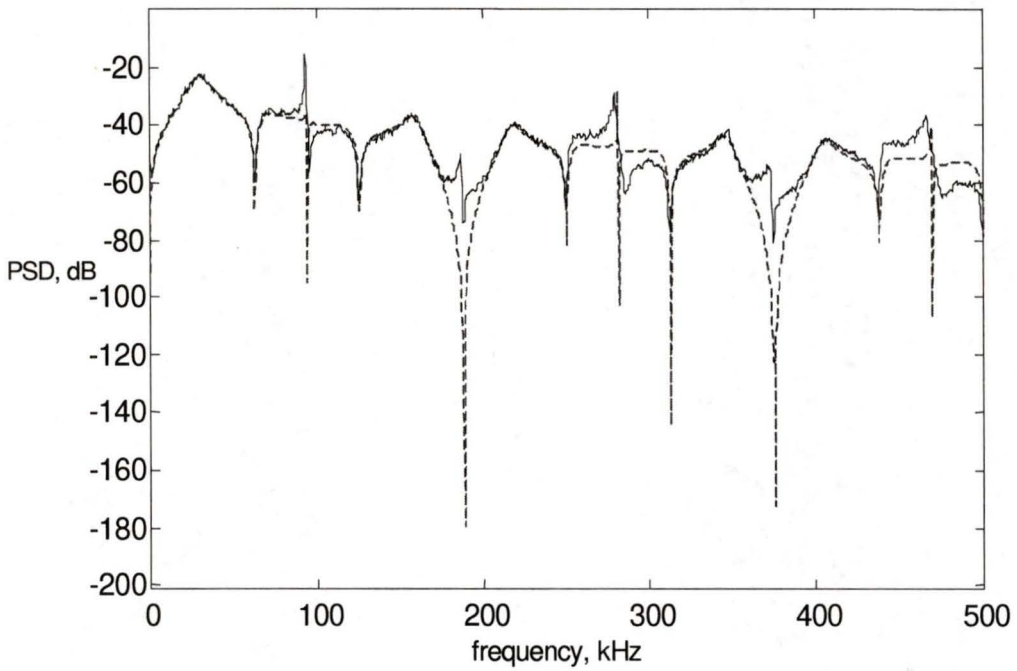

Figure 3.16. Results for experimental parameters given in Table 3.4, duty cycle 50%. Unconstrained $f_{s\min}$, $f_{s\max}$. The Dotted plot represents the theorectical result, while the solid plot represents the simulation result.

Analysis of $1 - E\{e^{j2\pi f\tau}\}$ for experiment 3.1:

We have nulled both terms in equation (3.1) at f_0 = 62.5 kHz (for 50% duty cycle) by using switching frequency 31.3 kHz , found by simply solving $E\{\sin^2(\pi f\alpha\tau)\} = 0$ (or setting the sine argument equal to an integer multiple of π). The composite angle vector

from $E\{e^{j2\pi f\tau}\}$ is simply that of the (equally weighted) sum of the two switching frequencies' complex exponential. We calculate their two angles at $f = f_0$:

$$\theta_{\max} = \frac{2f_0\pi}{f_{s\min}} = \frac{2 \times 62.5\pi}{31.3} = 3.99\pi \approx 718^\circ$$

$$\theta_{\min} = \frac{2f_0\pi}{f_{s\max}} = \frac{2 \times 62.5\pi}{93.7} = 1.33\pi \approx 240^\circ$$

The complex vectors (half unit magnitude) associated with these terms are shown in Figure 3.17. For equal probabilities the angle of the expectation is approximately 300 degrees. That angle is not good for maximizing the denominator factor $1 - E\{e^{j2\pi f\tau}\}$. Thus in the next experiment we will not only null at f_0 = 62.5 kHz, but also we will maximize $1 - E\{e^{j2\pi f\tau}\}$.

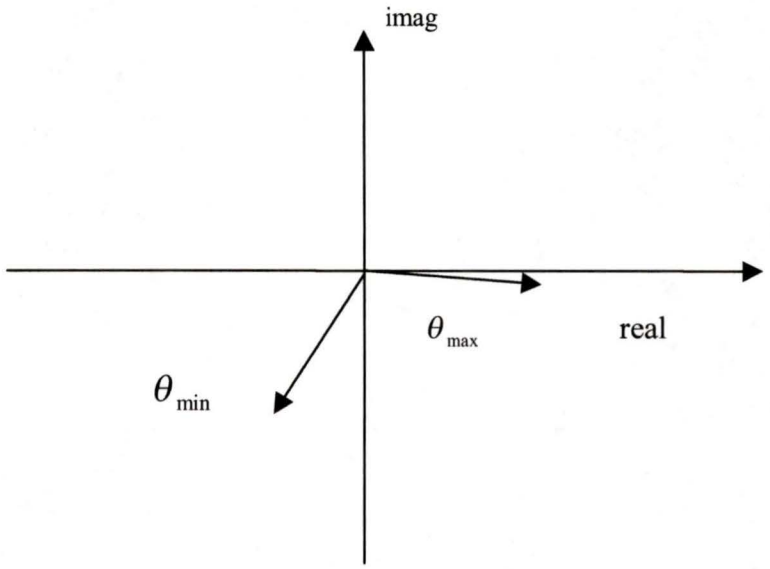

Figure 3.17. Complex exponential vectors for experiment 3.1 for f_0 = 62.5 kHz.

Experiment 3.2. Widely spread frequencies that maximize $1 - E\{e^{j2\pi f\tau}\}$

Now we choose the two switching frequencies to be 18.3 and 106.7 kHz, very much outside the [55, 75] kHz band constraint. The two angles of the exponential terms in the expectation in the denominator term $1 - E\{e^{j2\pi f\tau}\}$ at $f = f_0$ are:

$$\theta_{\max} = \frac{2f\pi}{f_{s\min}} = \frac{2 \times 62.5\pi}{18.3} = 6.83\pi \approx 1230^\circ = 360 \times 3 + 150^\circ$$

$$\theta_{\min} = \frac{2f\pi}{f_{s\max}} = \frac{2 \times 62.5\pi}{106.7} = 1.17\pi \approx 211^\circ$$

The complex vectors associated with these terms are shown in Figure 3.18. The experiment's parameters used are as in Table 3.5.

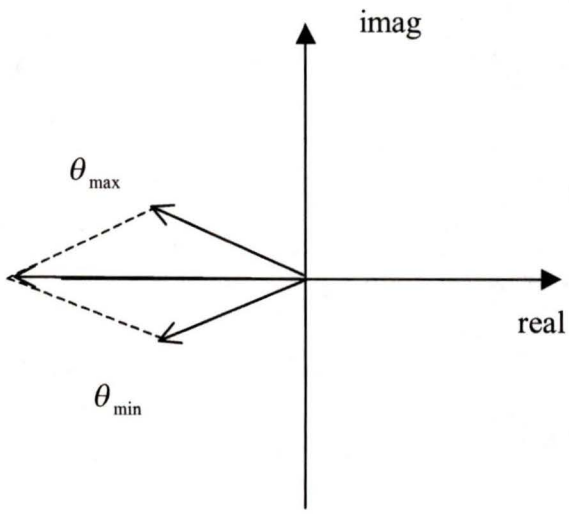

Figure 3.18. Complex exponential vectors for experiment 3.2, maximizing the denominator at the constrained mean frequency 62.5 kHz.

Switching frequencies	18.3, 106.7 kHz, equal probabilities
The Average of switching frequencies	62.5 kHz
Initial Dc voltage value	1 volt
Sampling frequency	1000 kHz
Bandwidth	500 kHz
Constant duty cycle	50%
Periodogram characteristics	Hamming window, 30 averages 10 samples overlap

Table 3.5. Experiment 3.2.

The simulation and analytical results are shown in figure 3.19. The PSD value at f_0 = 62.5 kHz is –34.6 dB, a reduction from –22dB of experiment 1.1 (shown in Figure 3.4). Although we have not placed a null at f_0 as in experiment 3.1, the reduction by design from the arbitrary selection in experiment 1.1 is good.

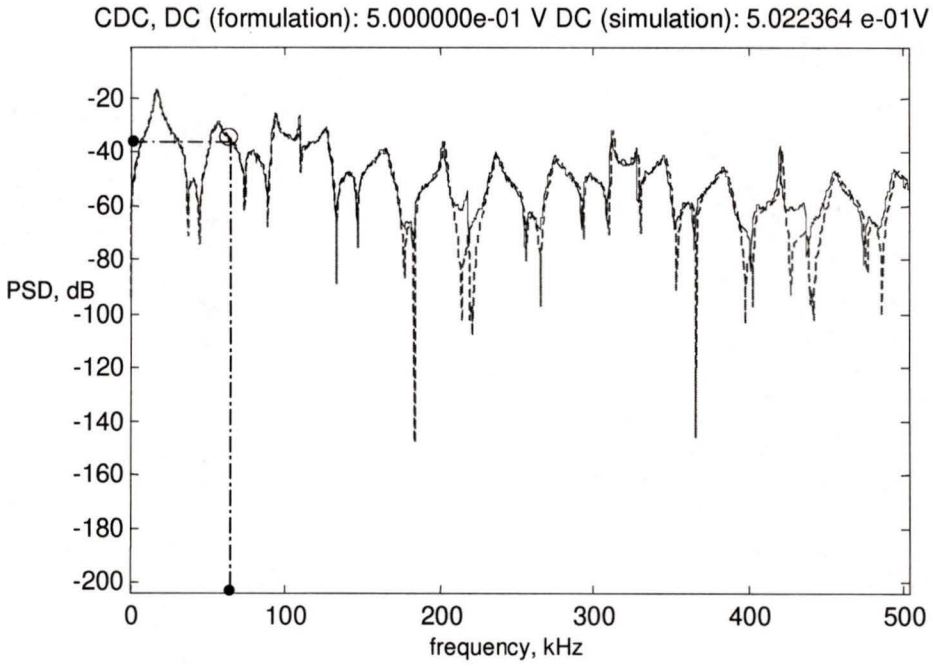

Figure 3.19. Results for parameters as given in Table 3.5, duty cycle 50%. Dotted plot represents the result from equation. Solid plot represents the result from simulation.

Experiment 3.3. Narrow frequency spread that maximizes $1 - E\{e^{j2\pi f\tau}\}$

Now let us change the switching frequencies to 26.4 and 98.6 kHz, a narrower range than those in experiment 3.2. The two angles of the equal-probable exponential terms in the expectation $E\{e^{j2\pi f\tau}\}$ at $f = f_0$ are:

$$\theta_{\max} = \frac{2f\pi}{f_{s\min}} = \frac{2 \times 62.5\pi}{26.4} = 4.73\pi \approx 852^\circ = 360 \times 2 + 132^\circ$$

$$\theta_{\min} = \frac{2f\pi}{f_{s\max}} = \frac{2 \times 62.5\pi}{98.6} = 1.27\pi \approx 228^\circ$$

and their composite vector has angle 180 degrees. The complex vectors associated with these terms are shown in Figure 3.20.

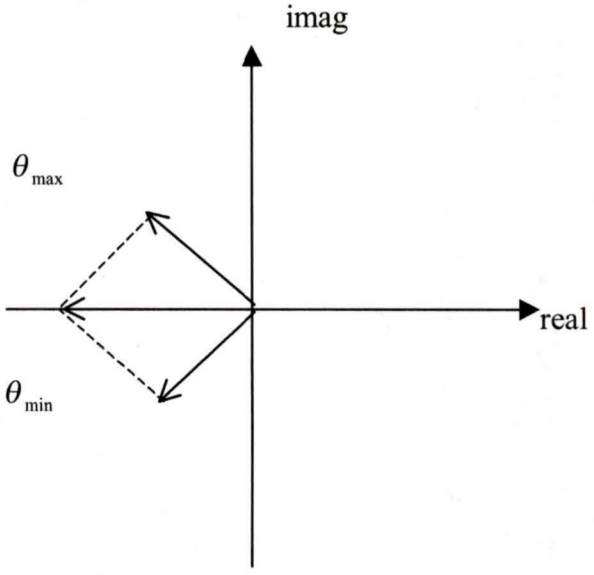

Figure 3.20. Complex vectors in $E\{e^{j2\pi f\tau}\}$ for experiment 3.3.

Our experimental parameters are given in Table 3.6, and the experimental results are shown in Figure 3.21. The PSD value at f_0 = 62.5 kHz is –42.7dB, a reduction from –22 dB of experiment 1.1.

Switching frequencies	26.4, 98.6 kHz, equal probabilities
The Average of switching frequencies	62.5 kHz
Initial Dc voltage value	1 volt
Sampling frequency	1000 kHz
Bandwidth	500 kHz
Constant duty cycle	50%
Periodogram characteristics	Hamming window, 30 averages 10 samples overlap

Table 3.6. Experiment 3.3.

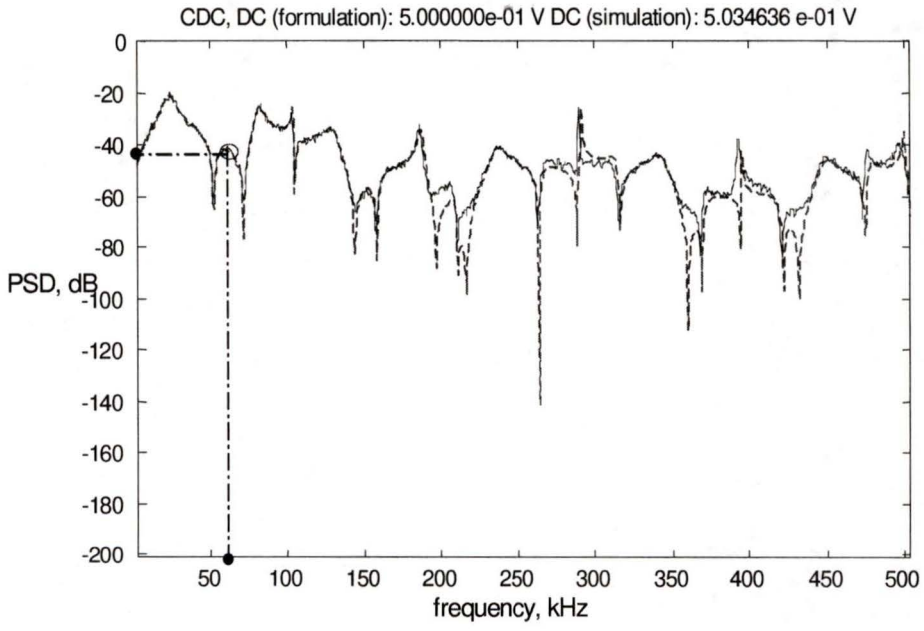

Figure 3.21. Results for parameters as given in Table 3.6, duty cycle 50%. Dotted plot represents the result from equation. Solid plot represents the result from simulation.

This result is actually better than that of experiment 3.2, where the composite vector of $E\{e^{j2\pi f\tau}\}$ is actually smaller, which should make the denominator of the effective PSD

term larger. However, the numerator factor is being ignored, and its effect between the two experiments is not clear. We are led to yet one more experiment to illustrate the expansion to more switching frequencies.

Experiment 3.4. Maximization of $1 - E\{e^{j2\pi f\tau}\}$ with 3 frequencies

Here we again try to minimize the spectrum at f_0 = 62.5 kHz with the constraint that average switching frequency is 62.5 kHz, but this time we use three switching frequencies. We have used numerical search methods to find sets of switching frequencies whose corresponding exponential phase factors compose a vector along the negative part of the real axis (shown in Figure 3.22). More than one solution can be found and we label these experiments 3.4-a and 3.4-b.

Experiment 3.4-a. Solution No. 1.

For the first of the 3-frequency solutions, we get [17, 48,122.5] kHz, and the corresponding equally likely exponential terms are shown in Figure 3.22. The three angles of exponential terms in the expectation at f_0 are:

$$\theta_1 = \frac{2f\pi}{f_{s1}} = \frac{2 \times 62.5\pi}{17} \approx 7.35\pi \approx 1323.5^\circ = 360 \times 3 + 243.5^\circ$$

$$\theta_2 = \frac{2f\pi}{f_{s2}} = \frac{2 \times 62.5\pi}{48} \approx 2.60\pi = 468.75^\circ = 360 + 108.75^\circ$$

$$\theta_3 = \frac{2f\pi}{f_{s3}} = \frac{2 \times 62.5\pi}{122.5} \approx 1.02\pi \approx 183.7^\circ$$

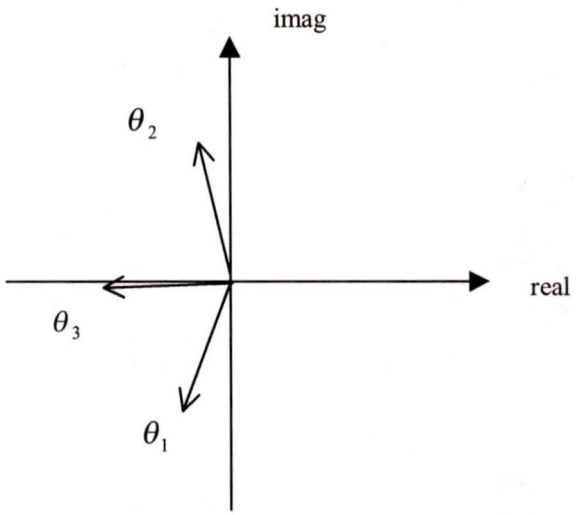

Figure 3.22. The three equally likely complex exponential vectors for experiment 3.4-a at f = 62.5 kHz.

Our experimental parameters are given in Table 3.7, and the experimental results are shown in Figure 3.23. The theoretical PSD value at f_0 = 62.5 kHz is –35.5dB, a reduction from –22dB of experiment 1.1.

Switching frequencies	17, 48 and 122.5 kHz (uniform)
The Average of switching frequencies	62.5 kHz
Initial Dc voltage value	1 volt
Sampling frequency	1000 kHz
Bandwidth	500 kHz
Constant duty cycle	50%
Periodogram characteristics	Hamming window, 30 averages 10 samples overlap

Table 3.7. Experiment 3.4-a.

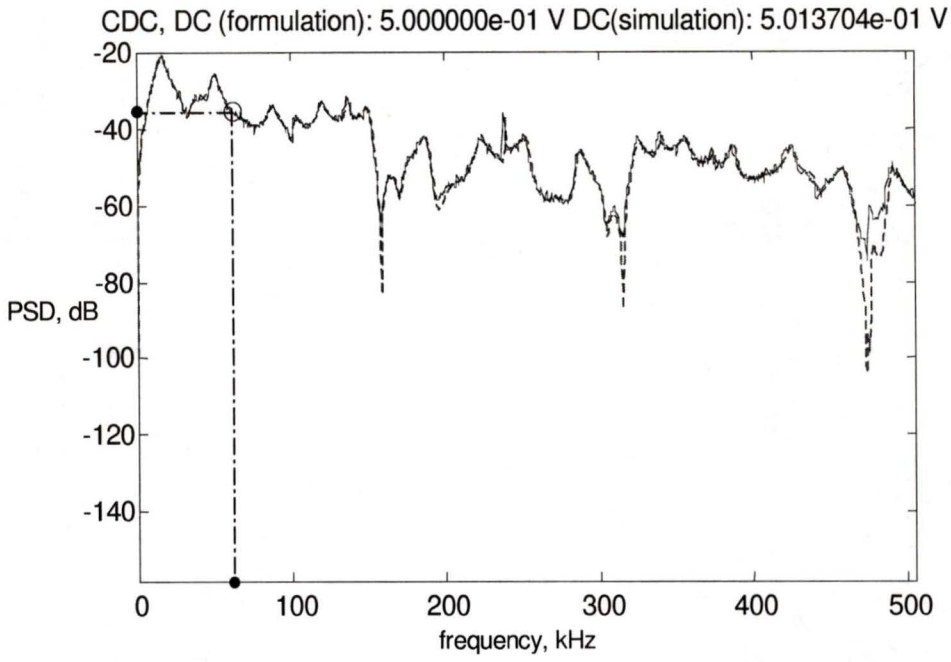

Figure 3.23. Experiment 3.4-a results for parameters as given in Table 3.7, duty cycle 50%. The dotted plot represents the theoretical result, solid plot represents the simulation.

Experiment 3.4-b. Solution No. 2.

The composite vector angle criteria also gives a solution set of switching frequencies [43.1, 56.1, 88.3] kHz. The experimental parameters used are given in Table 3.8.

Switching frequencies	43.1, 56.1 and 88.3 kHz (uniform)
The Average of switching frequencies	62.5 kHz
Initial Dc voltage value	1 volt
Sampling frequency	1000 kHz
Bandwidth	500 kHz
Constant duty cycle	50%
Periodogram characteristics	Hamming window, 30 averages 10 samples overlap

Table 3.8. Experiment 3.4-b.

The continuous power spectrum and its simulation are shown in Figure 3.24. The theoretical PSD value at f_0 = 62.5 kHz is –28dB, is not as good as that in experiment 3.4-a.

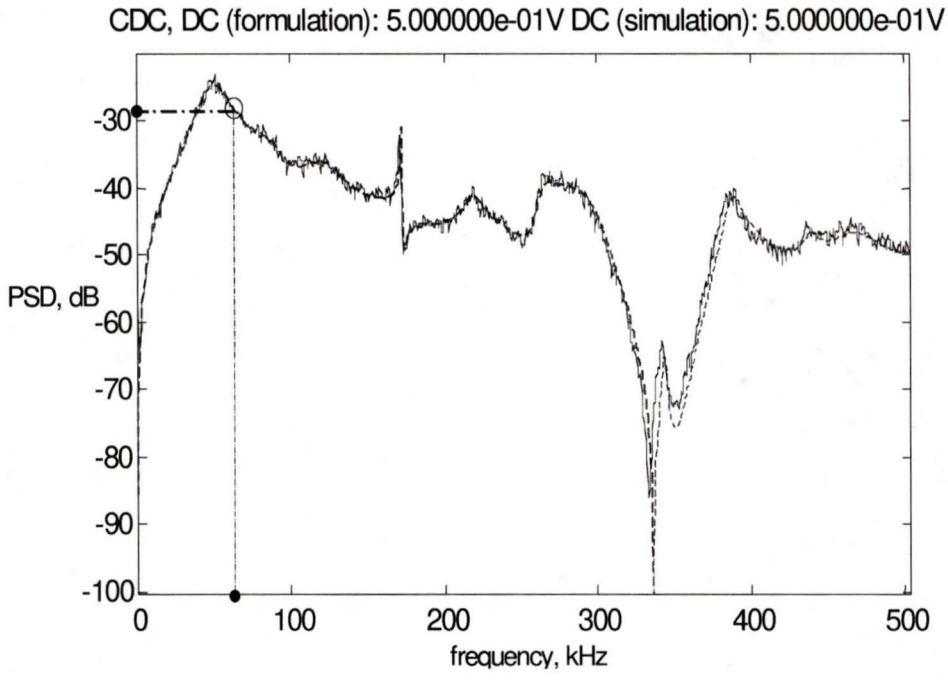

Figure 3.24. Experiment 3.4-b results for parameters as given in Table 3.8, duty cycle 50%. Dotted represents the theoretical result, solid represents the simulation.

Experiment 3.5. Maximization of $1 - E\{e^{j2\pi f\tau}\}$ with 4 frequencies

Now we use the same composite angle constraint as in experiment 3.4 to choose 4 rather than 3 switching frequencies. We choose the solution [43.6, 50.8, 67.3, 88.3] kHz. The experiment's parameters are in Table 3.9. The PSD value at f_0 = 62.5 kHz is –27.2dB. The continuous power spectrum and its simulation are shown in Figure 3.25. Again, this level is not nearly as deep as an unconstrained design null, but the density has smoothed

out considerably since 4 frequencies are used instead of just 2 or 3. Peakiness appears at higher multiples of the switching frequencies however.

Switching frequencies	43.6, 50.8, 67.3 and 88.3 kHz (uniform)
The Average of switching frequencies	62.5 kHz
Initial Dc voltage value	1 volt
Sampling frequency	1000 kHz
Bandwidth	500 kHz
Constant duty cycle	50%
Periodogram characteristics	Hamming window, 30 averages 10 samples overlap

Table 3.9. Experiment 3.5.

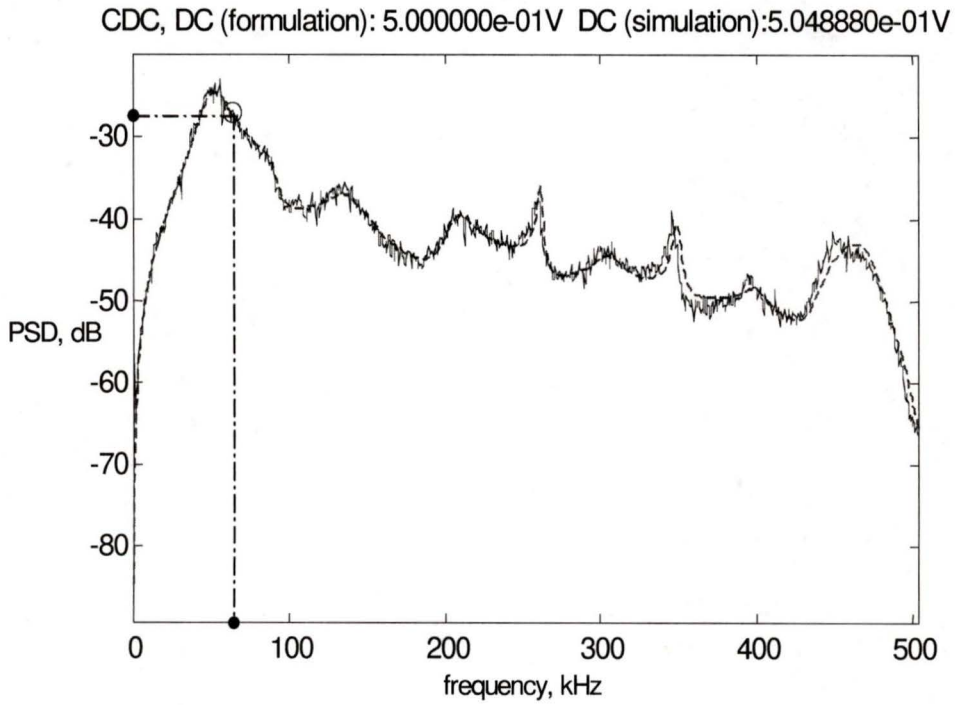

Figure 3.25. Results for parameters as given in Table 3.9, duty cycle 50%. The dotted plot represents the theoretical result while solid represents the simulation.

3.4 Conclusions

We have shown in the preceding experiments that although there are constraints, we are able to exert considerable control of the PSD at any particular frequency in the PSD of CDC RSFPWM. A spectral null may be placed almost anywhere by choosing switching frequencies that are harmonically related, however, that freedom is not allowed by narrow bandwidth constraints. When pure nulls are not allowed, we still have control over the PSD level at a particular frequency by designing the composite phase of the denominator term $1 - E\{e^{j2\pi f\tau}\}$ to cause it to maximize at the desired frequency. In most cases there are multiple solutions and we must sort through to find satisfactory switching frequency sets, as the denominator term is not the only term affecting the PSD level.

A narrow switching band constraint severely limits our flexibility in design for PSD minimization at a desired frequency; we have demonstrated what can be gained by weakening the constraints. Further minimization can of course be accomplished by full numerical search of the frequency set members. Further study along those lines is suggested and further study of the flexibility of the discrete probability distribution is also warranted, but the most important factor affecting the PSD peaks is the denominator term $1 - E\{e^{j2\pi f\tau}\}$, and its most important feature is the composite phase of the exponential terms to be averaged.

The minimum and maximum switching frequencies specify the range of control of the individual phases. Experiments 1.1 and 1.2 illustrate the minimum and maximum phases offered by the switching frequency range extremes. Phases of the terms in

$E\{e^{j2\pi f\tau}\}$ must lie in the range of the corresponding minimum and maximum switching frequencies, and therefore the composite phase of the mean of these is constrained. The phase range is a function of the chosen frequency for PSD minimization.

When the PSD is minimized at a particular frequency, the chosen switching frequencies will necessarily cause peaking to move from the positions that existed with other designs in order to minimize at the f_0 specified. That effect may be undesirable, and more research on total spectral control is warranted.

Chapter 4

Spectrum Design Problems for a Band of Frequencies

4.1 Introduction

We have studied the power spectrum design problems for a single frequency in chapter 3 for the CDC RSFPWM, however it is sometimes important to suppress the PSD over a band of frequencies. In this chapter we will focus on the spectrum design problems for a band of frequencies.

We will analyze the power spectrum equation (3.1) of CDC RSFPWM from another point of view in order to get a further understanding of the reason for peaks in the PSD and to find a reasonable way to control the PSD level over a band of frequencies. Again we will put our emphasis on the denominator in the second term of equation (3.1) since we have found that to be the cause of peaks in the PSD. We factor the frequency domain expression into a "modulating function" and a "carrier function", and by design of the modulating function we effect suppression of the PSD over a band of frequencies. In our analysis we set a constraint on the switching intervals by forcing them "evenly spaced".

4.2 Theory and Formulation

Both the first term and the numerator of the second term in the PSD expression in equation (3.1) have maxima at multiple frequencies, however the maxima are at most unity, aside from the constant scale factors in the PSD expression. The only significant factor in the location and value of PSD peaks is the denominator expression $1-E\left\{e^{j2\pi f\tau}\right\}$, which derives from the infinite geometric series of delay factors in the auto-correlation function of the whole RSFPWM waveform.

We write the denominator of the second major and complex term in the PSD expression (3.1) as follows:

$$\begin{aligned} D(f) &= 1-E\left\{e^{j2\pi f\tau}\right\} \\ &= 1-\sum_{k=1}^{N_\tau} p_k e^{j2\pi\frac{f}{f_{s_k}}} \\ &= 1-\sum_{k=1}^{N_\tau} p_k e^{j2\pi f m_k / f_{LCM}} \\ &= 1-\sum_{k=1}^{N_\tau} p_k z^{m_k}, \quad z = e^{j2\pi f / f_{LCM}} \end{aligned} \tag{4.1}$$

where p_k are the corresponding probabilities, $f_{LCM} = m_k f_{s_k}$, $k = 1,2,...,N_\tau$, is the least common multiple of the switching frequencies f_{s_k}, the m_k are associated integers and N_τ is the number of switching frequencies. Note that the highest power of z is m_1 considering that the switching frequencies increase from f_{s_1} to $f_{s_{N_\tau}}$, therefore m_1 is the number of z-plane poles for this 2nd PSD term. The frequency f_{LCM} acts much like a sampling frequency in sampled data, and the other frequencies can be considered to be normalized by f_{LCM}, so that the unit circle in the complex z-plane marks the domain of f

between dc and f_{LCM}. We can also think of the zeros of $D(f)$ as poles of the function (3.1). There is a pole at z = 1, but the frequency response of $1/D(f)$ is periodic and shows an infinite response magnitude at all harmonics of f_{LCM}. At those frequencies, the expression for harmonic power and not density must be used.

Now we further focus on the second term of (4.1), which if nearly unity causes a peak in the spectrum. We will determine how to predict and control such peaks. Thus,

$$E\left\{e^{j2\pi f\tau}\right\} = \sum_{k=1}^{N_\tau} p_k e^{j2\pi(fm_k/f_{LCM})} = e^{j2\pi f(\bar{m}/f_{LCM})} \sum_{k=1}^{N_\tau} p_k e^{j2\pi f(m_k-\bar{m})/f_{LCM}}$$

Suppose

$$R(f) = \sum_{k=1}^{N_\tau} p_k e^{j2\pi f(m_k-\bar{m})/f_{LCM}}$$

then

$$E\left\{e^{j2\pi f\tau}\right\} = e^{j2\pi f(\bar{m}/f_{LCM})} R(f) \tag{4.2}$$

where we have used $\bar{m}$ to express the average of the m_k. In the last form of the expression (4.2), the summation $R(f)$ can be interpreted as an envelope function on the exponential "carrier" function, $e^{j2\pi f(\bar{m}/f_{LCM})}$ having $\dfrac{\bar{m}}{f_{LCM}}$ cycles per Hz. What is required to cause (4.2) to approach unity is to have the phase of the "carrier" be a multiple of 2π and the (real) envelope to be nearly unity. This term can exactly equal 1 only when f = K f_{LCM} for some integer K, but it is nearly unity whenever f is an integer multiple of $f_{LCM}/\bar{m}$, the average switching frequency, and the envelope magnitude is near unity. So next we will find frequencies for which the envelope magnitude is near unity.

Now we can see that the frequency envelope function is essentially the Discrete Fourier Transform of the "window" sequence of probability weights in "time" (switching intervals or periods): $w(p) = (p_1, p_2, ..., p_{N_\tau})$ where the "time delay" factors in the frequency domain are

$$e^{j2\pi f(m_i - \bar{m})/f_{LCM}} = e^{j2\pi f((m_1 - \bar{m}) - (i-1)\Delta_m)/f_{LCM}},$$

and we have assumed that the spacing Δ_m / f_{LCM} between switching intervals is constant, as shown in Figure 4.1.

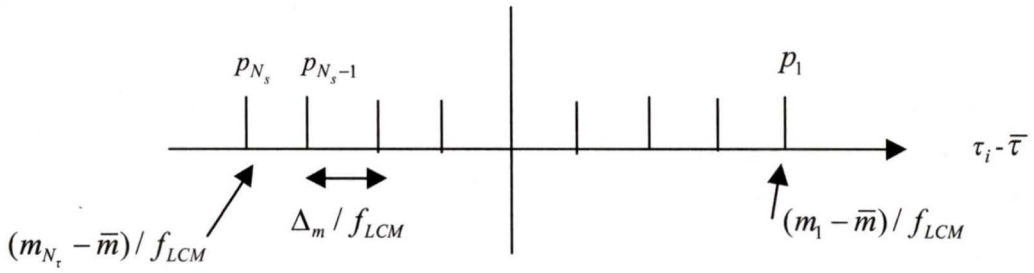

Figure 4.1. Switching intervals relocated to the origin by subtracting the mean $\bar{m}/f_{LCM}$ and weighted by their probabilities.

The DFT of the vector of probabilities spaced as shown in Figure 4.1 is an even and real function of f as long as the probabilities are symmetric around the origin. That means if we want a real envelope, then switching intervals should have probabilities symmetric around the (or generally around $\bar{m}$). We momentarily choose a real envelope for simplicity of analysis and to further our understanding. In this case the envelope can be written:

$$R(f)=\sum_{k=1}^{N_\tau} p_k e^{j2\pi f((m_1-\bar{m})-(k-1)\Delta_m)/f_{LCM}}$$

$$=\begin{cases} 2\sum_{k=1}^{N_\tau/2} p_k \cos(2\pi f((m_1-\bar{m})-(k-1)\Delta_m)/f_{LCM}),\ N_\tau \text{ even} \\ p_{(N_\tau+1)/2}+2\sum_{k=1}^{(N_\tau-1)/2} p_k \cos(2\pi f((m_1-\bar{m})-(k-1)\Delta_m)/f_{LCM}),\ N_\tau \text{ odd} \end{cases} \quad (4.3)$$

When the distribution of probabilities is not symmetrical or when the spacing of switching intervals is not constant, the envelope is complex but still has a magnitude similar to that in (4.3). It also has a phase that is significant in determining at which frequencies (4.2) is close to 1+j0. In general, we could write:

$$R(f)=R_{ev}(f)+jR_{od}(f) \quad (4.4)$$

and

$$\frac{1}{D(f)}=\frac{1}{1-\left(e^{j2\pi f(\bar{m}/f_{LCM})}R(f)\right)} \quad (4.5)$$

Here we are mostly concerned with $e^{j2\pi f(\bar{m}/f_L)}R(f)$ approaching 1+j0.

The general criterion for a nearly zero $D(f)$ is that $|R(f)|\cong 1$ and the phase angle of $e^{j2\pi f(\bar{m}/f_{LCM})}$ is the negative of the angle of $R(f)$.

Clearly it is easiest to design with symmetric probabilities and equally spaced switching intervals τ. Considering Figure 4.1, we find that the frequency domain envelope has the same properties as any DFT of a window function. The envelope for equally distributed and weighted samples in time is the discrete equivalent of a sinc function, but the sinc function will be periodic with period in frequency equal to the reciprocal of the spacing Δ_m / f_{LCM}. That is, there will be a peak in the envelope every multiple of f_{LCM}/Δ_m Hz.

4.3 Analysis and Results with Constraints on Switching Frequency Range

Now we set limitations on the switching frequencies and let $f_{s_{\min}}$ be the lower bound and $f_{s_{\max}}$ be the upper bound. These yield the following inequalities for any f_s:

$$
\begin{aligned}
f_{s_{\min}} \le \frac{f_{LCM}}{m_{\max}} \le f_s \le \frac{f_{LCM}}{m_{\min}} \le f_{s_{\max}} \\
m_{\min} \ge \frac{f_{LCM}}{f_{s_{\max}}} \\
m_{\max} \le \frac{f_{LCM}}{f_{s_{\min}}}
\end{aligned}
\tag{4.6}
$$

where m_k are integer and have greatest common divisor (GCD) = 1.

Since it is hard to control the least common multiple of a set of switching frequencies, we will not choose switching frequencies directly. On the contrary we will first choose a proper f_{LCM}, which is large enough. Then we will choose a proper set of integers m_k within the constraints according to equation (4.6) and calculate the corresponding switching frequencies. It is obvious that we need to note the following points:

a) We should not choose a prime number as the f_{LCM}.

b) When we choose the m_k we should make sure that their greatest common divisor is equal to 1. This constraint adds to those in expression (4.6).

c) The resulting switching frequencies are probably not integers.

d) Due to c), in practicality due to round-off error the true least common multiple of the resulting switching frequencies is probably not exactly f_{LCM}. That implies that the process is not revertible. The true f_{LCM} will be far larger than the selected f_{LCM} in general, and that is actually desirable. However the design f_{LCM} gives a PSD that is a very good approximation of the resulting PSD.

4.3.1 Experiment 4.1: Three Switching Frequencies

Suppose we choose f_{LCM}=3300 kHz, and the upper and lower bound of switching frequencies are 50 and 75 kHz respectively. So the range of multiples according to expression (4.6) is $44 \le m \le 66$. Suppose we choose to use three switching frequencies corresponding to the uniformly distributed set of $1/f_{LCM}$ multiples [53 56 59] for the intervals. The corresponding switching frequencies are [55.9 58.9 62.3] kHz (accurate to one decimal place). According to (4.2) and (4.3) the envelope and carrier are:

$$\left[1+2\cos(2\pi\frac{\Delta_m}{f_{LCM}}f)\right]=\left[1+2\cos(2\pi\frac{3}{3300}f)\right]=\left[1+2\cos(2\pi\cdot 3\cdot\frac{f}{3300})\right]$$
$$\frac{1}{3}e^{j2\pi fm_2/f_{LCM}}=\frac{1}{3}e^{j2\pi f\cdot 56/3300}=\frac{1}{3}e^{j2\pi\cdot 56\frac{f}{3300}} \qquad (4.7)$$

Figures 4.2 and 4.3 show the magnitude of the envelope $R(f)$ and the magnitude of the $1/D(f)$ respectively. From Figure 4.2 we find that there are Δ_m=3 cycles during the range [0, f_{LCM}], and in Figure 4.3 we see that there are $\bar{m}=m_2$=56 peaks in [0, f_{LCM}]. Also these peaks appear periodically at the multiples of $\frac{f_{LCM}}{\bar{m}}$=58.9 kHz. As with our previous analysis, when the "carrier" $e^{j2\pi f\bar{m}/f_{LCM}}$ has real value=1 at the same frequency

as large envelope magnitude, there are values of the denominator $D(f)$ that are nearly zero. We can observe that there appear sharp peaks around 58.9 kHz and 1119 kHz in Figure 4.3 just as predicted.

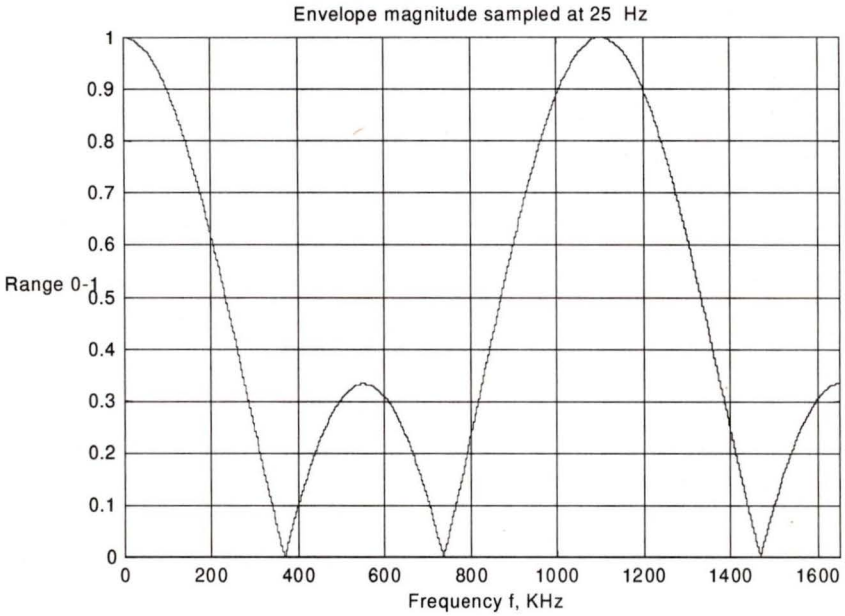

Figure 4.2. The magnitude of the envelope. $0 \le f \le \frac{f_{LCM}}{2}$.

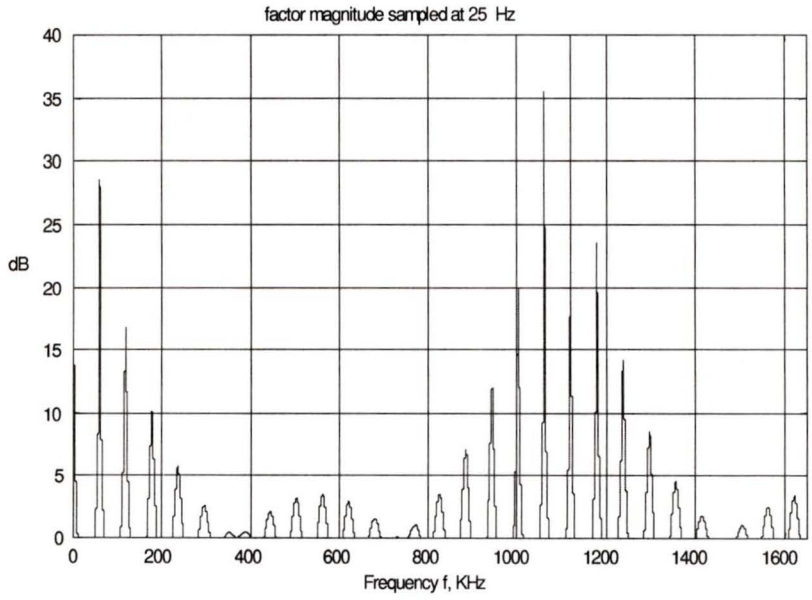

Figure 4.3. The magnitude of $1/D(f)$ $0 \le f \le \frac{f_{LCM}}{2}$.

The simulation with parameters shown in Table 4.1 resulting in Figure 4.4 verifies our analysis, since we can find these peaks appearing at the same frequencies and approximate magnitude gains as predicted by $1/D(f)$ in Figure 4.3.

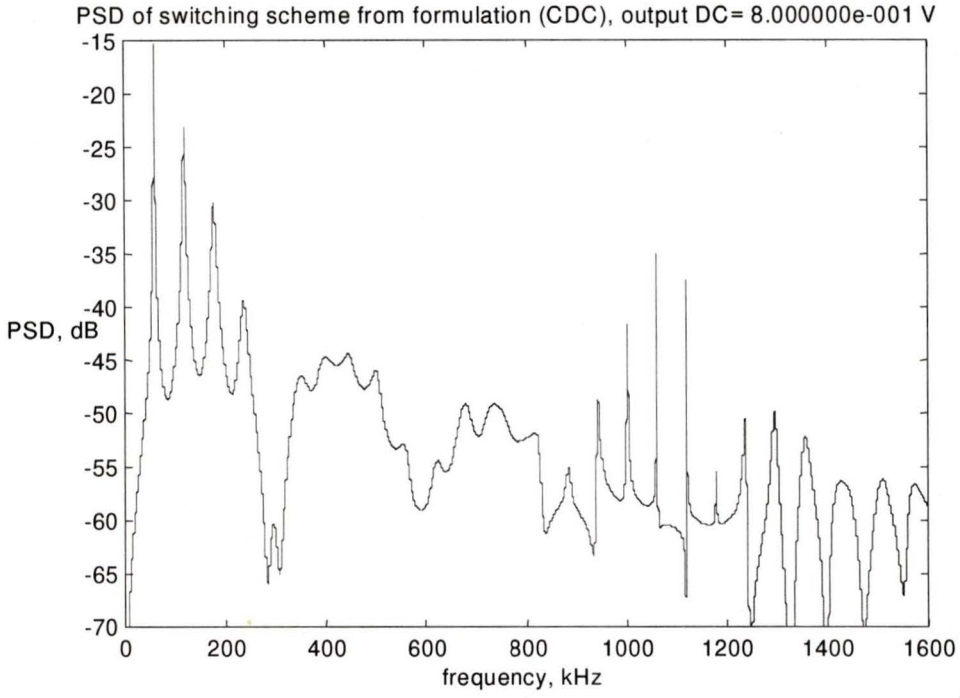

Figure 4.4. The PSD results. Duty cycle=80%.

The multiples m of switching frequencies	m_1=53, m_2=56, and m_3=59
The switching frequencies	$f_{s_1} = 55.9, f_{s_2} = 58.9, f_{s_3} = 62.3$ kHz
The probabilities of switching frequencies	$p_1 = p_2 = p_3 = \frac{1}{3}$
Δ_m	$m_2 - m_1 = m_3 - m_2 = 3$
Least common multiple f_{LCM}	3300 kHz
Duty cycle	80%

Table 4.1 Parameters for Figures 4.2, 4.3 and 4.4.

Now we widen the range of switching frequencies' intervals by using Δ_m=5. The magnitudes of envelope and $1/D(f)$ are shown in Figure 4.5 and Figure 4.6 respectively. The parameters are shown in Table 4.2.

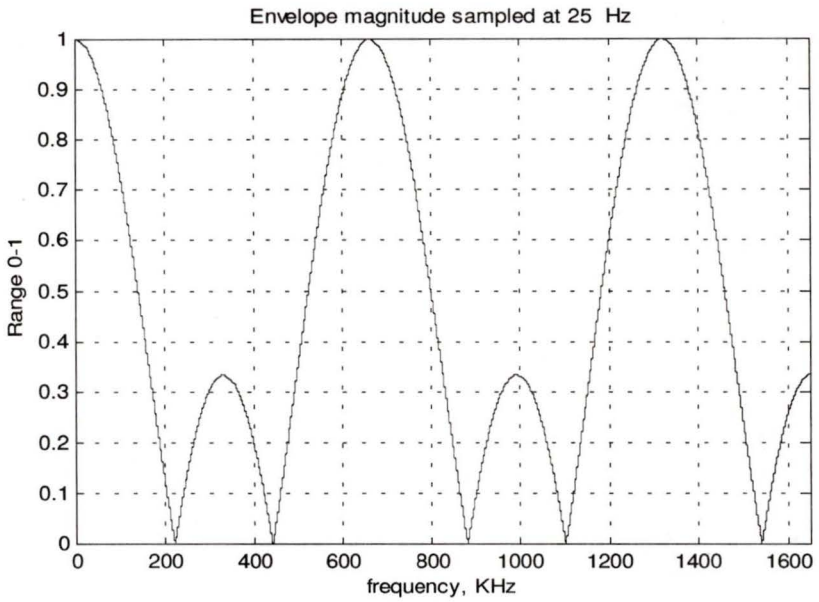

Figure 4.5. The magnitude of the envelope. $0 \le f \le \frac{f_{LCM}}{2}$.

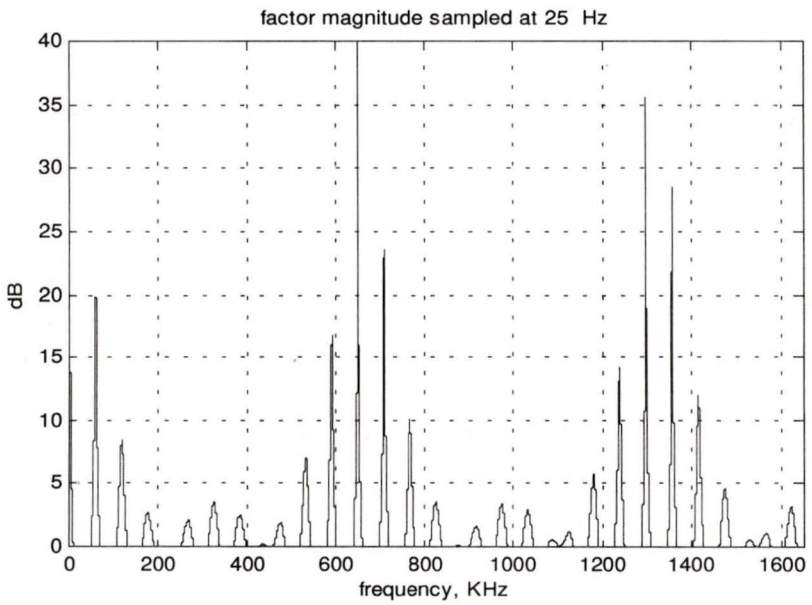

Figure 4.6. The magnitude of $1/D(f)$, $0 \le f \le \frac{f_{LCM}}{2}$.

In Figure 4.5 we notice there are Δ_m=5 cycles over the range [0, f_{LCM}]. In Figure 4.6 we can observe the sharp $1/D(f)$ peaks around the frequencies for which $|R(f)|$ peaks appeared in Figure 4.5, in agreement with our analysis. Figure 4.7 is the corresponding simulation PSD using parameters of Table 4.2.

The multiples m of switching frequencies	m_1=51, m_2=56, and m_3=61
The switching frequencies	$f_{s_1} = 54.1, f_{s_2} = 58.9, f_{s_3} = 64.7$ kHz
The possibilities of switching frequencies	$p_1 = p_2 = p_3 = \frac{1}{3}$
Δ_m	$m_2 - m_1 = m_3 - m_2 = 5$
Least common multiple f_{LCM}	3300 kHz
Duty cycle	80%

Table 4.2. Parameters for Figures 4.5, 4.6 and 4.7.

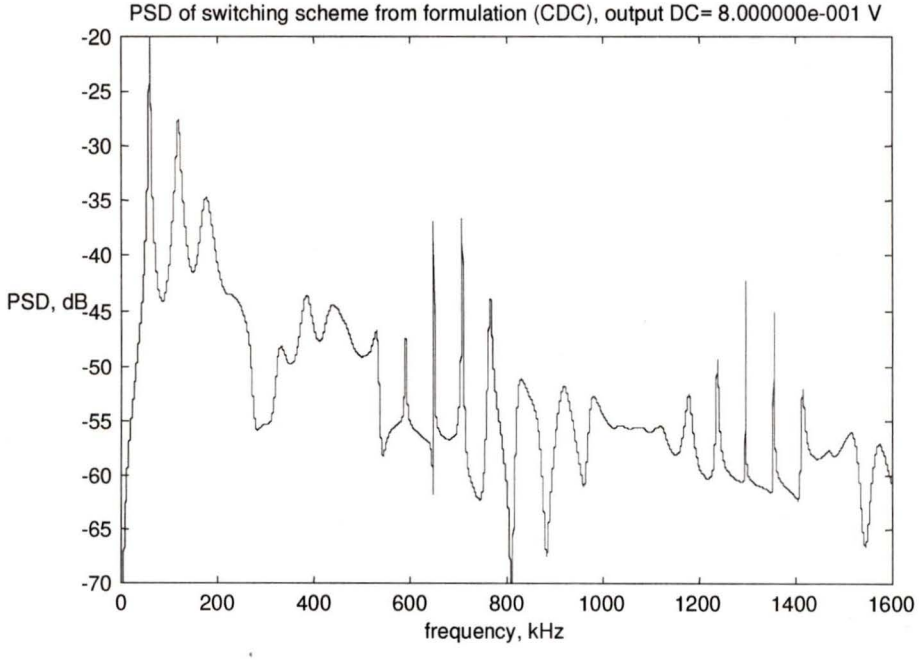

Figure 4.7. The PSD results. Duty cycle=80%.

Now we narrow the range of these switching intervals to Δ_m=1. The magnitudes of envelope and $1/D(f)$ are shown in Figure 4.8 and Figure 4.9 respectively for simulation parameters shown in Table 4.3, and the simulation result is shown in Figure 4.10. Again these figures are consistent with our analysis.

The multiples m of switching frequencies	m_1=55, m_2=56, and m_3=57
The switching frequencies	$f_{s_1} = 57.9, f_{s_2} = 58.9, f_{s_3} = 60$ kHz
The Probabilities of switching frequencies	$p_1 = p_2 = p_3 = \frac{1}{3}$
Δ_m	$m_2 - m_1 = m_3 - m_2 = 1$
Least common multiple f_{LCM}	3300 kHz
Duty cycle	80%

Table 4.3. Parameters for Figures 4.8, 4.9 and 4.10.

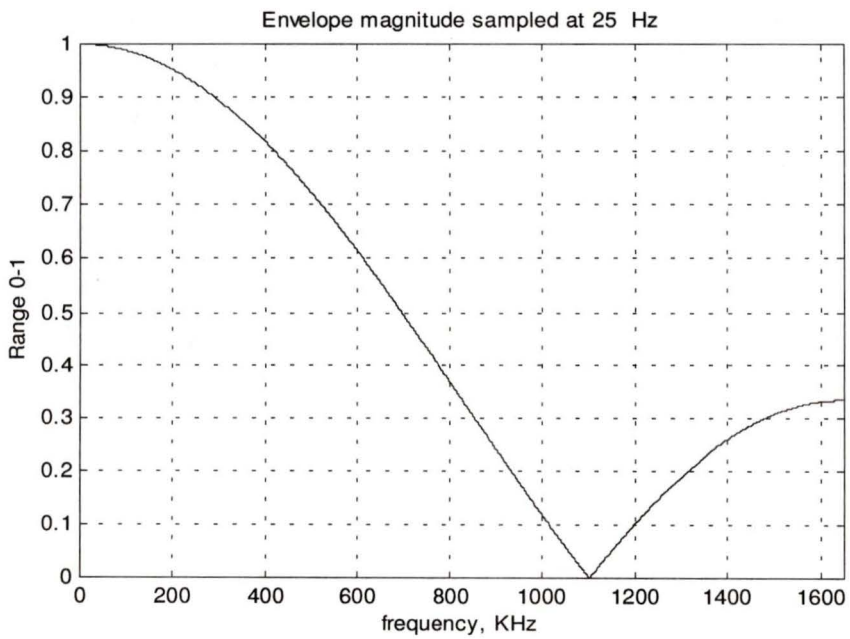

Figure 4.8. The magnitude of the envelope, $0 \le f \le \frac{f_{LCM}}{2}$.

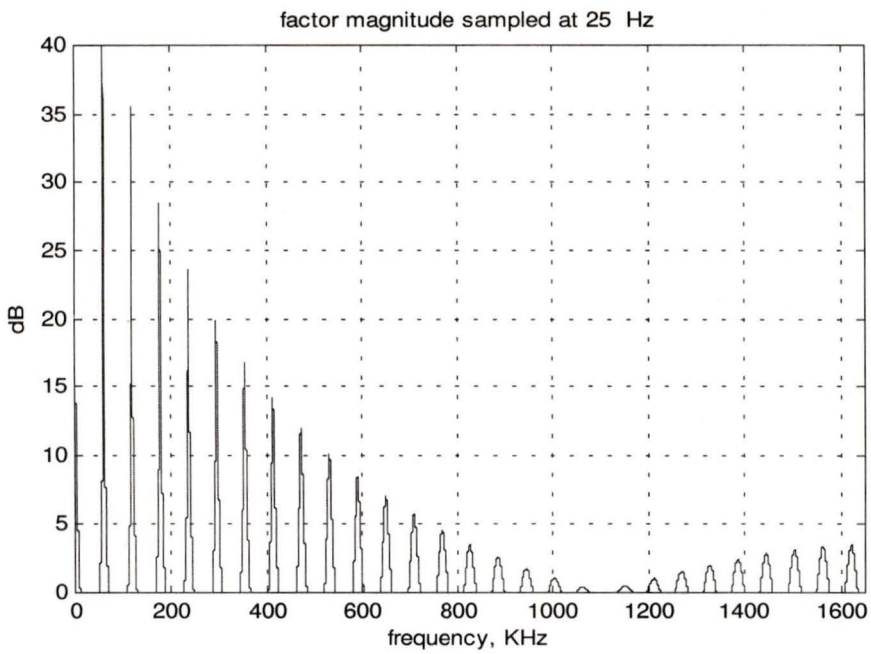

Figure 4.9. The magnitude of $1/D(f)$ $0 \le f \le \frac{f_{LCM}}{2}$.

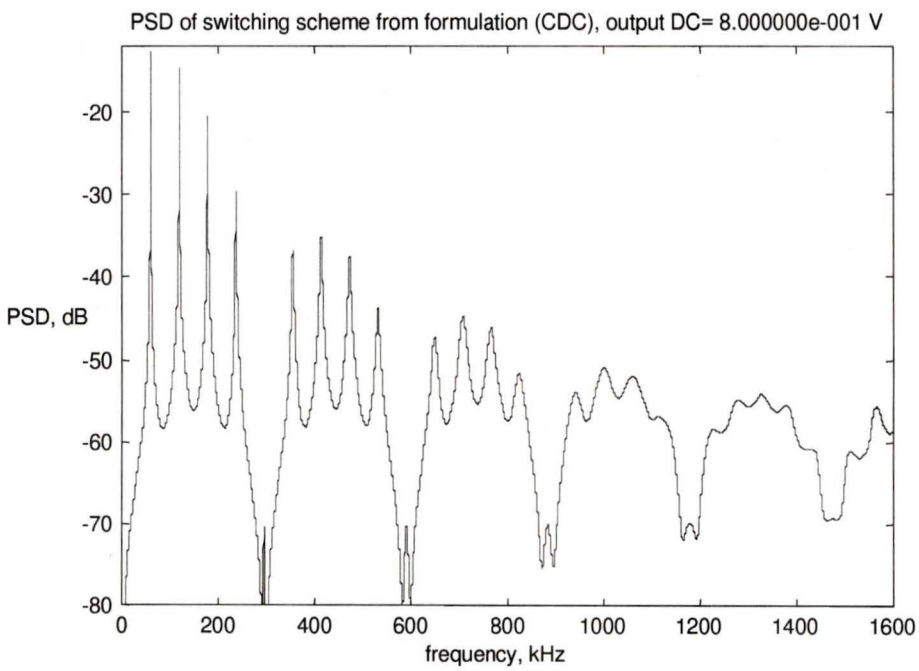

Figure 4.10. The PSD results. Duty cycle=80%.

4.3.2 Experiment 4.2: Five Switching Frequencies

According to equations (4.2) and (4.3) the envelope and carrier are:

$$R(f) = \left[1 + 2\cos(2\pi \frac{\Delta_m}{f_{LCM}} f) + 2\cos(2\pi \frac{2\Delta_m}{f_{LCM}} f)\right]$$
$$= \left[1 + 2\cos(2\pi \frac{3}{3300} f) + 2\cos(2\pi \frac{6}{3300} f)\right] \quad (4.8)$$
$$\frac{1}{5} e^{j2\pi f m_3 / f_{LCM}} = \frac{1}{5} e^{j2\pi f \cdot 56/3300} = \frac{1}{5} e^{j2\pi \cdot 56 \frac{f}{3300}}, \quad m_3 = \overline{m}$$

The magnitude of the envelope and the magnitude of the $1/D(f)$ are shown in Figure 4.11 and Figure 4.12 respectively. From Figure 4.11 we find that there are Δ_m=3 cycles during the range [0, f_{LCM}]. Also these peaks appear periodically at the multiples of $\frac{f_{LCM}}{\overline{m}}$=58.9 kHz. We can observe that there appear sharp peaks around 58.9 kHz in Figure 4.13 as we expect. The parameters are shown in Table 4.4. The total PSD is shown in Figure 4.13.

The multiples m of switching frequencies	m_1=50, m_2=53, m_3=56, m_4=59, m_5=62
The switching frequencies	$f_{s_1} = 53.2, f_{s_2} = 55.9, f_{s_3} = 58.9,$ $f_{s_4} = 62.3, f_{s_5} = 66$ kHz
The probabilities of switching frequencies	$p_1 = p_2 = p_3 = p_4 = p_5 = \frac{1}{5}$
Δ_m	3
Least common multiple f_{LCM}	3300 kHz
Duty cycle	80%

Table 4.4. Parameters for Figures 4.11, 4.12 and 4.13.

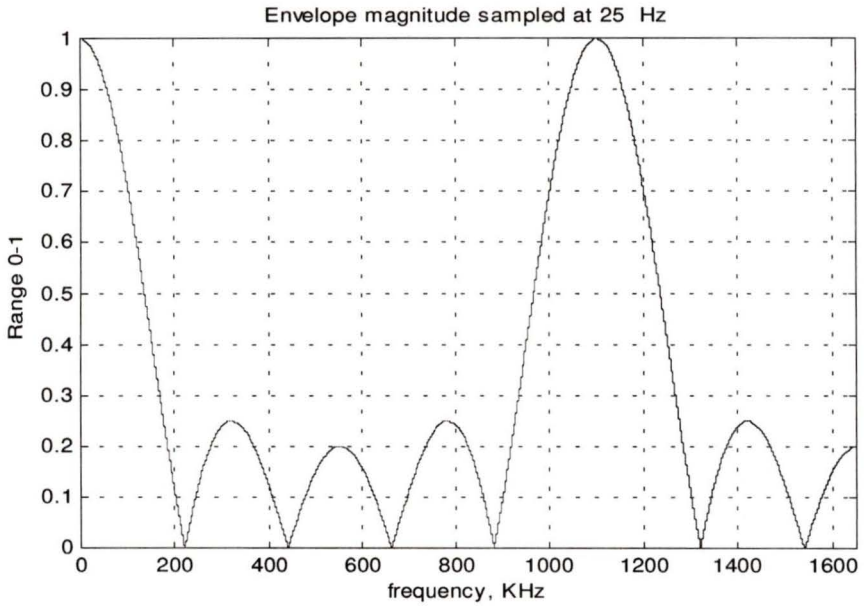

Figure 4.11. Envelope $R(f)$ for equal probabilities, $\Delta_m = 3$ (indicating 3 cycles over [0, f_{LCM}]).

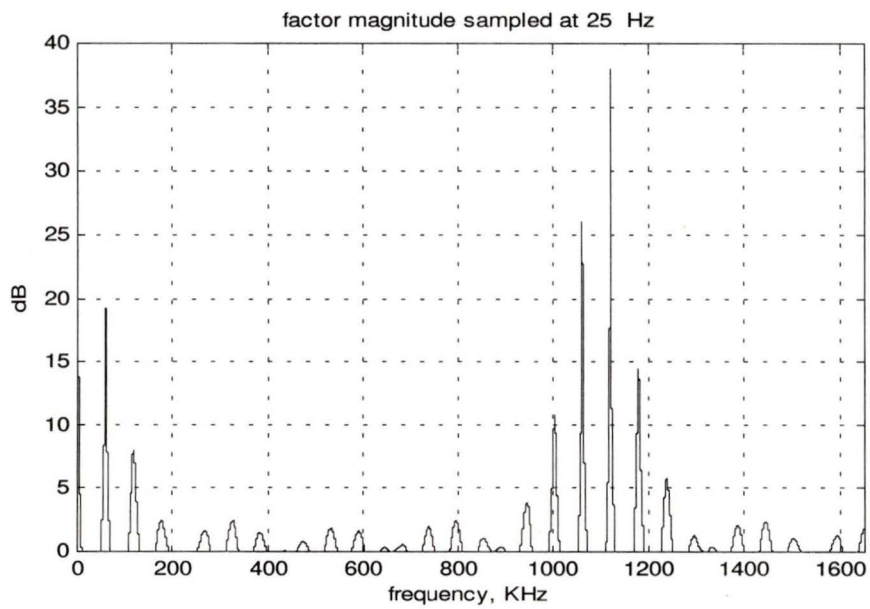

Figure 4.12. The magnitude of $1/D(f)$, $0 \le f \le \frac{f_{LCM}}{2}$.

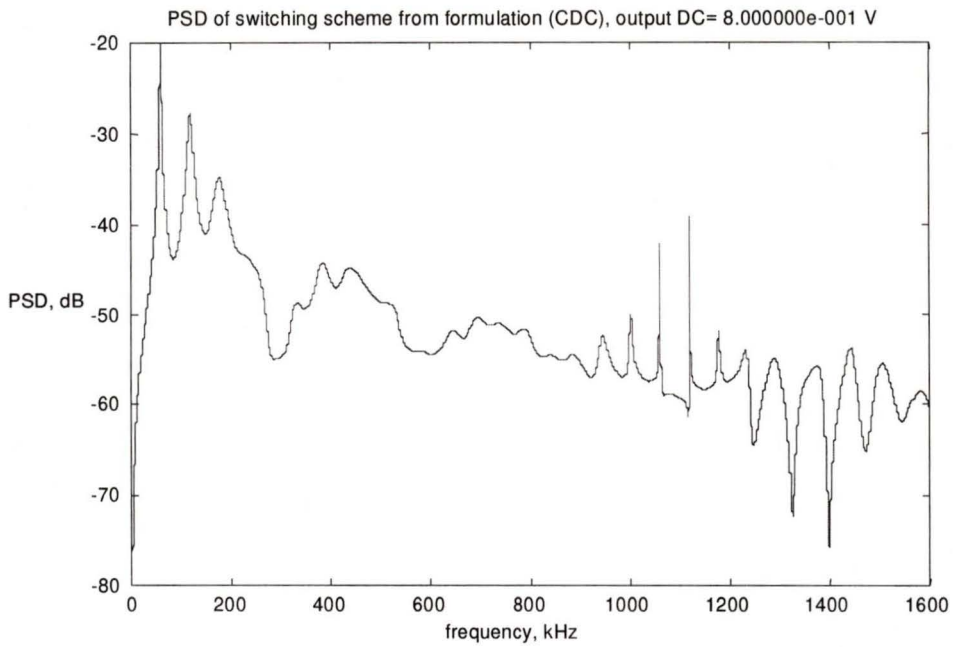

Figure 4.13. The PSD results. Duty cycle=80%.

4.3.3 Experiment 4.3: The Effects of the Switching Frequencies' Probabilities on the Poles

Suppose we use the same parameters as shown in Table 4.1 except that we change the probabilities into p_1=0.15, p_2=0.7 and p_3=0.15. The magnitude of the envelope is shown in Figure 4.14 and the magnitude of $1/D(f)$ is shown in Figure 4.15. These results show that tapering the probabilities produces worse results because $R(f)$ is near unity over a broader range of f. The best we can do is to use uniform probability weights, producing the narrow sinx/x $R(f)$, dropping to zero quickly. Although the side-lobes may be broader for the sinc function, they are small with respect to unity and do not cause $D(f)$ to be near zero.

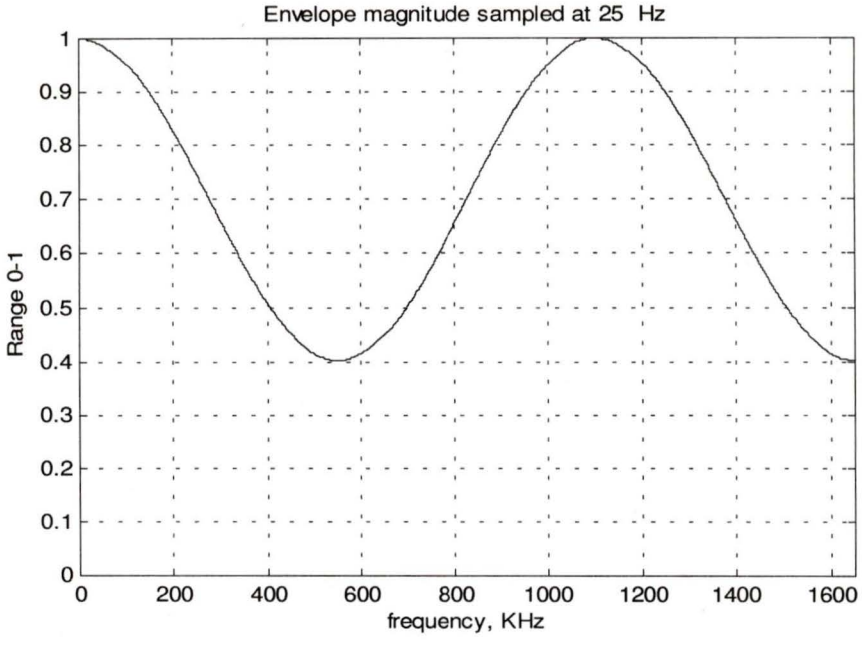

Figure 4.14. The magnitude of the envelope. $0 \le f \le \frac{f_{LCM}}{2}$.

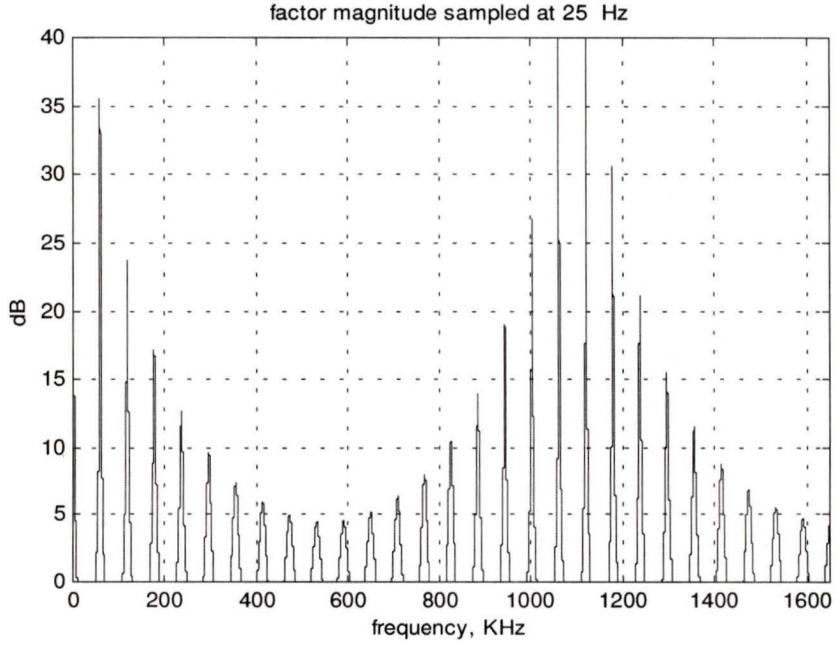

Figure 4.15. The magnitude of $1/D(f)$ $0 \le f \le \frac{f_{LCM}}{2}$.

4.3.4 Conclusions

From the above three experiments, we find that:

a) By comparing Figure 4.2, Figure 4.5 and Figure 4.8 we know that the wider the range of switching intervals, the narrower the envelope $|R(f)|$, thus $D(f) \approx 0$ over a narrower f range.

b) The smaller the spacing between switching intervals, the greater the distance between repetitions of the modes of the envelope.

c) The higher the average frequency $\frac{1}{\bar{\tau}}$, the more often the envelope is sampled creating more peaks in $1/D(f)$ at harmonics.

d) The equally weighted window gives the narrowest envelope (sinc-function) $R(f)$, dropping quickly down to zero but having large but insignificant "side-lobes", whereas rounded windows give slower drops to zero and produce more large peaks in $1/D(f)$. We conclude that the uniform distribution gives the best results.

4.4 Design Examples and Results Without Constraints on Switching Frequencies

In this section, we attempt to minimize the PSD over a specified band of frequencies without any constraints on the switching frequencies. For this propose we make assumptions as follows:

a) There are a finite number of switching frequencies; we choose three and five.

b) The interval probability distribution is symmetric and uniform such as $p_1 = p_3 = p_2 = 1/3$.

c) The spacing of the switching frequencies' multiples is constant, Δ_m.

d) There are no maximum and minimum constraints on the switching frequencies.

Equation (4.2) for three switching frequencies becomes:

$$E\{e^{j2\pi f\tau}\} = \sum_{k=1}^{3} p_k \exp(j2\pi f m_k / f_{LCM}) = \frac{1}{3} e^{j2\pi f m_2 / f_{LCM}} [1 + 2\cos(2\pi f(m_2 - m_1) / f_{LCM})]$$
$$= \frac{1}{3} e^{j2\pi f m_2 / f_{LCM}} \left[1 + 2\cos(2\pi \frac{\Delta_m}{f_{LCM}} f)\right] \tag{4.9}$$

In this case it can be seen that over the normalizing range $[0, f_{LCM})$ there are $\bar{m} = m_2$ cycles of the carrier factor $e^{j2\pi f\bar{m}/f_{LCM}}$, and this is modulated by an envelope $R(f) = \left[1 + 2\cos(2\pi \frac{\Delta_m}{f_{LCM}} f)\right]$ which has $(m_2 - m_1) = \Delta_m$ cycles over the range $[0, f_{LCM})$.

When the carrier $e^{j2\pi f m_2 / f_{LCM}}$ has large real magnitude that is coincident with large envelope magnitude, there will be peaks appearing at the PSD.

Consider that we want to minimize peaks in the power spectrum over a band of frequencies whose average frequency is f_0. We can achieve this goal by controlling the peak location of the cosine term in equation (4.9). We let the cosine term be zero at the average frequency of the band so we have:

$$2\pi f_0 \frac{\Delta_m}{f_{LCM}} = \frac{\pi}{2} + k\pi \qquad k = 0,1,2\cdots \tag{4.10}$$

From (4.10) we can get:

$$f_0 = \frac{f_{LCM}}{2\Delta_m}\left(\frac{1}{2} + k\right) \tag{4.11}$$

Example 1

Suppose we design the lobe of $R(f)$ at DC ($k=0$), $f_{LCM}=1300kHz$, $\Delta_m=5$ and m_1=20. They obviously satisfy equation (4.11). From this set of data, we get the switching frequencies:

$$f_{s_1}=43.3kHz,\quad f_{s_2}=52kHz,\quad f_{s_3}=65kHz$$

The corresponding power spectrum is shown in Figure 4.16. It is obvious that the PSD around f_0 = 65kHz resulting from the design set of switching frequencies is reduced dramatically from that of the arbitrary chosen switching frequencies.

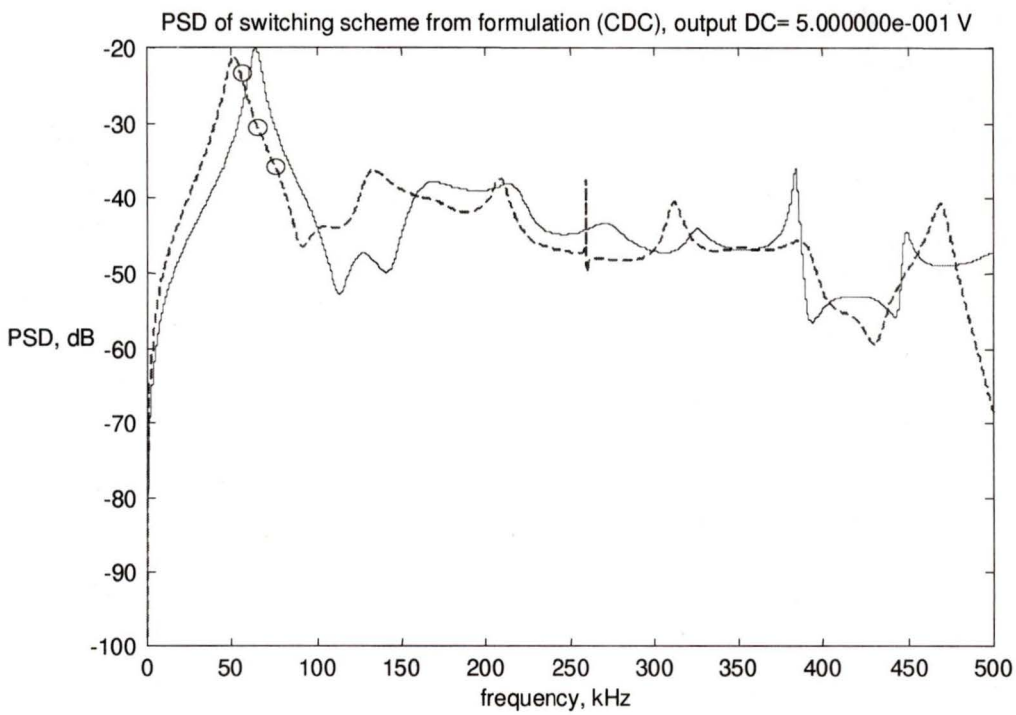

Figure 4.16. Duty cycle 50%. Dotted trace: PSD with design switching frequencies [43.3 52 65] kHz. Solid trace: PSD with arbitrary switching frequencies [55 65 75] kHz. The second circle marks f_0 = 65 kHz.

Example 2

Now suppose we want to control the band around 2*65=130kHz and again design for the dc ($k=0$) lobe of $R(f)$ and $\Delta_m = 5$ and m_1=40. From equation (4.11) we can calculate $f_{LCM} = 2600kHz$. Then we get the set of switching frequencies $f_{s_1} = 52kHz$ $f_{s_2} = 57.7kHz$ and $f_{s_3} = 65kHz$. The corresponding power spectrum is shown in Figure 4.17. The results of the design vs. arbitrary frequencies are that the original PSD around the desired frequency is a peak but after design it becomes a valley.

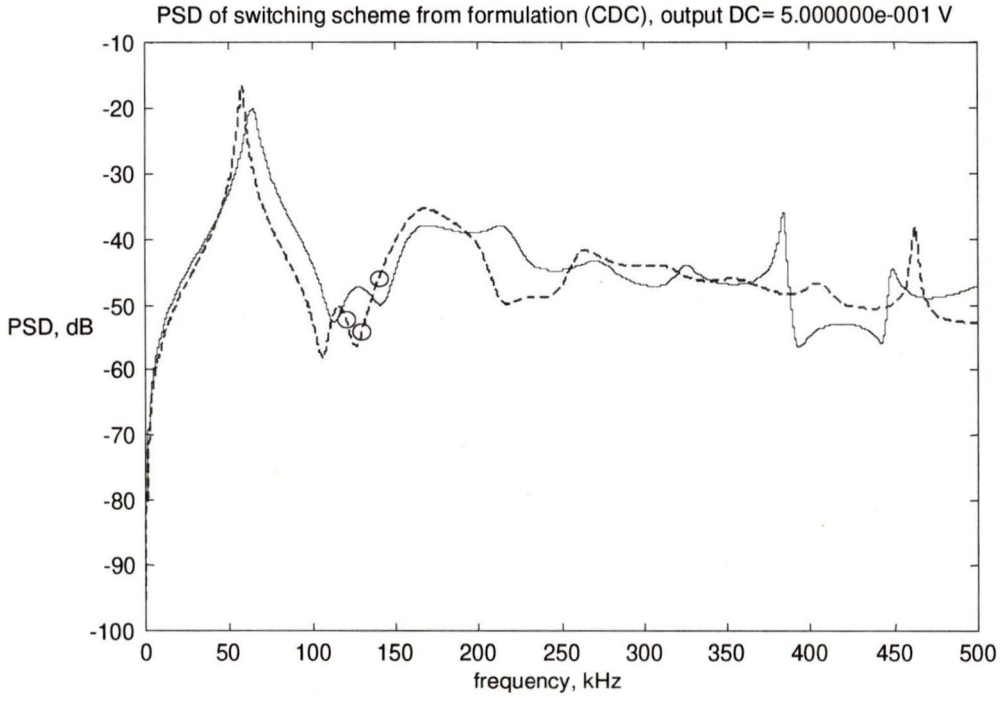

Figure 4.17. Duty cycle 50%. Dotted trace: PSD with design switching frequencies [52 57.8 65] kHz. Solid trace: PSD with arbitrary switching frequencies [55 65 75] kHz. The second circle marks the location of f_0 = 130 kHz.

Example 3

In this example we will utilize five switching frequencies. Five switching frequencies should narrow the $R(f)$ lobe and DC, reducing peaks at multiples of $\frac{f_{LCM}}{\bar{m}}$ compared to three switching frequencies. We give the formulation of equation (4.2) for 5 switching frequencies; wherein

$$\sum_{k=1}^{5} p_k \exp(j2\pi f m_k / f_L) = \frac{1}{5} e^{j2\pi f m_3 / f_L} \left[1 + 2\cos(2\pi \frac{\Delta_f}{f_L} f) + 2\cos(2\pi \frac{2\Delta_f}{f_L} f) \right] = \frac{1}{5} e^{j2\pi f m_3 / f_L} \times R(f) \tag{4.12}$$

The analysis is similar to that of three switching frequencies. Again we try to control the power spectrum over a band of frequencies whose average frequency equals to $f_0 = 65kHz$. We choose $\Delta_m = 5$ and m_1=15. We again achieve our goal by minimizing the magnitude of envelope $R(f)$, and utilizing equation (4.11) we get $f_{LCM} = 1300kHz$. The switching frequencies set is:

$$f_{s_1} = 37.1kHz \; f_{s_2} = 43.3kHz \; f_{s_3} = 52kHz \; f_{s_4} = 65kHz \; f_{s_5} = 86.7kHz$$

The corresponding power spectrum is shown in Figure 4.18. Compared to example 1's result shown in Figure 4.16, we see that there is a dramatic reduction in the 1st peak around 65 kHz. One reason can be seen clearly by comparing equations (4.9) and (4.12) where the scalars are 1/3 and 1/5, respectively. Also the f-domain envelope falls to zero more quickly since a broader band of frequencies is used. The PSD over a band of frequencies centered at 65 kHz is much flattened compared to that before design.

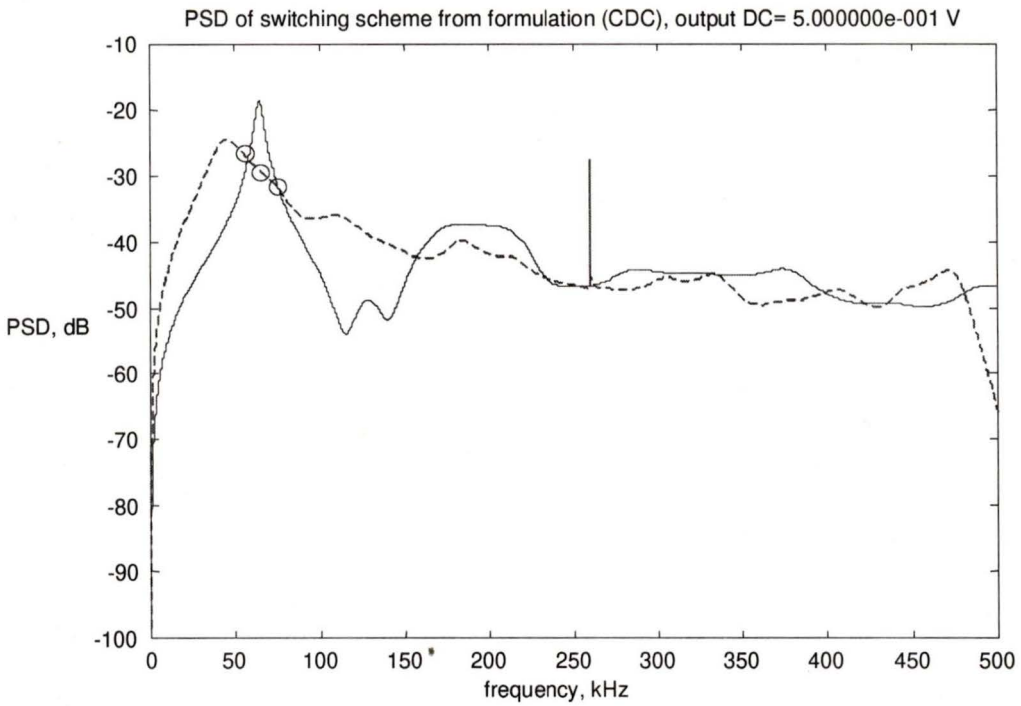

Figure 4.18. Duty cycle 50%. Dotted trace: PSD with design switching frequencies [37.1 43.3 52 65 86.7] kHz. Solid trace: PSD with arbitrary switching frequencies [55 60 65 70 75] kHz. The second circle marks f_0 = 65 kHz.

4.5 Summary

In this chapter we have studied the control of PSD over a band of frequencies. We have factored the denominator of equation (3.1) into a carrier and envelope $R(f)$ just as with amplitude modulation, and we can suppress the PSD by manipulating the $R(f)$. Under the assumption of equally spaced switching intervals with a uniform distribution, we have carried out some design examples without constraints on the switching frequencies and

show that the resulting PSDs are satisfactory. In addition, we find from example 3 that as a broader band and more switching frequencies are used, a better PSD results.

If we want to confine the switching frequencies within a band $F_1 \le f_s \le F_2$, from (4.11) with $k = 0$ and three switching frequencies we have

$$F_1 \le \frac{f_{LCM}}{m_1 + 2\Delta_m} < \frac{f_{LCM}}{m_1} \le F_2 \quad and \quad 4f_0 = \frac{f_{LCM}}{\Delta_m} \tag{4.13}$$

Equation (4.13) shows that it is hard to find a proper set of switching frequencies when f_0 is small.

Chapter 5

Application of Optimization Methods in Spectrum Design

5.1 Introduction

We have studied the power spectrum design problems for a single frequency in chapter 3 and show that proper selection of the switching frequencies and their PDF gives control over the output noise PSD at a specified frequency, whose value we want to minimize. Also we have developed some design procedures for choosing the switching frequencies in order to minimize the spectral power at the specified frequency. These procedures are only partially effective under practical constraints on the switching frequencies. Since the related equation is so complex that there is no an obvious way for designing the switching frequencies under all the constraints, we must resort to numerical optimization methods to perform the desired minimization at a general specified frequency f_0.

In this chapter we first use numerical optimization methods to find a constrained set of equally likely switching frequencies that will minimize the spectral power at a specified frequency. We formulate the minimization problem, apply optimization

methods and then give experiment results. Further we will study the use of numerical optimization methods to find a constrained set of switching frequencies and their probabilities to minimize the spectral power at a specified frequency.

All our methods and experiments are based on the CDC RSFPWM scheme. The switching frequencies resulting from the experiments are constrained to lie between 55 kHz and 75 kHz, and the average switching frequency is constrained to equal 62.5 kHz. We select the specified frequency $f_0 = 62.5$ kHz to minimize because it is presumed to be the most difficult frequency to minimize under the above constraints.

5.2 Optimum Selection of Switching Frequencies

In this section we use conventional optimization methods to find the best set of a specified number of switching frequencies having equal probabilities which will minimize the spectral power at a specified frequency. We first formulate the objective function and then give simulation results.

5.2.1 Formulation with Constraints on Switching Frequencies Range

We have known that the power spectrum expression with constant duty cycle α_0 at the specified frequency f_0 (see chapter 2 equation (2.7)) is as follows:

$$F(\tau_1, \tau_2, \cdots, \tau_m) = \frac{A_0^2}{\bar{\tau}\pi^2 f_0^2}\left(E\{\sin^2(\pi\alpha_0 f_0 \tau)\} + 2\,\mathrm{Re}\left[\frac{\left(E\{\sin(\pi\alpha_0 f_0 \tau)e^{j\pi f_0 \tau}\}\right)^2}{1 - E\{e^{j2\pi f_0 \tau}\}}\right]\right) \quad (5.1)$$

We can formulate our minimizing problem from above equation as follow:

$$F(\tau_1,\tau_2,\cdots,\tau_m)=\frac{{A_0}^2}{\sum_{i=1}^{m}p_i\tau_i\pi^2{f_0}^2}\left(\sum_{i=1}^{m}p_i\sin^2(\pi\alpha_0 f_0\tau_i)+2\,\mathrm{Re}\left[\frac{\left(\sum_{i=1}^{m}p_i\sin(\pi\alpha_0 f_0\tau_i)e^{j\pi f_0\tau_i}\right)^2}{1-\sum_{i=1}^{m}p_i e^{j2\pi f_0\tau_i}}\right]\right)$$

$$=\frac{A_0^2}{\sum_{i=1}^{m}p_i\tau_i\pi^2 f_0^2}\left(\sum_{i=1}^{m}p_i\sin^2(\pi\alpha_0 f_0\tau_i)+2\mathrm{Re}\left[\frac{\left(\sum_{i=1}^{m}p_i\sin(\pi\alpha_0 f_0\tau_i)\cos(\pi f_0\tau_i)+j\sum_{i=1}^{m}p_i\sin(\pi\alpha_0 f_0\tau_i)\sin(\pi f_0\tau_i)\right)^2}{(1-\sum_{i=1}^{m}p_i\cos(2\pi f_0\tau_i))-j\sum_{i=1}^{m}p_i\sin(2\pi f_0\tau_i)}\right]\right)$$

$$=\frac{2{A_0}^2}{\sum_{i=1}^{m}p_i\tau_i\pi^2{f_0}^2}\left(\begin{array}{l}\left(\left(\sum_{i=1}^{m}p_i\{\sin(\pi\alpha_0 f_0\tau_i)\cos(\pi f_0\tau_i)\}\right)^2-\left(\sum_{i=1}^{m}p_i\{\sin(\pi\alpha_0 f_0\tau_i)\sin(\pi f_0\tau_i)\}\right)^2\right)\\ \qquad\times\left(1-\sum_{i=1}^{m}p_i\{\cos(2\pi f_0\tau_i)\}\right)\\ -2\left(\sum_{i=1}^{m}p_i\{\sin(\pi\alpha_0 f_0\tau_i)\cos(\pi f_0\tau_i)\}\right)\left(\sum_{i=1}^{m}p_i\{\sin(\pi\alpha_0 f_0\tau_i)\sin(\pi f_0\tau_i)\}\right)\\ \qquad\times\left(\sum_{i=1}^{m}p_i\{\sin(2\pi f_0\tau_i)\}\right)\end{array}\right)$$

$$/\left[\left(1-\sum_{i=1}^{m}p_i\cos(2\pi f_0\tau_i)\right)^2+\left(\sum_{i=1}^{m}p_i\sin(2\pi f_0\tau_i)\right)^2\right]+\frac{{A_0}^2}{\sum_{i=1}^{m}p_i\tau_i\pi^2{f_0}^2}\sum_{i=1}^{m}p_i\sin^2(\pi\alpha_0 f_0\tau_i)$$

(5.2)

Subject to the switching frequency range constraints and usual probability constraints:

$$\frac{1}{75}\le\tau_1,\tau_2,\cdots,\tau_m\le\frac{1}{55},\ p_1,p_2,\cdots,p_m\ge 0,\ \sum_{i=1}^{m}p_i=1 \tag{5.3}$$

Obviously it is a constrained problem to minimize. We first try to transfer it into unconstrained problem then we will use optimization methods to minimize it. We let

$\tau_i = \frac{\frac{1}{55} + \frac{1}{75} e^{-2x_i}}{1 + e^{-2x_i}}$ $(-\infty \le x_i \le +\infty)$ and $\bar{p}_i^2 = p_i$ then we can get the unconstrained problem objective function as equation (B.3) derived in Appendix B.

In section 5.2.2 we assume that the selection probabilities of the switching frequencies and therefore the switching intervals are equally likely. Under these conditions, we can simplify the objective function as (B.4) shown in Appendix B. Also we derive the gradient of the objective function in Appendix B.

5.2.2 Application Experiments and Results

Since we have the objective function and its gradient (see Appendix B) we can apply the conventional optimization method. We use the Davidon-Fletcher-Powell (DFP) and Broyden-Fletcher-Goldfarb-Shanno (BFGS) methods on the objective function. Without the loss of generality in all our experiments we use the constant duty cycle α_0=0.5 and the specified frequency $f_0 = 62.5$ kHz. The following two experiments differ only in starting points for the solution vector $\boldsymbol{x}$. Results are summarized in Table 5.1. Comparison of the two methods follows.

Experiment 5.1

We first use the DFP method and the initial point x0 = [1 -1 -0.4 0 0.4], and tolerance epsilon = 1e-30.

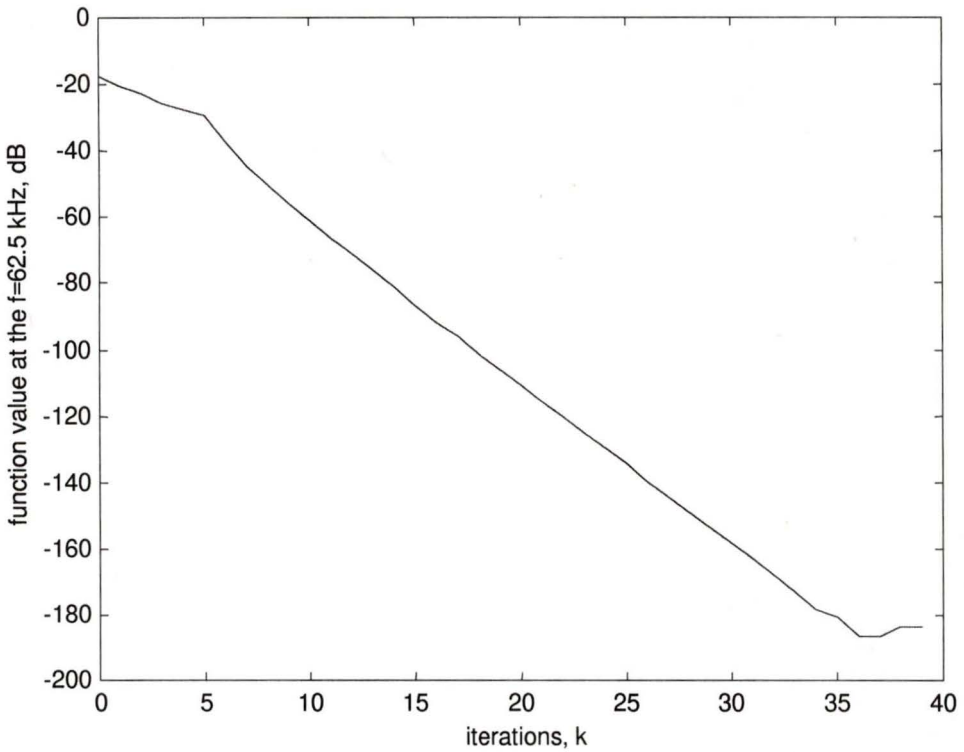

Figure 5.1. The result of using DFP method to minimize the objective function.

The solution we get is $x = \begin{bmatrix} -10.00081911377267 \\ -15.06467751479793 \\ -31.88936384654919 \\ -36.60269164957070 \\ -28.43440749228487 \end{bmatrix}$, and this corresponds to switching frequencies that are all 75 kHz. The optimization result is shown in Figure 5.1. From Figure 5.1, we can see the value of the objective function reduces from –17.7 dB to –180 dB and 39 iterations are required.

Then as a comparison we use the BFGS method starting with the same initial point x0. The result is shown in Figure 5.2. The required iteration is 34. And it takes less time and fewer flops to obtain the same result as with the DFP method.

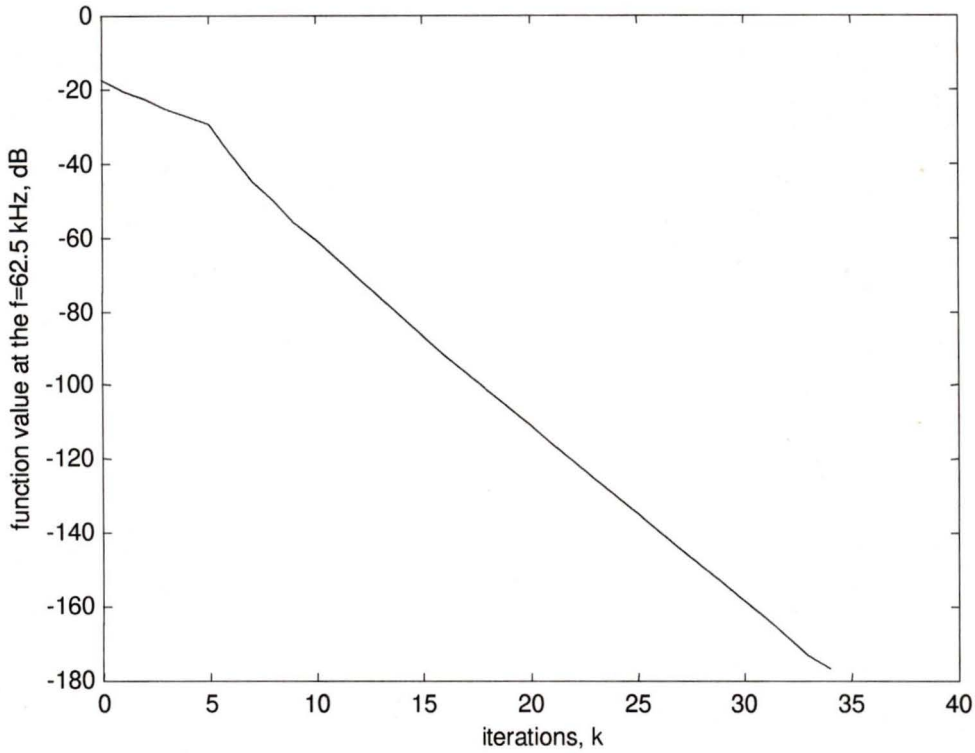

Figure 5.2. The result of using BFGS method to minimize the objective function.

Experiment 5.2

Here We use another initial point x0 = [0.8 -0.8 0 0.1 -0.1], and tolerance epsilon = 1e-30. First using the DFP method we obtain the optimization result shown in Figure 5.3. We can see that the value of the objective function reduces from –17.7 dB to –183.6 dB and 37 iterations are required. The solution we get is $x = \begin{bmatrix} -17.15372324131126 \\ -8.632359877412405 \\ -24.63369478054297 \\ -25.67311406786958 \\ -23.08727051129367 \end{bmatrix}$, and this corresponds to frequencies that are all 75 kHz.

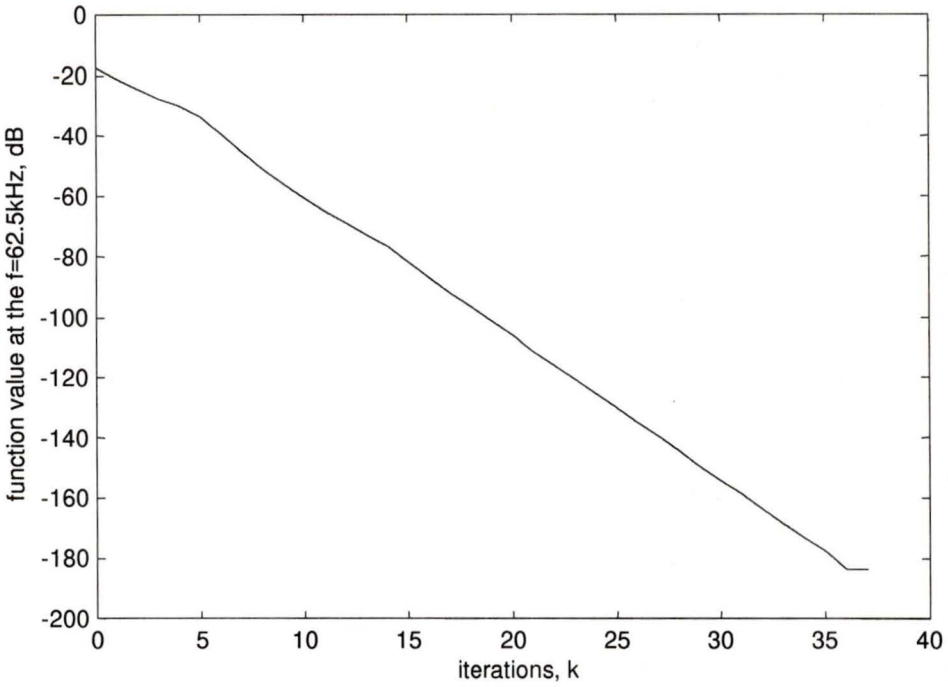

Figure 5.3. The result of using DFP method to minimize the objective function.

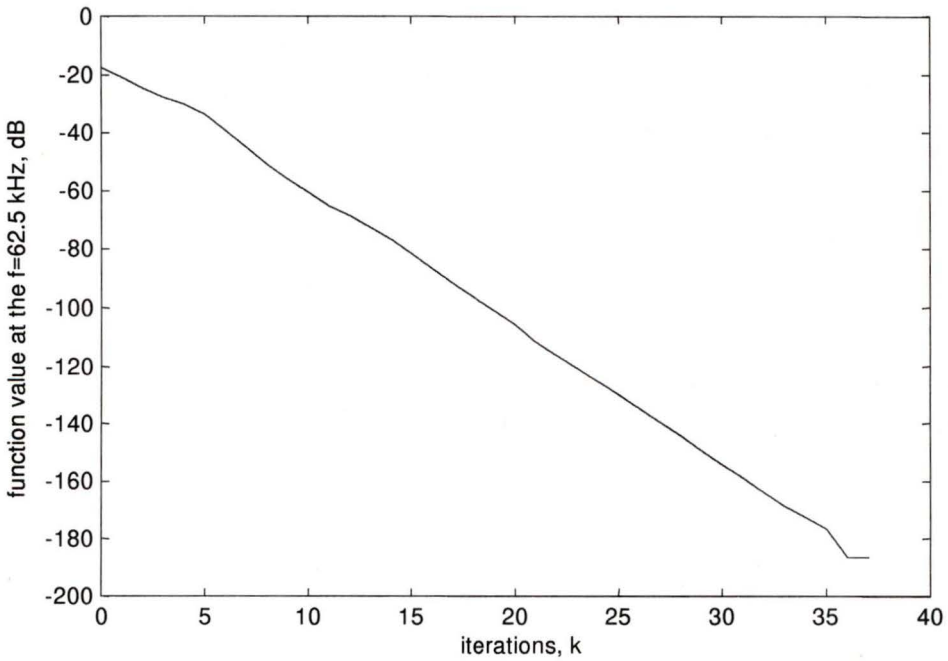

Figure 5.4. The result of using BFGS method to minimize the objective function.

Then as a comparison, using the BFGS method starting with the same initial point x0, the result is shown in Figure 5.4. In this experiment the BFGS is almost the same as the DFP method and with the same number of iterations.

5.2.3 Conclusions

From the above two experiments and in Table 5.1 we can see the BFGS method is a little better than the DFP method in general since it uses fewer iterations to get the same results.

	DFP method $\varepsilon = 1e-30$			**BFGS method** $\varepsilon = 1e-30$		
X^*	**Xs**	**No. Iter**	**Flops**	**Xs**	**No. Iter**	**Flops**
$\begin{bmatrix} 1 \\ -1 \\ -0.4 \\ 0 \\ 0.4 \end{bmatrix}$	$\begin{bmatrix} -9.449261886 \\ -14.361818094 \\ -30.315690967 \\ -34.773114461 \\ -26.991931335 \end{bmatrix}$	39	251180	$\begin{bmatrix} -8.750206121 \\ -13.212414044 \\ -27.798591855 \\ -32.004767315 \\ -24.996131534 \end{bmatrix}$	36	237184
$\begin{bmatrix} 0.8 \\ -0.8 \\ 0 \\ 0.1 \\ -0.1 \end{bmatrix}$	$\begin{bmatrix} -17.153723241 \\ -8.632359877 \\ -24.633694780 \\ -25.673114067 \\ -23.087270511 \end{bmatrix}$	37	250677	$\begin{bmatrix} -17.289026474 \\ -8.630545076 \\ -24.724440530 \\ -25.783892239 \\ -23.158517313 \end{bmatrix}$	37	251746

Table 5.1. A comparison of these two optimization methods.

However this optimization procedure only results in a set of switching frequencies whose values are identical. This is not practical, and we require at least two different switching frequencies to give a high f_{LCM}. Therefore in the next section we add one more constraint to the variables in our objective function.

5.2.4 Formulation with Constraints on Both Range and Average of Switching Frequencies

In this section we consider the constraints on both switching frequency range and average. We add the average switching frequency $\bar{f}_s = 62.5$ kHz to the variables constraints. All derivations can be found in Appendix C. The new objective function is

$$F(x_1, x_2, \cdots, x_{m-1}) = \frac{2A_0^{\,2}}{\sum_{i=1}^{m} \frac{1}{m} \tau_i \pi^2 f_0^{\,2}}$$

$$\times \left(\left(\sum_{i=1}^{m} \frac{1}{m} \left\{ \sin(\pi\alpha_0 f_0 \frac{\frac{1}{55}+\frac{1}{75}e^{-2x_i}}{1+e^{-2x_i}}) \cos(\pi f_0 \frac{\frac{1}{55}+\frac{1}{75}e^{-2x_i}}{1+e^{-2x_i}}) \right\} \right)^2 \left(1 - \sum_{i=1}^{m} \frac{1}{m} \left\{ \cos(2\pi f_0 \frac{\frac{1}{55}+\frac{1}{75}e^{-2x_i}}{1+e^{-2x_i}}) \right\} \right) \right.$$

$$\left. + \left(-\sum_{i=1}^{m} \frac{1}{m} \left\{ \sin(\pi\alpha_0 f_0 \frac{\frac{1}{55}+\frac{1}{75}e^{-2x_i}}{1+e^{-2x_i}}) \sin(\pi f_0 \frac{\frac{1}{55}+\frac{1}{75}e^{-2x_i}}{1+e^{-2x_i}}) \right\} \right)^2 \right.$$

$$\left. - 2 \left(\sum_{i=1}^{m} \frac{1}{m} \left\{ \sin(\pi\alpha_0 f_0 \frac{\frac{1}{55}+\frac{1}{75}e^{-2x_i}}{1+e^{-2x_i}}) \cos(\pi f_0 \frac{\frac{1}{55}+\frac{1}{75}e^{-2x_i}}{1+e^{-2x_i}}) \right\} \right) \right.$$

$$\left. \times \left(\sum_{i=1}^{m} \frac{1}{m} \left\{ \sin(\pi\alpha_0 f_0 \frac{\frac{1}{55}+\frac{1}{75}e^{-2x_i}}{1+e^{-2x_i}}) \sin(\pi f_0 \frac{\frac{1}{55}+\frac{1}{75}e^{-2x_i}}{1+e^{-2x_i}}) \right\} \right) \left(\sum_{i=1}^{m} \frac{1}{m} \left\{ \sin(2\pi f_0 \frac{\frac{1}{55}+\frac{1}{75}e^{-2x_i}}{1+e^{-2x_i}}) \right\} \right) \right)$$

$$/\left[\left(1-\sum_{i=1}^{m}\frac{1}{m}\cos(2\pi f_0\frac{\frac{1}{55}+\frac{1}{75}e^{-2x_i}}{1+e^{-2x_i}})\right)^2+\left(\sum_{i=1}^{m}\frac{1}{m}\sin(2\pi f_0\frac{\frac{1}{55}+\frac{1}{75}e^{-2x_i}}{1+e^{-2x_i}})\right)^2\right]$$

$$+\frac{A_0^{\,2}}{\sum_{i=1}^{m}\frac{1}{m}\frac{\frac{1}{55}+\frac{1}{75}e^{-2x_i}}{1+e^{-2x_i}}\pi^2 f_0^{\,2}}\sum_{i=1}^{m}\frac{1}{m}\sin^2(\pi\alpha_0 f_0\frac{\frac{1}{55}+\frac{1}{75}e^{-2x_i}}{1+e^{-2x_i}})$$

(5.4)

We notice that in the above function x_m (or at least one of the x_i) is not a free variable. In fact it is determined by the other x_i. Although the form of the objective function does not change we must get the new form of the gradient of the objective function, since now x_m is a function of the other x_i. The derivation of the gradient can be found in Appendix C.

5.2.5 Application Experiments and Results

Here again we test the two methods of optimization in objective function (5.4) with three experiments, each starting with a different initial guess at the vector $\boldsymbol{x}$. Results are summarized in Table 5.2 and discussed in the following conclusions. The evolution of the PSD with optimization iteration index is also produced in the 3-D plots of Figures 5.6, 7, 9, 10, 12, 13, 15, 16, 18, 19, 21 and 22.

Experiment 5.3

We first use BFGS method and the initial point x0 = [10 -10 50 6] and tolerance epsilon = 1e-30. The optimization result is shown in Figure 5.5.

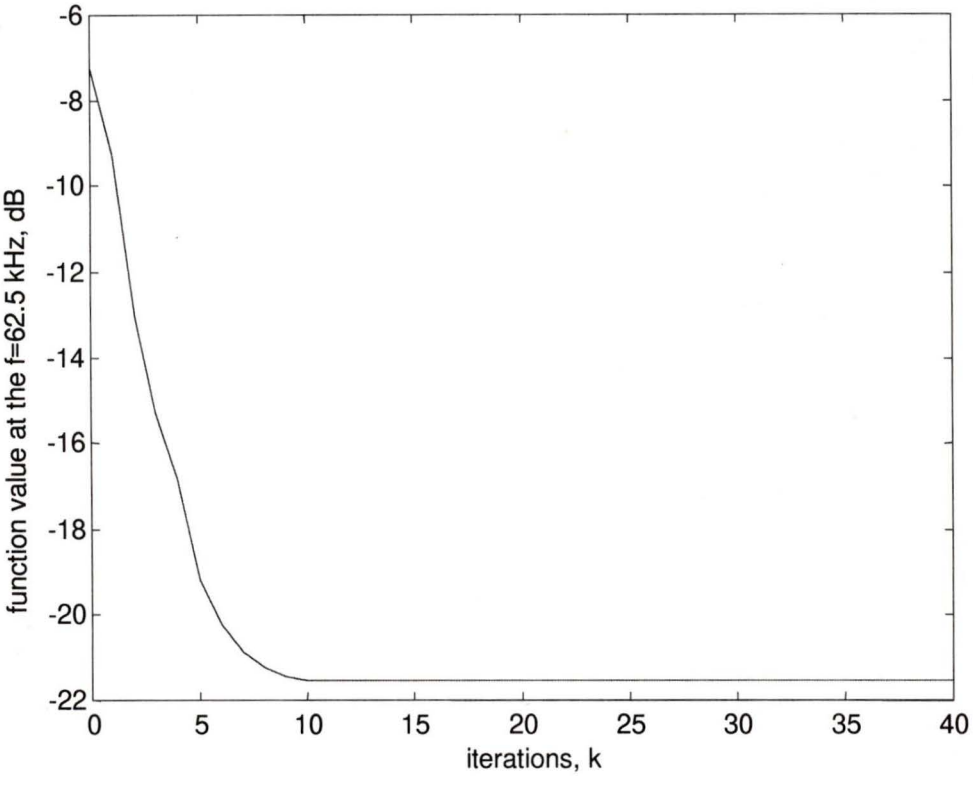

Figure 5.5. The result of using BFGS method to minimize the objective function.

The solution is $x = \begin{bmatrix} 3240.2482340729 \\ -4561.9069459701 \\ 12255.7711497748 \\ 1746.7453399396 \end{bmatrix}$ which corresponds to switching frequencies [55, 75, 55, 55 and 72.5] kHz and 40 iterations are required. The objective function's value reduces from 0.182 to 0.007(-7.4dB to –21.5dB).

Now we give the sequential 3-D plot of the PSD vs. iteration index in Figure 5.6. Figure 5.7 is a detail of the PSD around $f_0 = 62.5$ kHz.

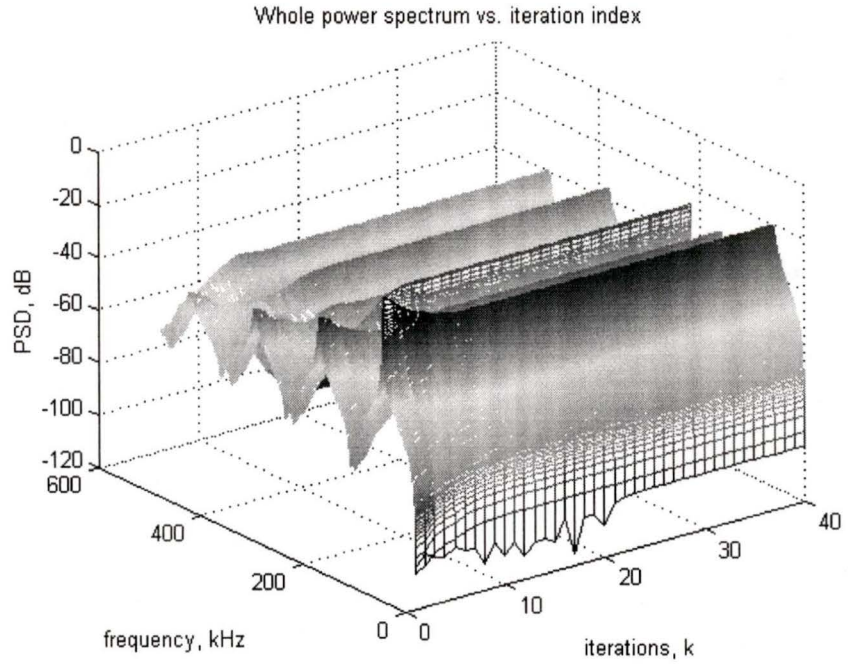

Figure 5.6. 3-D plot of the PSD vs. iteration index.

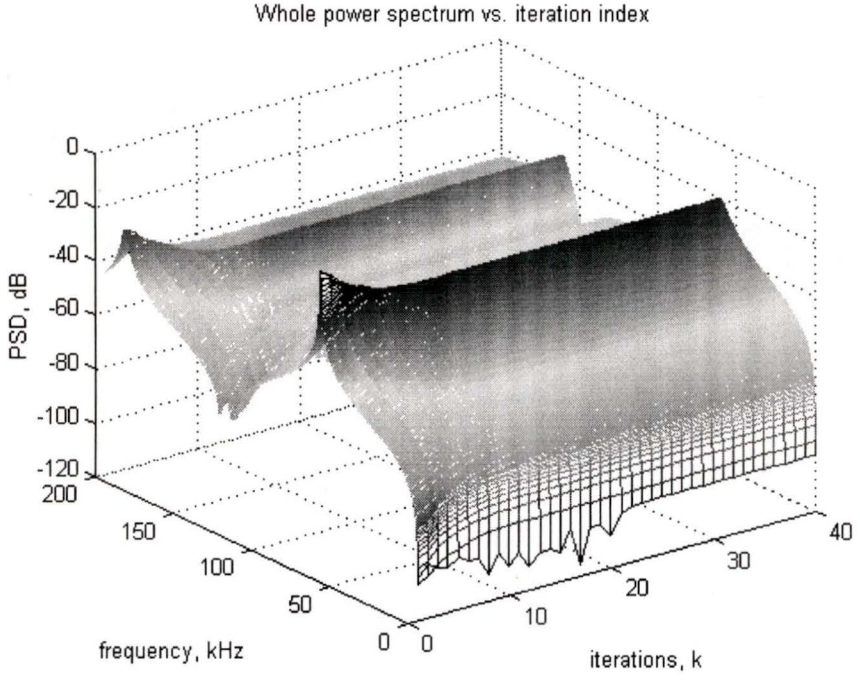

Figure 5.7. Detail of the PSD around $f_0 = 62.5\,kHz$.

Using the DFP method with the same parameters and initial point, the result is shown in Figure 5.8.

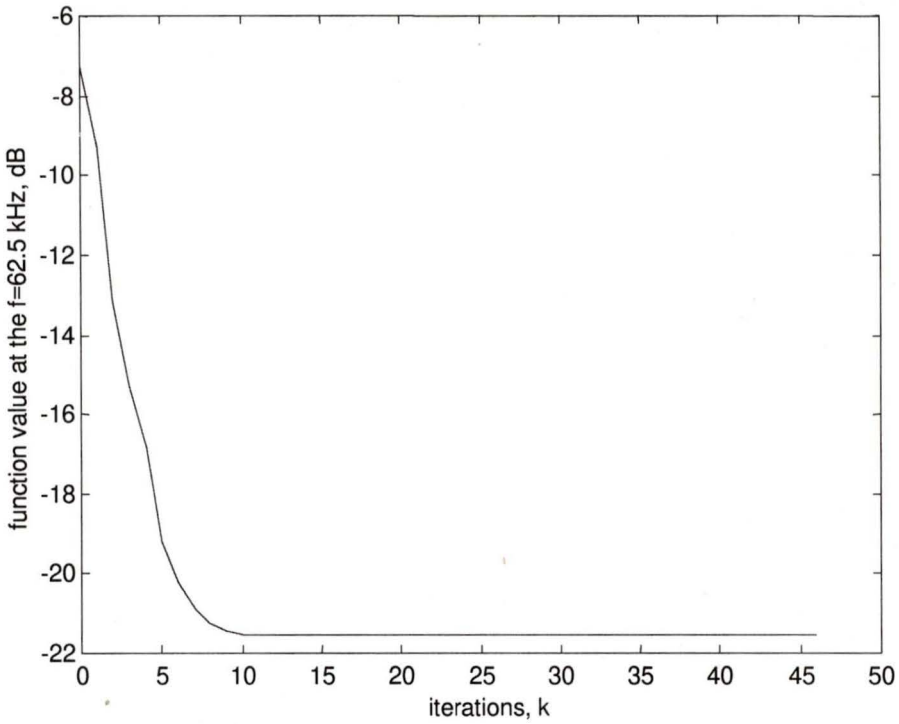

Figure 5.8. The result of using DFP method to minimize the objective function.

The solution is $x = \begin{bmatrix} 3243.4601122836 \\ -4566.6879751655 \\ 12268.3893463918 \\ 1748.4238959882 \end{bmatrix}$, which corresponds to switching frequencies [55, 75, 55, 55 and 72.5] kHz, and 46 iterations are required. The objective function's value reduces from 0.182 to 0.007(-7.4dB to –21.5dB). We give the sequential 3-D plot of the PSD vs. iteration index in Figure 5.9. Figure 5.10 is a detail of the PSD around $f_0 = 62.5$ kHz.

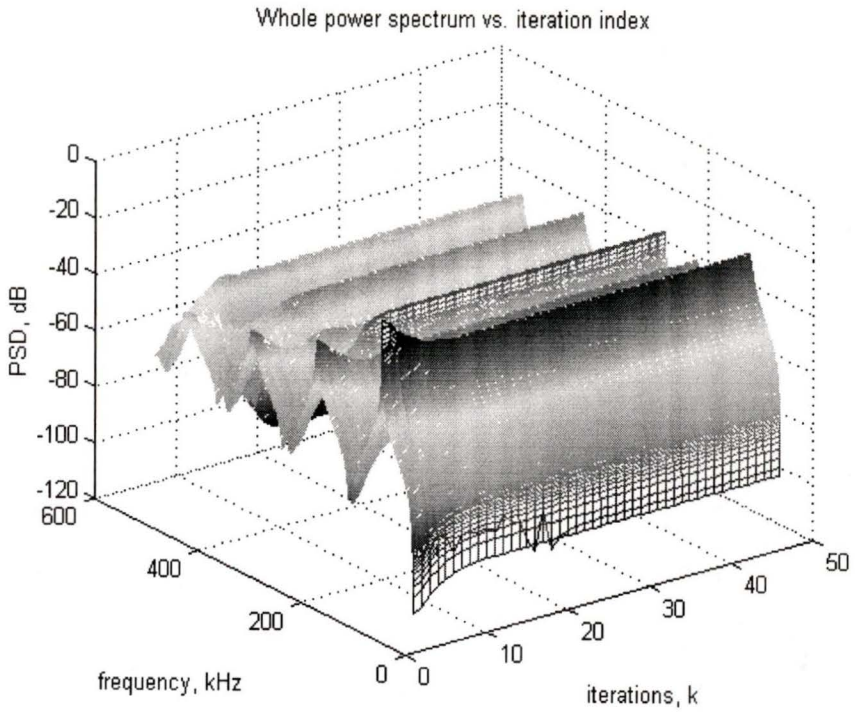

Figure 5.9. 3-D plot of the PSD vs. iteration index.

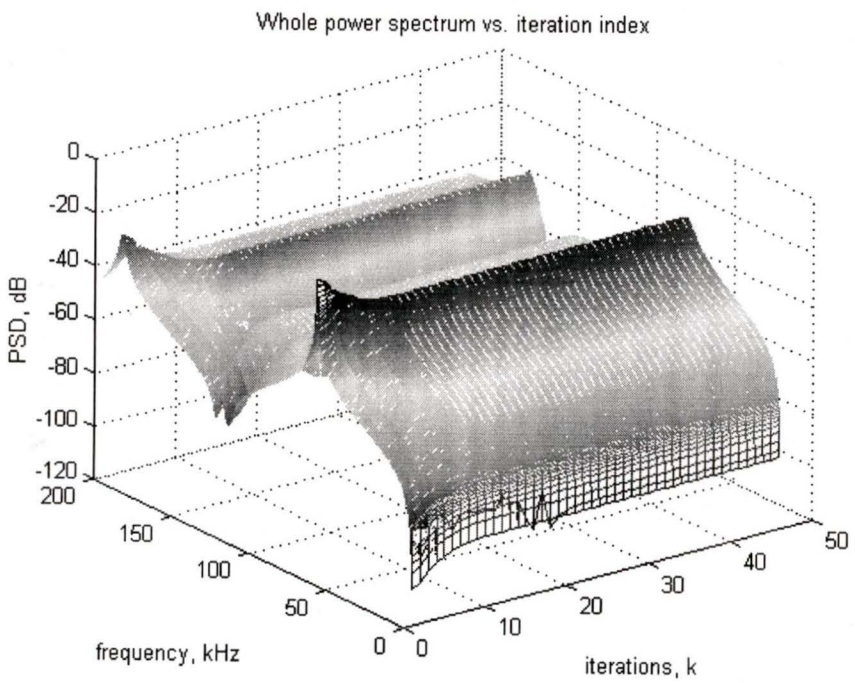

Figure 5.10. Detail of the PSD around $f_0 = 62.5\,kHz$.

Experiment 5.4

We use a different initial point x0 = [40 -40 50 10] and tolerance epsilon = 1e-30. The optimization result is shown in Figure 5.11.

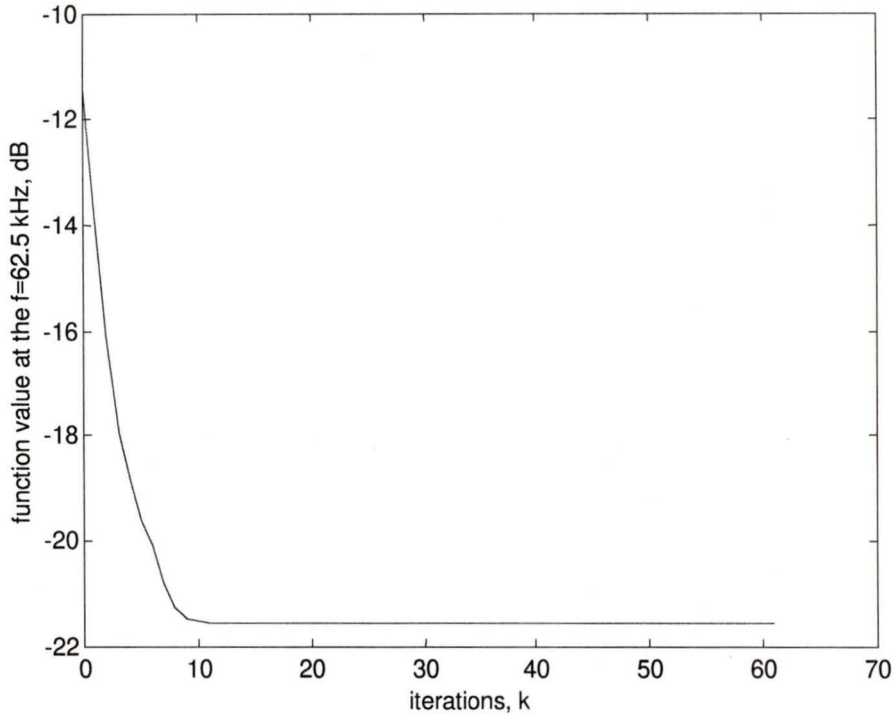

Figure 5.11. The result of using DFP method to minimize the objective function.

The solution is $x = \begin{bmatrix} 7323.5995286207 \\ -11105.062184213 \\ 8023.3036894773 \\ 1802.7645263504 \end{bmatrix}$, which corresponds to switching frequencies [55, 75, 55, 55 and 72.5] kHz and 61 iterations are required. The objective function's value reduces from 0.07 to 0.007(-11.5dB to –21.5dB). We give the sequential 3-D plot of the PSD vs. iteration index in Figure 5.12. Figure 5.13 is a detail of the PSD around $f_0 = 62.5$ kHz.

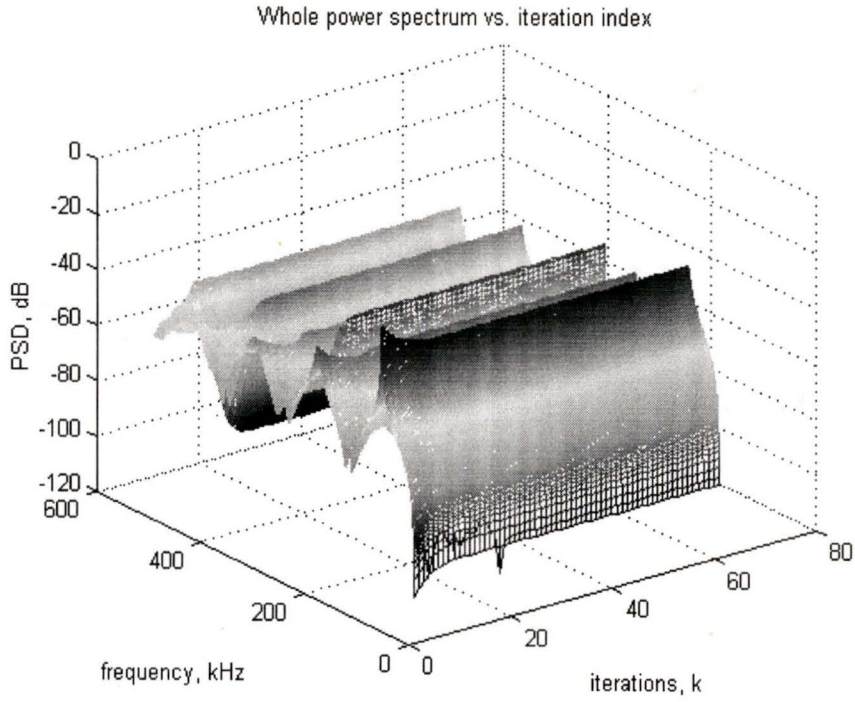

Figure 5.12. 3-D plot of the PSD vs. iteration index.

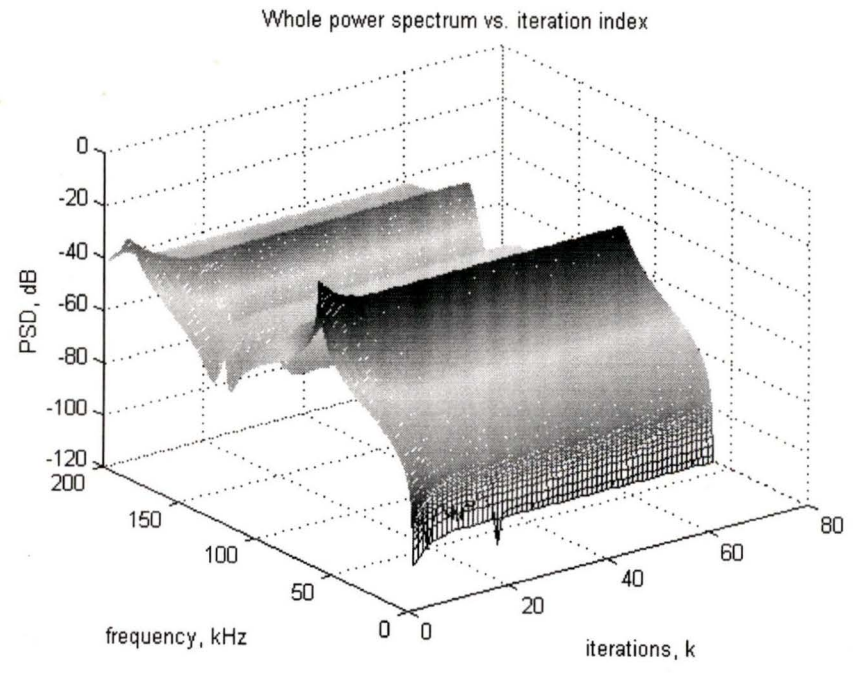

Figure 5.13. Detail of the PSD around $f_0 = 62.5\,kHz$.

Now we use the BFGS method with the same input and same parameters. The experiment result is shown in Figure 5.14.

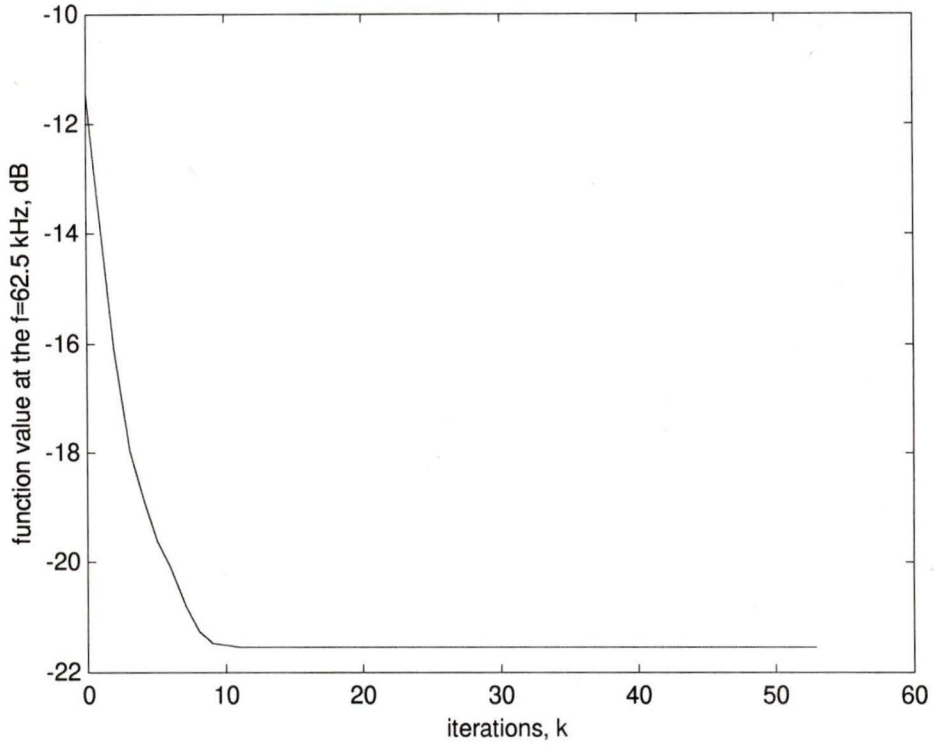

Figure 5.14. The result of using BFGS method to minimize the objective function.

The solution is $x = \begin{bmatrix} 7246.1048860987 \\ -10987.334313555 \\ 7938.4707266985 \\ 1783.6903716423 \end{bmatrix}$, which corresponds to switching frequencies [55, 75, 55, 55 and 72.5] kHz and 53 iterations. The objective value reduces from 0.07 to 0.007 (-11.5dB to –21.5dB). We give the sequential 3-D plot of the PSD vs. iteration index in Figure 5.15. Figure 5.16 is a detail of the PSD around $f_0 = 62.5$ kHz.

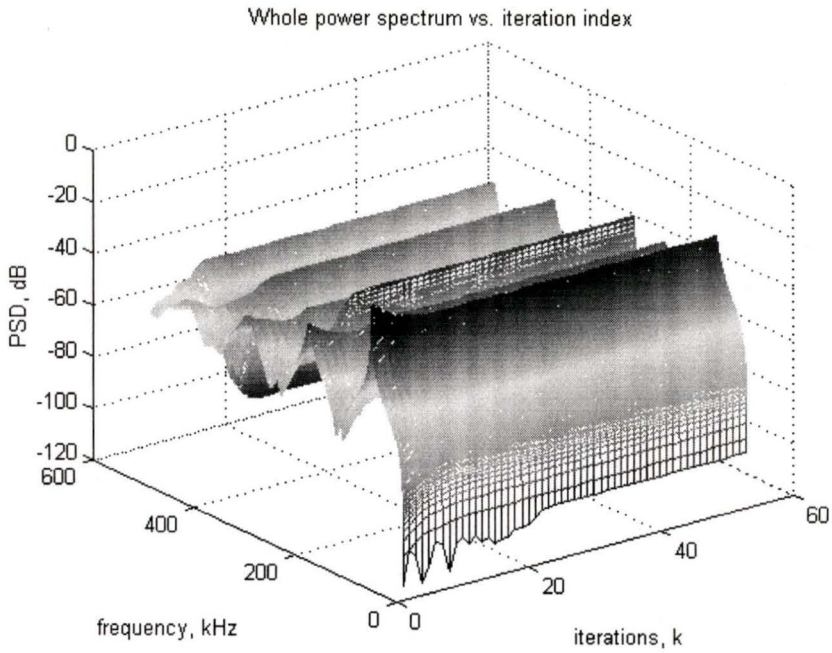

Figure 5.15. 3-D plot of the PSD vs. iteration index.

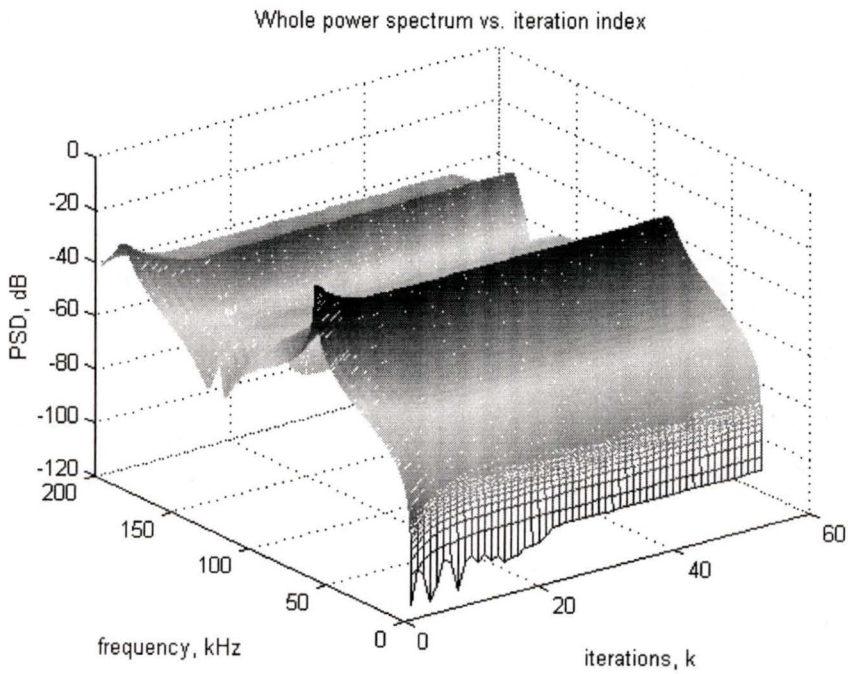

Figure 5.16. Detail of the PSD around $f_0 = 62.5\,kHz$.

Experiment 5.5

We use the different initial point x0 = [20 -20 50 5] and tolerance epsilon = 1e-30. First we use the DFP method. The optimization result is shown in Figure 5.17. The solution is $x = \begin{bmatrix} 16255.1611443584 \\ -26227.2903139028 \\ 32139.2267091684 \\ 1406.2175570742 \end{bmatrix}$, which corresponds to switching frequencies [55, 75, 55, 55 and 72.5] kHz and 27 iterations are required. The objective value reduces from 0.14 to 0.007 (-8.5 dB to –21.5 dB).

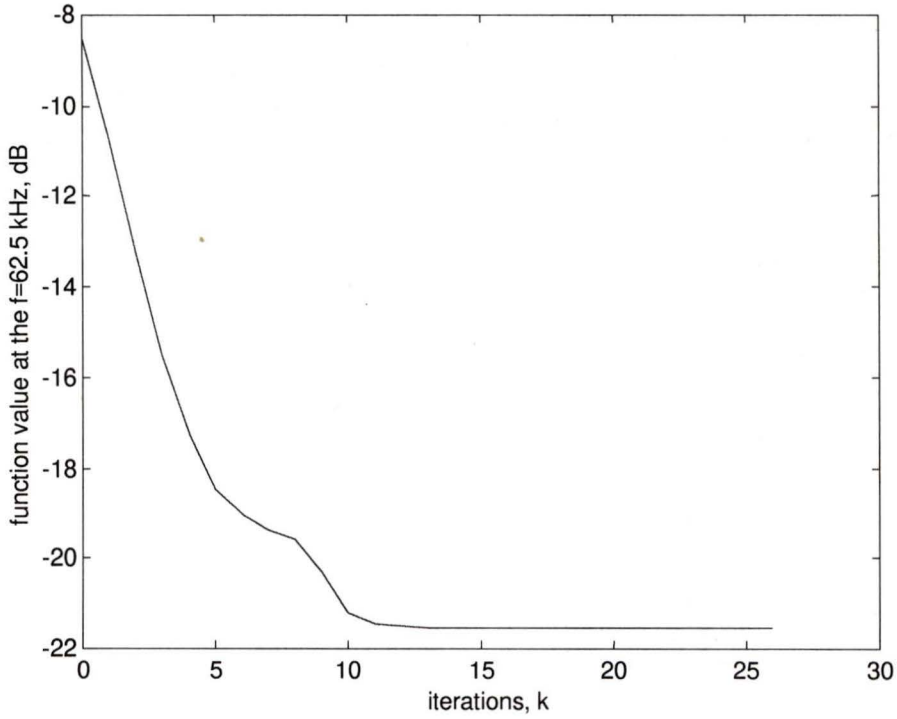

Figure 5.17. The result of using DFP method to minimize the objective function.

We give the sequential 3-D plot of the PSD vs. iteration index in Figure 5.18. Figure 5.19 is a detail of the PSD around $f_0 = 62.5$ kHz.

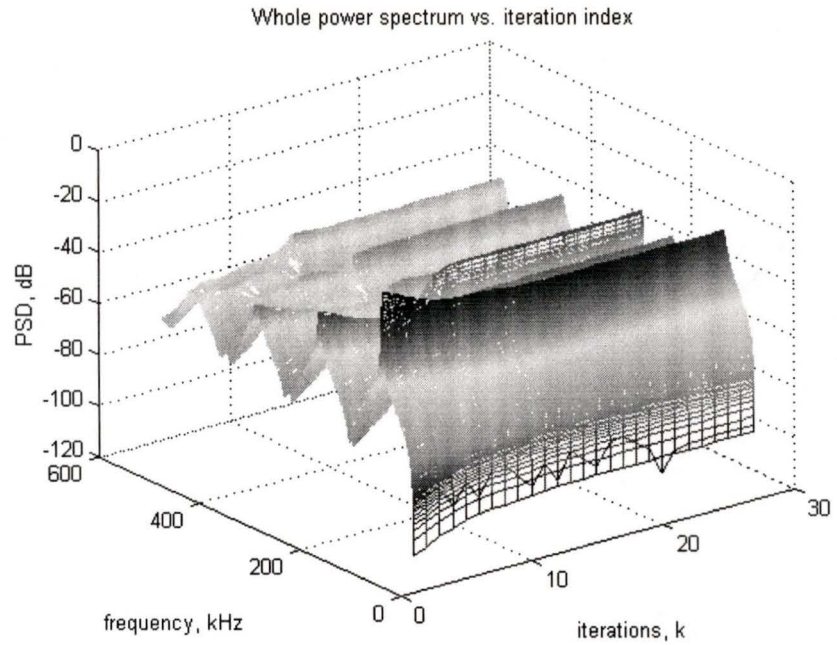

Figure 5.18. 3-D plot of the PSD vs. iteration index.

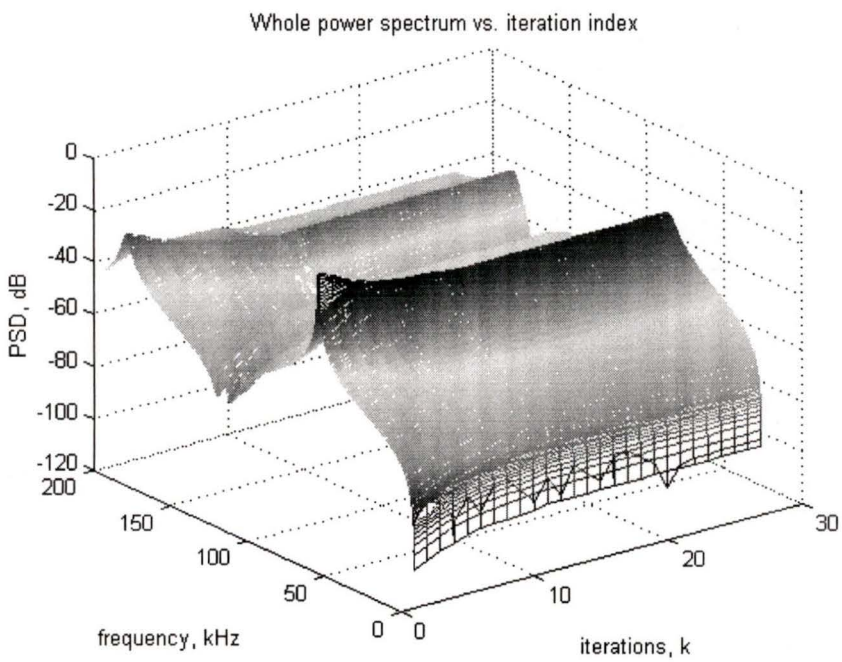

Figure 5.19. Detail of the PSD around $f_0 = 62.5\,kHz$.

Now we use the BFGS method with the same input and same parameters. The experiment result is shown in Figure 5.20.

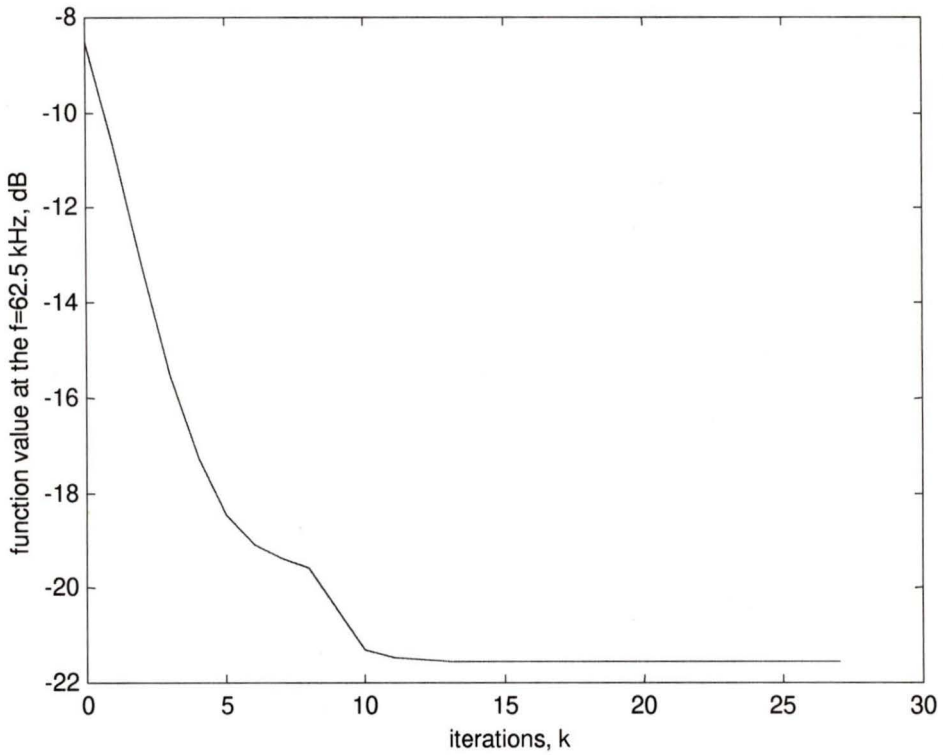

Figure 5.20. The result of using BFGS method to minimize the objective function.

The solution is $x = \begin{bmatrix} 13722.1639020688 \\ -22138.3898241159 \\ 27132.6179135244 \\ 1187.6262410727 \end{bmatrix}$, which corresponds to switching frequencies [55, 75, 55, 55 and 72.5] kHz and 27 iterations are required. The objective value reduces from 0.14 to 0.007 (-8.5dB to –21.5dB). We give the sequential 3-D plot of the PSD vs. iteration index in Figure 5.21. Figure 5.22 is a detail of the PSD around $f_0 = 62.5$ kHz.

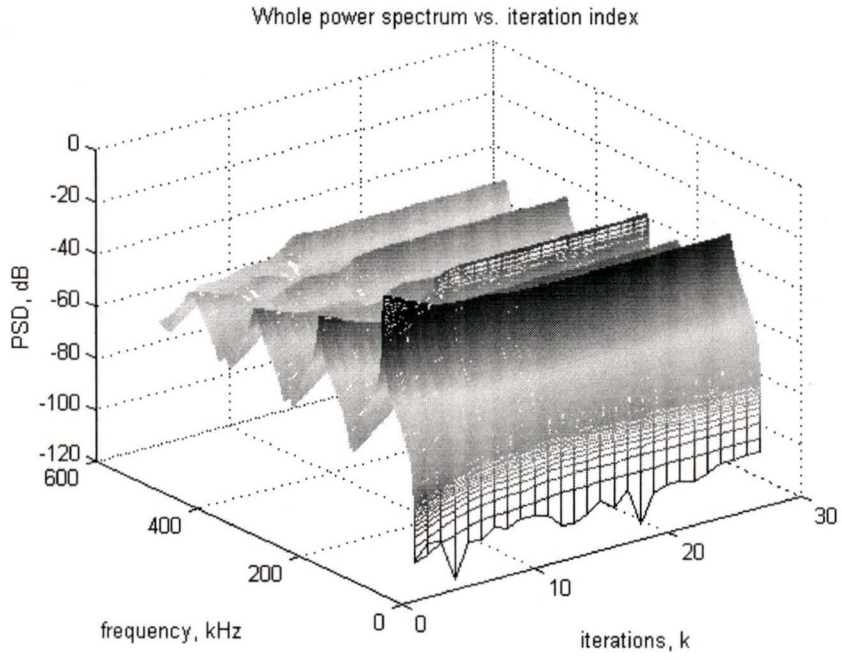

Figure 5.21. 3-D plot of the PSD vs. iteration index.

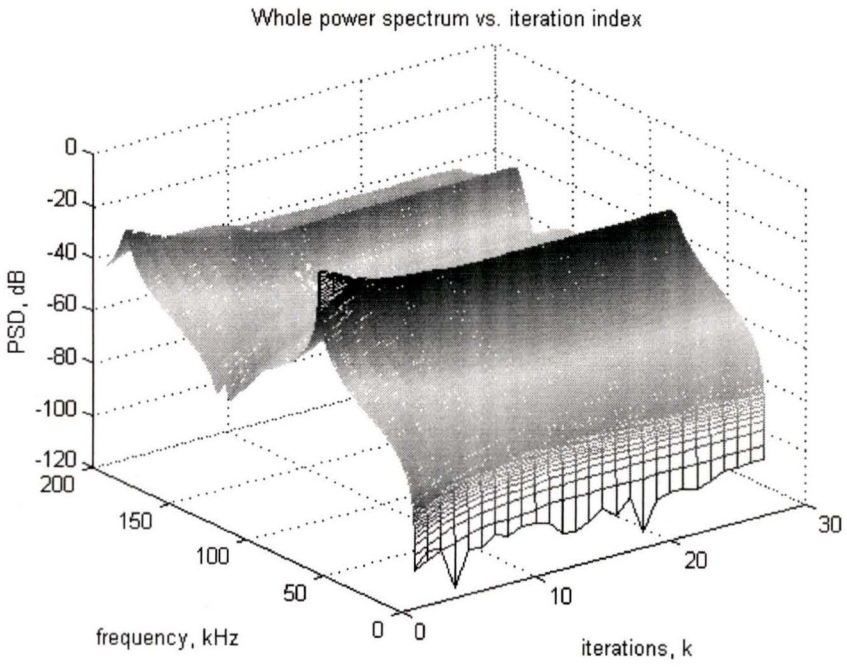

Figure 5.22. Detail of the PSD around $f_0 = 62.5\,kHz$.

	DFP method $\varepsilon = 1e-30$			**BFGS method** $\varepsilon = 1e-30$		
X^*	**Xs**	**No. Iter**	**Flops**	**Xs**	**No. Iter**	**Flops**
$\begin{bmatrix} 10 \\ -10 \\ 50 \\ 6 \end{bmatrix}$	$\begin{bmatrix} 3243.460112283 \\ -4566.68797516 \\ 12268.38934639 \\ 1748.423895988 \end{bmatrix}$	46	1003417	$\begin{bmatrix} 3240.248234072 \\ -4561.906945970 \\ 12255.7711497 \\ 1746.745339939 \end{bmatrix}$	40	569222
$\begin{bmatrix} 40 \\ -40 \\ 50 \\ 10 \end{bmatrix}$	$\begin{bmatrix} 7323.599528620 \\ -11105.06218421 \\ 8023.303689477 \\ 1802.764526350 \end{bmatrix}$	61	975167	$\begin{bmatrix} 7246.104886098 \\ -10987.33431355 \\ 7938.470726698 \\ 1783.690371642 \end{bmatrix}$	53	742649
$\begin{bmatrix} 20 \\ -20 \\ 50 \\ 5 \end{bmatrix}$	$\begin{bmatrix} 16255.16114435 \\ -26227.29031390 \\ 32139.226709168 \\ 1406.2175570742 \end{bmatrix}$	27	292304	$\begin{bmatrix} 13722.163902068 \\ -22138.38982411 \\ 27132.61791352 \\ 1187.626241072 \end{bmatrix}$	27	316312

Table 5.2. A comparison of the two optimization methods under all constraints.

Comments summarizing comparisons in Table 5.2 and the experiments are given in the next section.

5.2.6 Discussion on Experimental Results of Section 5.2.5

If we translate all the solutions which are obtained from experiments 5.3, 5.4 and 5.5 into switching frequencies we can find that they all reach the same set of switching frequencies 55, 75, 55, 55 and 72.5KHz. (Recall that only 4 of the solutions are independent; the fifth is dependent on the other 4). This is equivalent to saying that we use only three switching frequencies 55, 72.5 and 75 with the probabilities $\frac{3}{5}, \frac{1}{5}, \frac{1}{5}$ respectively. The least common multiple of these three is 23.925×10^6 Hz.

From the experiments and Table 5.2 we can see that for this objective function the BFGS method is a little better than the DFP method. It usually needs fewer iterations and more robust than the DFP.

We point out that a reasonable initial starting point must be chosen to assure convergence of the algorithm. In section 5.2.5 the numerical results of the optimization maybe complex. To eliminate that possibility we can use some alternative programming techniques.

Note that up to now all the experiments in this chapter use switching frequencies that have an equally likely chance of being selected, that is to say all the switching frequencies have the same probability of selection. In next section we will consider the probabilities as variables to optimize together with the switching frequencies.

5.3 Optimum Joint Selection of Switching Frequencies and Their Probabilities

In this section we apply nonlinear optimization methods to jointly find a constrained set of switching frequencies and their corresponding probabilities that will minimize the spectral power at a specified frequency. We consider both the switching frequencies and their possibilities as variables; that is to say we try to find the set of switching frequencies and their corresponding probabilities that minimize the objective function in equation (5.5). We formulate the problem, apply optimization methods and then give experiment results.

5.3.1 Formulation

We can formulate our minimization problem as follows:

$$F(\tau_1, \tau_2, \cdots, \tau_m)$$

$$= \frac{{A_0}^2}{\sum_{i=1}^{m} p_i \tau_i \pi^2 {f_0}^2} \left(\sum_{i=1}^{m} p_i \sin^2(\pi \alpha_0 f_0 \tau_i) + 2\,\mathrm{Re}\left[\frac{\left(\sum_{i=1}^{m} p_i \sin(\pi \alpha_0 f_0 \tau_i) e^{j\pi f_0 \tau_i} \right)^2}{1 - \sum_{i=1}^{m} p_i e^{j2\pi f_0 \tau_i}} \right] \right)$$

$$= \frac{{A_0}^2}{\sum_{i=1}^{m} p_i \tau_i \pi^2 {f_0}^2} \left(\sum_{i=1}^{m} p_i \sin^2(\pi \alpha_0 f_0 \tau_i) + 2\,\mathrm{Re}\left[\frac{\left(\sum_{i=1}^{m} p_i \sin(\pi \alpha_0 f_0 \tau_i)\cos(\pi f_0 \tau_i) + j \sum_{i=1}^{m} p_i \sin(\pi \alpha_0 f_0 \tau_i)\sin(\pi f_0 \tau_i) \right)^2}{(1 - \sum_{i=1}^{m} p_i \cos(2\pi f_0 \tau_i)) - j \sum_{i=1}^{m} p_i \sin(2\pi f_0 \tau_i)} \right] \right)$$

$$= \frac{2{A_0}^2}{\sum_{i=1}^{m} p_i \tau_i \pi^2 {f_0}^2} \left(\begin{array}{l} \left(\sum_{i=1}^{m} {p_i}^2 \{\sin(\pi \alpha_0 f_0 \tau_i)\cos(\pi f_0 \tau_i)\} - \sum_{i=1}^{m} {p_i}^2 \{\sin(\pi \alpha_0 f_0 \tau_i)\sin(\pi f_0 \tau_i)\} \right) \\ \qquad \times \left(1 - \sum_{i=1}^{m} p_i \{\cos(2\pi f_0 \tau_i)\} \right) \\ -2 \left(\sum_{i=1}^{m} p_i \{\sin(\pi \alpha_0 f_0 \tau_i)\cos(\pi f_0 \tau_i)\} \right) \left(\sum_{i=1}^{m} p_i \{\sin(\pi \alpha_0 f_0 \tau_i)\sin(\pi f_0 \tau_i)\} \right) \\ \qquad \times \left(\sum_{i=1}^{m} p_i \{\sin(2\pi f_0 \tau_i)\} \right) \end{array} \right)$$

$$/ \left[\left(1 - \sum_{i=1}^{m} p_i \cos(2\pi f_0 \tau_i) \right)^2 + \left(\sum_{i=1}^{m} p_i \sin(2\pi f_0 \tau_i) \right)^2 \right] + \frac{{A_0}^2}{\sum_{i=1}^{m} p_i \tau_i \pi^2 {f_0}^2} \sum_{i=1}^{m} p_i \sin^2(\pi \alpha_0 f_0 \tau_i)$$

(5.5)

Subject to the constraints:

$$\begin{cases} \frac{1}{75} \le \tau_1, \tau_2, \cdots, \tau_m \le \frac{1}{55} \\ p_1, p_2, \cdots, p_m \ge 0 \\ \sum_{i=1}^{m} p_i = 1 \\ \sum_{i=1}^{m} \frac{p_i}{\tau_i} = 62.5 \end{cases} \tag{5.6}$$

5.3.2 Application Experiments and Results

Now we can apply the nonlinear numerical methods to the above objective function. Without loss of generality of method we use in all our experiments α_0= 0.5 and f_0= 62.5 kHz. This section consists of three experiments 5.6, 5.7 and 5.8. In these experiments we consider 2, 3 and 5 switching frequencies respectively.

Experiment 5.6

In this part we only use two switching frequencies and their probabilities as the variables to optimize. The following experiments differ only in starting points for the solution vector ***x,*** which is composed of the τ_i, the inverses of the switching frequencies, and their probabilities.

First we use the initial input vector x0 = $[\tau_1, \tau_2, p_1, p_2]$=[1/55 1/70 0.5 0.5] which corresponds to 55kHz and 75kHz switching frequencies having equal probability 0.5. We get the solution $x = \begin{bmatrix} 0.01818181818182 \\ 0.01333333333333 \\ 0.62499999997846 \\ 0.37500000002154 \end{bmatrix}$, which corresponds to the switching frequencies 55kHz and 75kHz with probabilities 0.625 and 0.375 respectively. The objective function value decreases from initial point 0.01023611641455 (-19.90 dB) to solution point 0.00638234397206 (-21.95 dB). The corresponding original and optimized PSDs are shown together for comparison in Figure 5.23. The detail is shown in Figure 5.24.

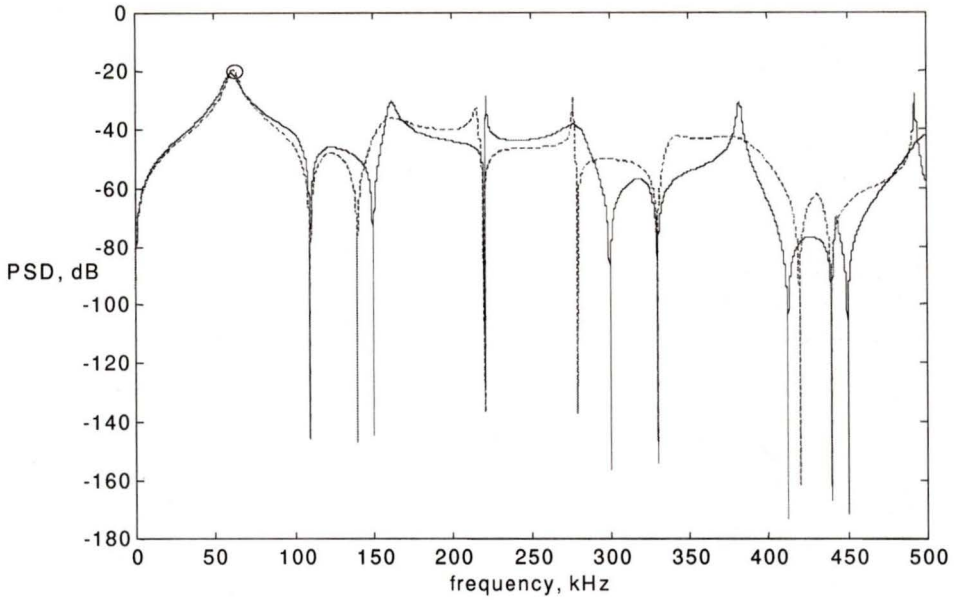

Figure 5.23. The PSD results. The Dotted trace represents the initial trial. The solid one represents the solution.

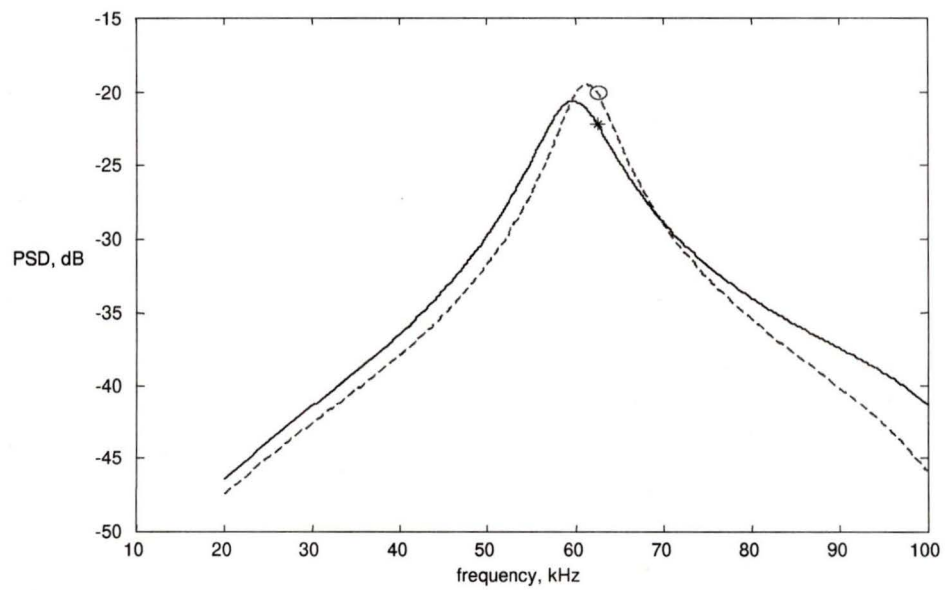

Figure 5.24. The detail around $f_0 = 62.5$ kHz.

With an alternate initial input vector x0 = [1/60 1/65 0.5 0.5] we get the solution $x = \begin{bmatrix} 0.01818181818182 \\ 0.01333333333333 \\ 0.62500000096261 \\ 0.37499999903739 \end{bmatrix}$, which corresponds to the switching frequencies 55 kHz and 75 kHz with probabilities 0.625 and 0.375 respectively. The objective function value decreases from initial point 0.09309793273259 (-10.31 dB) to solution point 0.00638234395145 (-21.95 dB). The corresponding original and optimized PSDs are shown together for comparison in Figure 5.25, and detail is shown in Figure 5.26.

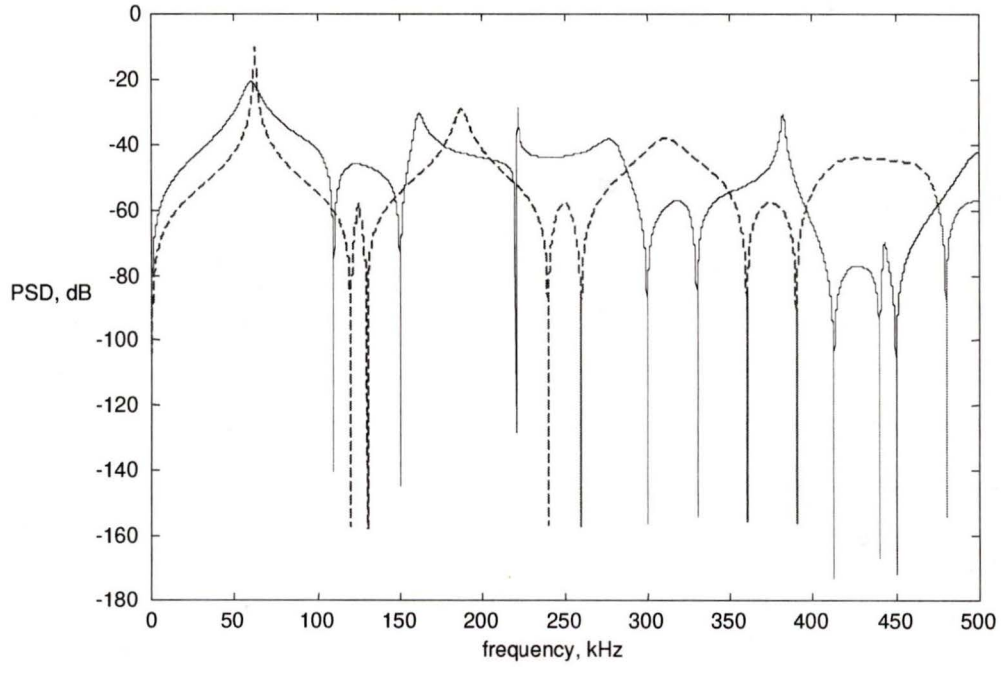

Figure 5.25. The PSD results. The Dotted plot represents the initial trial. The solid one represents the solution.

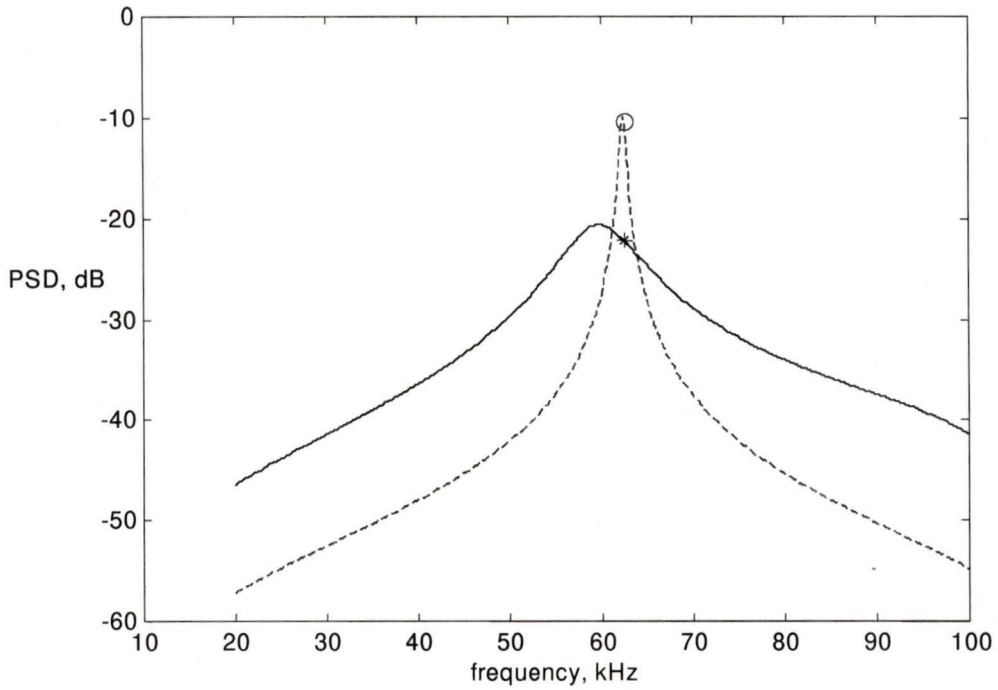

Figure 5.26. The detail around $f_0 = 62.5$ kHz.

Experiment 5.7

In this test we change the number of switching frequencies and their corresponding probabilities from 2 to 3. The following experiments differ only in starting points for the solution vector $\boldsymbol{x}$ which is composed of the τ_i and their probabilities.

First we use the initial input vector x0 = [1/55 1/60 1/72.5 1/3 1/3 1/3]. We get the

solution $x = \begin{bmatrix} 0.01818181818182 \\ 0.01818181818182 \\ 0.01333333333333 \\ 0.31772999980909 \\ 0.30727000023257 \\ 0.37499999995834 \end{bmatrix}$, which corresponds to the switching frequencies [55 55 75] kHz with probabilities 0.318, 0.307 and 0.375 respectively. The objective function value decreases from initial point 0.01026506091250 (-19.90 dB) to solution point

0.00638234397074 (-21.95 dB). The corresponding original and optimized PSDs are shown together for comparison in Figure 5.27. The detail is shown in Figure 5.28.

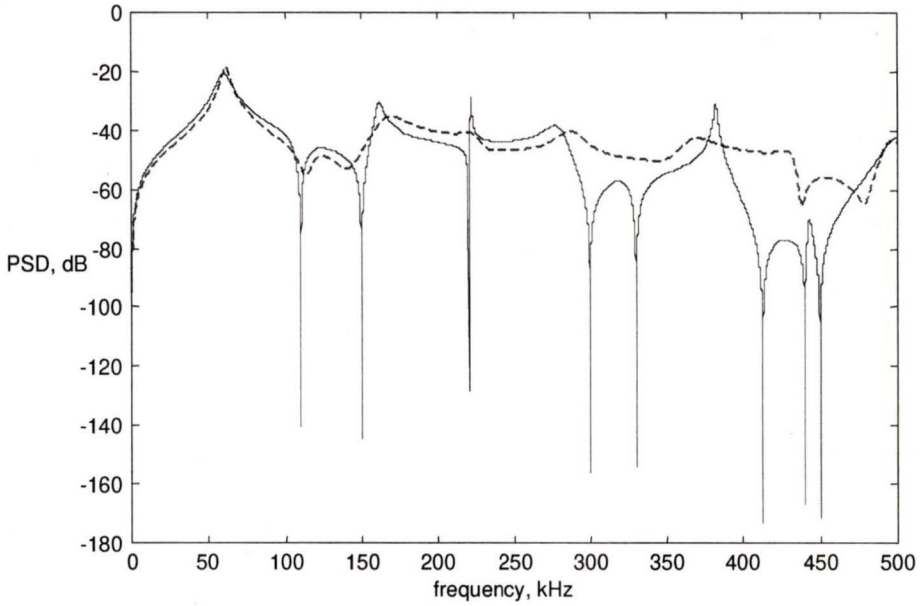

Figure 5.27. The PSD results. The Dotted trace represents the initial trial. The solid one represents the solution.

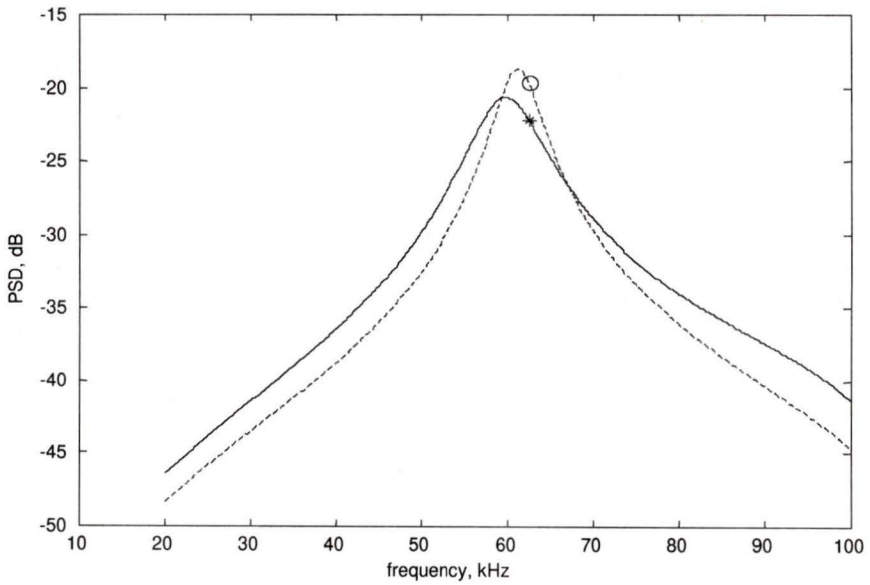

Figure 5.28. The detail around $f_0 = 62.5$ kHz.

We choose another initial input vector x0 = [1/56 1/62 1/69.5 1/3 1/3 1/3]. We get the solution $x = \begin{bmatrix} 0.01818181818182 \\ 0.01818181818182 \\ 0.01333333333333 \\ 0.32338586603824 \\ 0.30161413396123 \\ 0.37500000000052 \end{bmatrix}$, which corresponds to the switching frequencies [55 55 75] kHz with probabilities 0.323, 0.302 and 0.375 respectively. The objective function value decreases from initial point 0.01939332952049 (-17.1 dB) to solution point 0.00638234397162 (-21.95 dB). The corresponding original and optimized PSDs are shown together for comparison in Figure 5.29. The detail is shown in Figure 5.30.

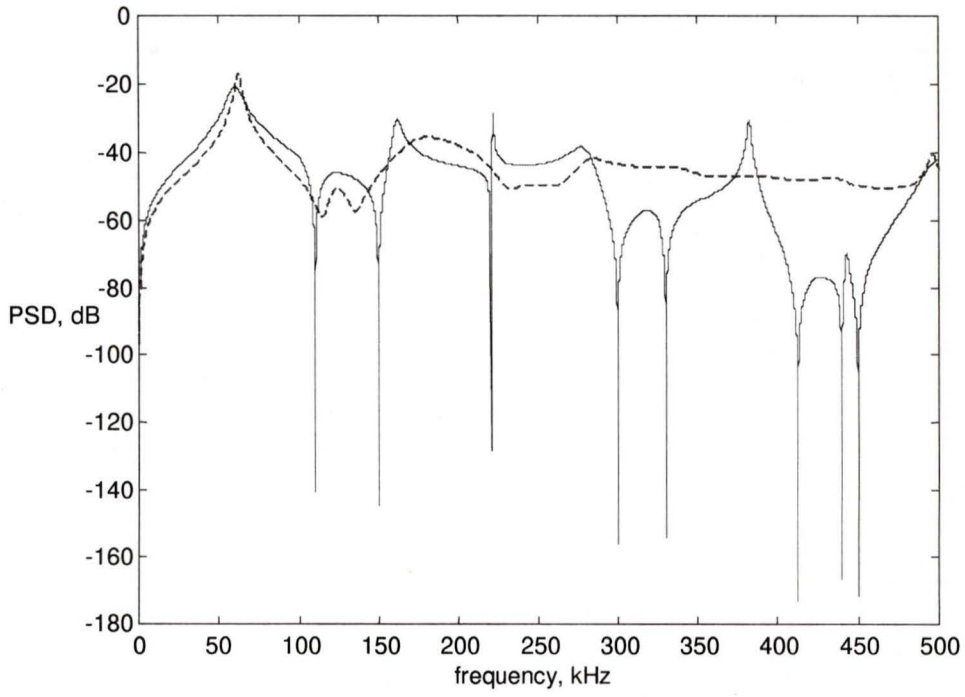

Figure 5.29. The PSD results. The Dotted plot represents the initial trial. The solid one represents the solution.

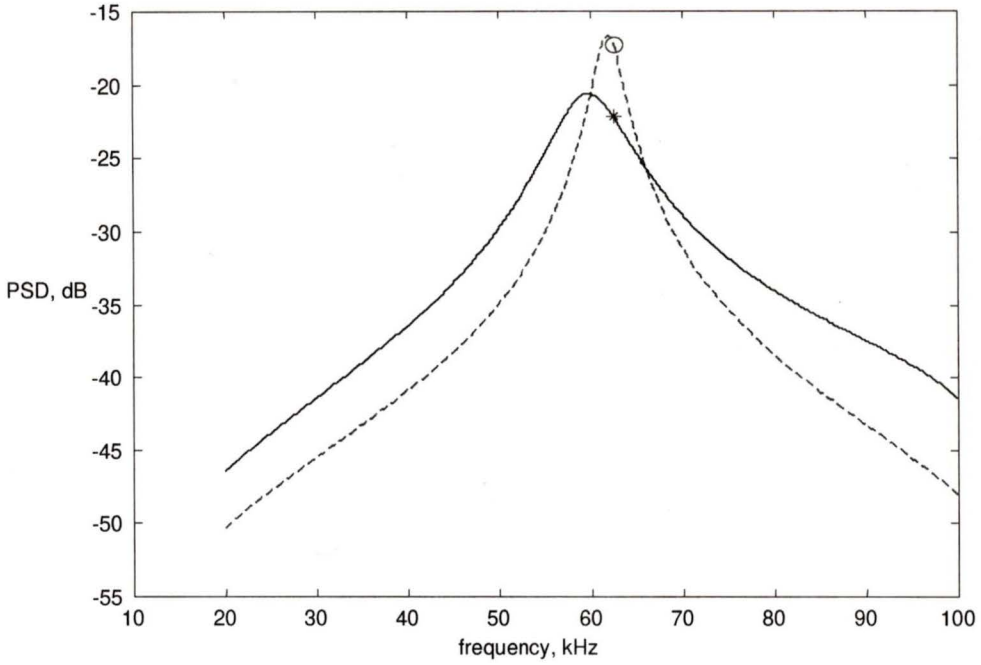

Figure 5.30. The detail around $f_0 = 62.5$ kHz.

Experiment 5.8

In this test we use five switching frequencies and their corresponding probabilities as the variable to optimize. The following two experiments differ only in starting points for the solution vector $\boldsymbol{x}$ which is composed of the τ_i and their probabilities.

In this experiment we first use the input vector x0 = [1/55 1/58 1/60 1/65 1/74.5 1/5 1/5 1/5 1/5 1/5]. We get the solution $x =$

$$\begin{bmatrix} 0.01818181818182 \\ 0.01818181818182 \\ 0.01818181818182 \\ 0.01333333333333 \\ 0.01333333333333 \\ 0.21148741908907 \\ 0.20769456400499 \\ 0.20581801690594 \\ 0.18119613142584 \\ 0.19380386857415 \end{bmatrix},$$

which corresponds to

the switching frequencies [55 55 55 75 75] kHz with probabilities 0.211, 0.208, 0.206, 0.181 and 0.194 respectively. The objective function value decreases from initial point 0.01334280661044 (-18.7 dB) to solution point 0.00638234397161 (-21.95 dB). The corresponding original and optimized PSDs are shown together for comparison in Figure 5.31. The detail is shown in Figure 5.32.

Then we try another input vector x0 = [1/56 1/58 1/60 1/62 1/76.5 1/5 1/5 1/5 1/5 1/5]. We get the solution $x = \begin{bmatrix} 0.01818181818182 \\ 0.01818181818182 \\ 0.01818181818182 \\ 0.01333333333333 \\ 0.01333333333333 \\ 0.20258077388015 \\ 0.20878890107156 \\ 0.21363032504874 \\ 0.20820395666444 \\ 0.16679604333511 \end{bmatrix}$, which corresponds to the switching frequencies [55 55 55 75 75] kHz with probabilities 0.202, 0.209, 0.214, 0.208 and 0.167 respectively. The objective function value decreases from initial point 0.0119116861775 (-19.2 dB) to solution point 0.00638234397160 (-21.95 dB). The corresponding original and optimized PSDs are shown together for comparison in Figure 5.33. The detail is shown in Figure 5.34.

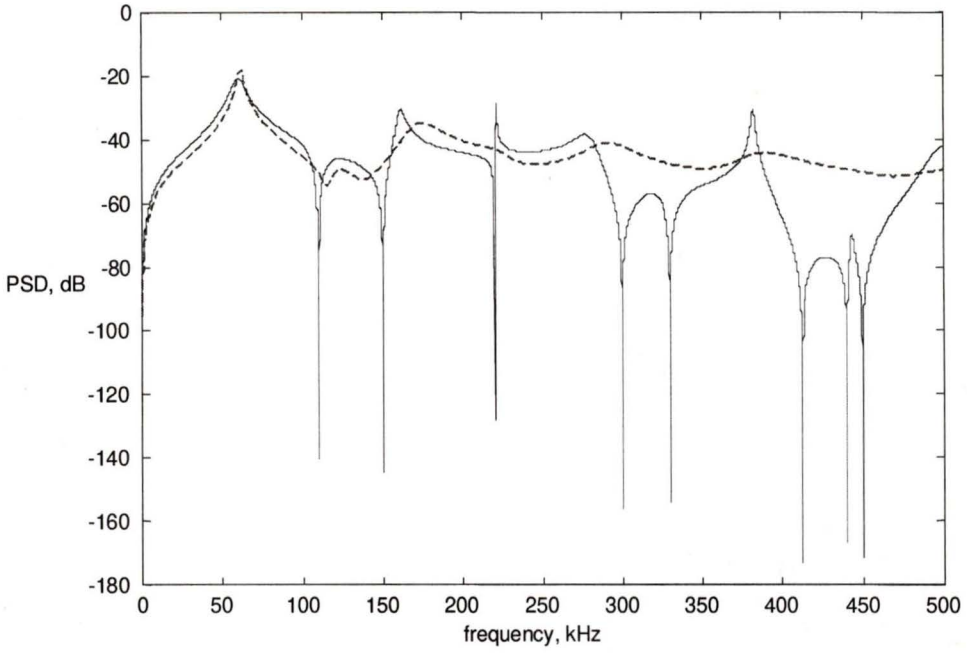

Figure 5.31. The PSD results. The Dotted trace represents the initial trial. The solid one represents the solution.

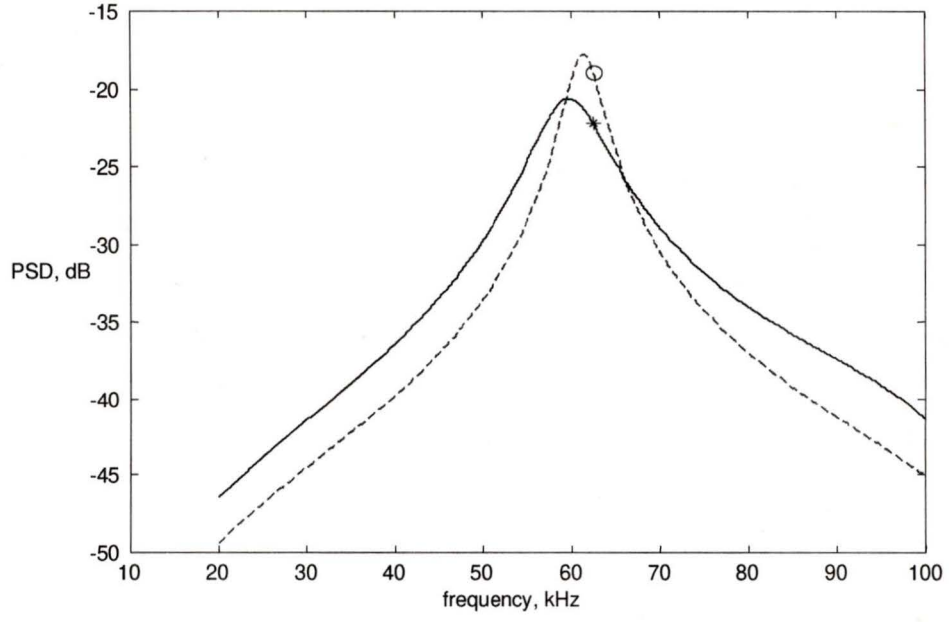

Figure 5.32. The detail around $f_0 = 62.5$ kHz.

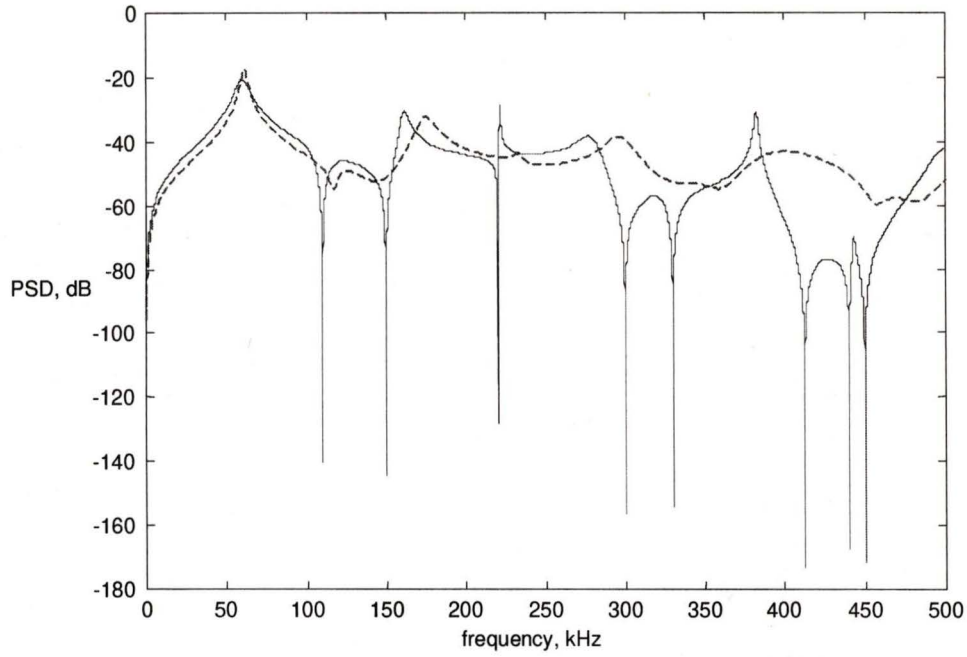

Figure 5.33. The PSD results. The Dotted trace represents the initial trial. The solid one represents the solution.

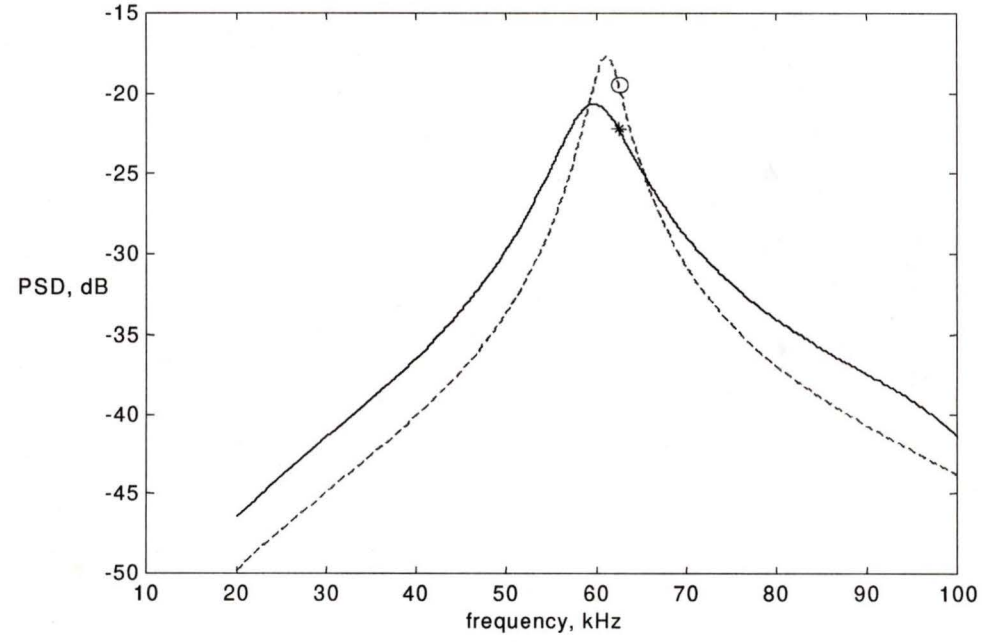

Figure 5.34. The detail around $f_0 = 62.5$ kHz.

5.3.3 Discussion of Results from Section 5.3.2

From all the experiments in section 5.3.2 we have found that all the solutions actually converge to the same switching frequencies 55 kHz and 75 kHz with probabilities 0.625 and 0.375 respectively. That is to say we have this optimal solution to the specified frequency $f_0 = 62.5$ kHz. However, we realize that some least common multiple frequency may not have been achieved, as it was not in the constraints. Some new constraints need to be found and added to the objective function to achieve better results in future study.

The result of the objective function value (minimized dB level at 62.5 kHz) is a little better than that we achieved in section 5.2.5.

Chapter 6

Conclusions and Future Research

6.1 Summary

We have analyzed the power spectral density formula for the CDC RSFPWM scheme in DC/DC conversion, and present design methods to control the continuous noise spectrum. The corresponding optimization methods are studied and applied. Simulations verify all our conclusions.

The background for this thesis is presented in chapter 2. We classify the RPWM schemes utilized in converters with conclusion on their characteristics in section 2.1. A survey of the existing literature on RPWM schemes is given in section 2.2, and RSFPWM is considered as the most successful. In section 2.3, we summarize the formulas for both a general RSFPWM scheme and two specific schemes CPW and CDC. We conclude the CPW scheme in section 2.3.2 and the CDC scheme in section 2.3.3. CDC allows controllability whereas CPW does not. A tight control of the continuous noise spectrum is more important in DC/DC converters than in DC/AC inverters since the noise will result in ripples in the output voltage.

In chapter 3 we develop two design methods to control the PSD of the CDC RSFPWM at discrete frequencies. We give the related analysis and derivation in section 3.2 and design examples with simulation verification in section 3.3. Method 1 can ideally put a null at any desired frequency, but we also point out the practical limitations of this method. Method 2 is a mild method since it cannot put a pure null at the desired frequency but avoids the peak appearing at that frequency, which is complementary to method 1. By combining methods 1 and 2 we are able to exert considerable control of the PSD at any particular frequency in the PSD of CDC RSFPWM, but we also present the limitation of these methods when there are practical constraints on switching frequencies. We demonstrate by experiments how a narrow switching band constraint severely limits our flexibility in design for PSD minimization at the desired frequency, and we also show what can be gained by weakening the constraints.

Chapter 4 continues our study to control the PSD over a band of frequencies. We first factor the denominator of the PSD express into carrier and envelope $R(f)$ in section 4.2, and analyze it under the assumption that switching intervals are equally spaced and have a symmetric distribution. In section 4.3 we further study the resulting PSD with constraints on the switching frequencies, and follow with simulation verification. In section 4.4 we suppress the PSD over a band of frequencies by controlling $R(f)$ without any constraints on the switching frequencies; design examples confirm our method. Although our approach is successful, all our analysis and design examples are based on the assumptions of equally spaced switching intervals with a symmetric distribution. The more general analysis is recommended as future research.

Optimization methods are applied in chapter 5 to minimize the PSD at a specified frequency under different constraints on the switching frequencies. The formulation details can be found in Appendix B and C. Although the solution provided by the optimization procedure reduces the PSD at the desired frequency, it contains only two different switching frequencies, which is not feasible in practice since the least common multiple switching frequency may not have been achieved and many peaks will appear in the PSD. Some new constraints need to be found and added to the objective function to achieve better results in future study.

6.2 Suggestions for Future Work

We hope the research addressed in this thesis contributes to better control of the continuous output noise spectrum in DC/DC converters using RSFPWM by optimal design rather than ad hoc methods for selecting the switching frequency set and its distribution. At the same time we suggest the following directions as future research work:

- Apply similar analysis procedure in DC/AC inverters using the CDC RSFPWM.
- Investigate the nonsymmetrical probabilities and unevenly spaced switching intervals in controlling the PSD over a band of frequencies.
- Find a new objective function with more constraints for minimizing the PSD at discrete frequencies in order to obtain a set of switching frequencies whose least common multiples are large enough.
- Explore more optimization methods for controlling the PSD over a band of frequencies.

Bibliography:

[1] N. Mohan, T. M. Undeland, W. P. Robbins, "Power electronics: converters, applications, and design", Second Edition, John Wiley & Sons, Inc. 1995.

[2] D. M. Mitchell, "Switching regulator analysis", McGraw-Hill, Inc. 1988.

[3] P. Wood, "Switching power converters", New York: Van Nostrand, Reprint Edition, 1984.

[4] K. Thorborg, "Power electronics", Prentice Hall, Inc. 1988.

[5] A. M. Stankovic, "Random pulse modulation with applications to power electronic converters", Ph.D. Thesis, Massachusetts Institute of Technology, February 1993.

[6] D. Middleton, "An introduction to statistical communication theory", New York: McGraw-Hill, 1960.

[7] A. M. Trzynadlowski, S. Legowski, R. L. Kirlin, "Random pulse-width modulation technique for voltage-controlled power inverters", IEEE, INT. J. Electronics, Vol. 68, No. 6, 1027-1037, 1990.

[8] T. Tanaka, T. Ninomiya, K. Harada, "Random-switching control in DC/DC switching converters", PESC'89 Record, pp.500-507, 1989.

[9] A. M. Stankovic, G. C. Verghese, D. J. Perreault, "Analysis and synthesis of randomized modulation schemes for power converters", IEEE Transactions on Power Electronics, Vol. 10, No. 6, pp.680-693, November 1995.

[10] S.Y. Hui, Y. Shrivastava, S. Sathiakumar, K.K. Tse, H. Chung, S. Hung, "Comparison of nondeterministic and deterministic switching methods for dc-dc power converters", IEEE Transactions on Power Electronics, Vol. 13, No. 6, pp. 1046-1055, November 1998.

[11] A. M. Trzynadlowski, S. Ji, S.Legowski, "Random pulse width modulation of delta inverter for automotive applications", 1991 Conference Rec. IEEE-IAS Ann. Mtg., pp. 826-833, 1991.

[12] P. W. Clarke, "Self-commutated thyristor DC-to-DC converter", IEEE Trans. On Magnetics, Vol. 6, pp.10-15, March 1970.

[13] A. M. Trzynadlowski, S. Legowski, R. L. Kirlin, "Random pulse width modulation technique for voltage-controlled power inverters", IEEE IAS Meeting, pp.863-868, 1987.

[14] T. Tanaka, H. Kameda, T. Ninomiya, "Noise analysis of DC-to-DC converter with random-switching control", Proc. Of Intelec'91, pp283-290, Nov. 1991.

[15] T. Tanaka, T. Ninomiya, "Random-switching control for DC-DC converters: Analysis of noise spectrum", IEEE PESC'92 Record, pp. 579-586, 1992.

[16] O. A. Z. Leneman, "Random sampling of random processes: Impulse processes", Information and Control, pp. 347-363, 1966.

[17] J. Holtz, "Pulsewidth modulation – a survey", IEEE PESC'92 Record, pp. 11-18, 1992.

[18] J. Holtz, "Pulsewidth modulation for electronic power conversion", Proc. of the IEEE, Vol. 82, No. 8, pp.1194-1214, August 1994.

[19] A. M. Trzynadlowski, S. Legowski, R. L. Kirlin, "Random pulse width modulation technique for voltage-controlled power inverters", IEEE-IAS Annual Meeting, pp. 863-868, 1987.

[20] S. Legowski, A. M. Trzynadlowski, "Hypersonic MOSFET-based power inverter with random pulse width modulation", 1989 Conference Rec. IEEE-IAS Ann. Mtg., pp. 901-903, 1989.

[21] S. Legowski, A. M. Trzynadlowski, "Power-MOSFET, hypersonic inverter with high-quality output current", Proceedings of IEEE APEC'90, pp3-7, 1990.

[22] S. Legowski, A. M. Trzynadlowski, "Advanced random pulse width modulation technique for voltage-controlled drive systems", IEEE APEC'91, pp. 100-106, 1991.

[23] A. M. Trzynadlowski, "Nonsinusoidal modulation functions for three-phase inverters", IEEE Trans. on Power Electronics, Vol. 4, No. 3, pp.331-338, 1989.

[24] P. G. Handley, M. Johnson, J. T. Boys, "Elimination of tonal acoustic noise in chopper-controlled DC drives", Applied Acoustics, Vol. 32, pp. 107-119, 1991.

[25] J. T. Boys, P. G. Handley, "Spread spectrum switching: low noise modulation technique for PWM inverter drives", IEE Proceedings-B, Vol. 139, No. 3, May 1992.

[26] J. T. Boys, "Theoretical spectra for narrow-band random PWM waveforms", IEE Proceedings-B, Vol. 140, No. 6, November 1993.

[27] K. D. Kryter, "Concepts of perceived noisiness, their implementation and application", J. Accoust. Soc. Am., 43 (2), pp. 344-361, 1968.

[28] K. D. Kryter, K. S. Pearson, "Some effects of spectral content and duration on perceived noise levels", J. Accoust. Soc. Am., Vol. 35, pp.866-883, 1963.

[29] J. T. Boys, M. Andrews, "Random PWM inverter drive systems: Theory and practice", Proc. of IEEE-IECON'93, pp. 695-700,1993.

[30] M. Andrews, J. T. Boys, "Improvements in estimating the spectra of random PWM waveforms", Electronics Letters, Vol. 29, No. 21, October 1993.

[31] F. Blaabjerg, J. K. Pedersen, "Digital implemented random modulation strategies for AC and switched reluctance drives", Proc. of IECON'93, pp. 676-682, 1993.

[32] J. K. Pedersen, F. Blaabjerg, "Digital Quasi-random modulated SFAVM PWM in an AC-Drive system", IEEE Trans. on Industrial Electronics, Vol. 41, No. 5, pp. 518-525, 1994.

[33] J. M. Retif, B. Allard, "A PWM ASIC using stochastic coding", IEEE PESC'92 Record, pp. 587-594, 1992.

[34] J. M. Retif, B. Allard, X. Jorda, A. Perez, "Use of ASIC's in PWM techniques for power converters", Proc. of IEEE-IECON'93, pp. 683-688, 1993.

[35] T. G. Habetler, D. M. Divan, "Acoustic noise reduction in sinusoidal PWM drives using a randomly modulated carrier", IEEE Transactions on Power Electronics, Vol. 6, No. 3, pp. 356-363, July 1991.

[36] S. Legowski, J. Bei, A. M. Trzynadlowski, "Analysis and implementation of a Grey-noise PWM technique based on voltage space vectors", IEEE-APEC'92, pp. 586-593, 1992.

[37] R. L. Kirlin, S. Legowski, A. M. Trzynadlowski, Y. Cui, S. Kwok, "Power spectra of a three phase inverter with random pulse width modulation modes", Third IEEE Workshop on Computers in Power Electronics, pp. 265-267, August 1992.

[38] R. L. Kirlin, S. Kwok, S. Legowski, A. M. Tryznadlowski, "Power spectra of a PWM inverter with randomized pulse position", IEEE Trans. on Power Electronics, Vol. 9, No. 5, pp. 463-472, September 1994.

[39] S. Kwok, "Power spectra of a three-phase inverter with random pulse width modulation modes", M.A.Sc. Thesis, University of Victoria, 1993.

[40] A. Wang, S. R. Sanders, "Random and programmed pulse-width modulation techniques for DC-DC converters", Proc. of the IEEE International Conference on Systems Engineering, pp. 589-592, 1990.

[41] A. Wang, S. R. Sanders, "On optimal programmed PWM waveforms for DC-DC converters", IEEE PESC'92, pp. 571-578, 1992.

[42] S. Y. R. Hui, I. Oppermann, F. Pasalic, S. Sathiakumar, "Microprocessor based mathematical and logical random PWM methods for power inverters", Proc. of EPE'95, pp. 707-712, 1995.

[43] S. Y. R. Hui, I. Oppermann, F. Pasalic, S. Sathiakumar, "Microprocessor based random PWM schemes for DC-AC power conversion", IEEE-PESC'95, pp. 307-312, 1995.

[44] S. Y. R. Hui, I. Oppermann, F. Pasalic, S. Sathiakumar, "Microprocessor-based random PWM schemes for DC-AC power conversion", IEEE Trans. on Power Electronics, Vol. 12, No. 2, March 1997.

[45] S. Ueda, K. Honda, T. Ikimi, M. Hombu, A. Ueda, "Magnetic noise reduction technique for an AC motor driven by a PWM inverter", IEEE Trans. on Power Electronics, Vol. 6, No. 3, pp. 470-475, July 1991.

[46] Y. Shrivastva, S. Sathiakumar, S. Y. R. Hui, "Random discrete PWM method for DC-DC power converters", Electronics Letters, Vol. 32, No. 23, pp. 2105-2106, November 1996.

[47] Y. Shrivastava, S. Y. R. Hui, S. Sathiakumar, H. Chung, K. K. Tse, "Effects of continuous noise in randomised switching DC-DC converters", Electronics Letters, pp. 919-921, April 1997.

[48] K. K. Tse, H. S. H. Chung, S. Y. R. Hui, H. C. So, "A Comparative Investigation on the Use of Random Modulation Schemes for DC/DC Converters", IEEE Trans on Industrial Electronics, Vol. 47, No. 2, pp. 253-263, April 2000.

[49] A. M. Trzynadlowski, F. Blaabjerg, J. K. Pedersen, R. L. Kirlin, S. Legowski, "Random pulse width modulation techniques for converter-fed drive system-A review", IEEE Trans. Industry Applications, Vol. 30, No. 5, pp.1166-1175, 1994.

[50] R. L. Kirlin, A. M. Trzynadlowski, "Spectral design of randomized pulse width modulation in DC to AC converters", IEE Proc. 7th SP Workshop on Statistical Signal and Array Processing, pp. 387-391, June 1994.

[51] F. Blaabjerg, J. K. Pedersen, L. Oestergaard, R. L. Kirlin, A. M. Trzynadlowski, S. Legowski, "Optimized and non-optimized random modulation techniques for VSI Drives", Proc. of EPE'95, Vol. 1, pp. 19-26, 1995.

[52] R. L. Kirlin, S. Legowski, A. M. Trzynadlowski, "An optimal approach to random pulse width modulation in power inverters", Proc. of IEEE-PESC'95, pp. 313-318, 1995.

[53] K. K. Tse, H. S. H. Chung, S. Y. R. Hui, H. C. So, "A Comparative study of Using Random Modulation Schemes for DC/DC Converters", IEEE-APEC'99, Vol. 1, pp. 160-167, 1999.

[54] R. L. Kirlin, A. M. Trzynadlowski, "A unified approach to analysis and design of random pulsewidth modulation in voltage-source inverters", IEEE Trans. on Circuits and Systems-1: Fundamental Theory and Applications, Vol. 44, No. 8, August 1997.

[55] R. L. Kirlin, A. M. Trzynadlowski, M. M Bech, F. Blaabjerg, J. K. Pedersen, "Analysis of spectral effects of random PWM strategies for voltage-source inverters", Proc. EPE'97, Vol. 1, pp. 146-151, 1997.

[56] A. M. Trzynadlowski, R. L. Kirlin, S. Legowski, "Space vector PWM technique with minimum switching Losses and a variable pulse rate", IEEE Trans. on Industrial Electronics, Vol. 44, No. 2, pp. 173-181. April 1997.

[57] M. M. Bech, F. Blaabjerg, J. K. Pedersen, A. M. Trzynadlowski, "Comparative investigation of random PWM techniques with variable switching frequency and pulse position for inverter-fed induction motors", Proc. EPE'97 vol. 1, pp. 343-349, 1997.

[58] M. M. Bech, F. Blaabjerg, J. K. Pedersen, A. M. Trzynadlowski, "A Methodology for True Comparison of Analytical and Measured Frequency Domain Spectra in Random PWM Converters", IEEE PESC'98, Vol. 1, pp. 36-43, 1998.

[59] M. M. Bech, F. Blaabjerg, J. K. Pedersen, A. M. Trzynadlowski, "A Methodology for True Comparison of Analytical and Measured Frequency Domain Spectra in Random PWM Converters", IEEE Trans. on Power Electronics, Vol. 14, No. 3, pp. 578-586, May 1999.

[60] M. M. Bech, F. Blaabjerg, J. K. Pedersen, "Random Modulation Techniques with Fixed Switching Frequency for Three-Phase Power Converters", IEEE PESC'99, Vol. 1, pp. 544-551, 1999.

[61] A. M. Trzynadlowski, M. M. Bech, F. Blaabjerg, J. K. Pedersen, R. L. Kirlin, Mauro Zigliotto, "Optimization of Switching Frequencies in the Limited-Pool Random Space Vector PWM Technique for Inverter-Fed Drives", IEEE APEC'99, Vol. 2, pp. 1013-1018, 1999.

[62] B. Kaku, I. Miyashita, S. Sone, "Novel random PWM method based on normally distributed random data", Proc. EPE'97, pp. 152, 1997.

[63] F. Mihalic, T. Bezjak, M. Milanovic, "Improved harmonic spectrum and reduced EMI in boost converter by using the random modulation", Proc. EPE'97, pp. 366-371, 1997.

[64] J. J. Stiffler, "Theory of synchronous communication", Englewood Cliffs, NJ: Prentice Hall, 1971.

[65] A. M. Stankovic, G. C. Verghese, D. J. Perreault, "Analysis and synthesis of random modulation schemes for power converters", IEEE-PESC'93, pp. 1068-1074, 1993.

[66] R. L. Kirlin, R. M. Dizaji, "Randomized switching design for DC/DC converters", Technical report, Electrical and Computer Engineering Department, University of Victoria, December 1998.

[67] A. M. Stankovic, G. C. Verghese, and D. J. Perrault, "Analysis and synthesis of random modulation schemes for power converters", Proc. 24th Ann. IEEE Power Electronics Specialists Conference, Seattle, 1993.

Appendix A

Evaluation of $E\left\{e^{j2\pi f\tau}\right\}$ for Uniform Distribution of τ

For uniform distribution of τ in $[f_{s\min}, f_{s\max}]$ we have the following algebraic development, ending in a magnitude-angle form of the result.

$$E\left\{e^{j2\pi f\tau}\right\} = \int_{1/f_{s\max}}^{1/f_{s\min}} \frac{1}{\frac{1}{f_{s\min}} - \frac{1}{f_{s\max}}} e^{j2\pi f\tau} d\tau$$

$$= \int_{1/f_{s\max}}^{1/f_{s\min}} \frac{f_{s\min} f_{s\max}}{f_{s\max} - f_{s\min}} e^{j2\pi f\tau} d\tau$$

$$= \frac{f_{s\min} f_{s\max}}{j2\pi f\left(f_{s\max} - f_{s\min}\right)}\left(e^{j2\pi f/f_{s\min}} - e^{j2\pi f/f_{s\max}}\right)$$

$$= \frac{f_{s\min} f_{s\max}}{j2\pi f\left(f_{s\max} - f_{s\min}\right)}\begin{pmatrix}\cos(2\pi f/f_{s\min}) + j\sin(2\pi f/f_{s\min}) \\ -\cos(2\pi f/f_{s\max}) - j\sin(2\pi f/f_{s\max})\end{pmatrix}$$

$$= \frac{f_{s\min} f_{s\max}}{j2\pi f\left(f_{s\max} - f_{s\min}\right)}\begin{pmatrix}\cos^2(2\pi f/f_{s\min}) + \cos^2(2\pi f/f_{s\max}) \\ -2\cos(2\pi f/f_{s\min})\cos(2\pi f/f_{s\max}) \\ \sin^2(2\pi f/f_{s\min}) + \sin^2(2\pi f/f_{s\max}) \\ -2\sin(2\pi f/f_{s\min})\sin(2\pi f/f_{s\max})\end{pmatrix}^{1/2} e^{j\theta}$$

$$= \frac{\sqrt{2} f_{s\min} f_{s\max}}{j2\pi f\left(f_{s\max} - f_{s\min}\right)} \begin{pmatrix} 1 - \cos(2\pi f / f_{s\min})\cos(2\pi f / f_{s\max}) \\ -\sin(2\pi f / f_{s\min})\sin(2\pi f / f_{s\max}) \end{pmatrix}^{1/2} e^{j\theta}$$

$$= \frac{\sqrt{2} f_{s\min} f_{s\max}}{j2\pi f\left(f_{s\max} - f_{s\min}\right)} \begin{pmatrix} 1 - \frac{1}{2}\left(\cos\left(2\pi f \frac{f_{s\max} + f_{s\min}}{f_{s\min} f_{s\max}}\right) + \cos\left(2\pi f \frac{f_{s\max} - f_{s\min}}{f_{s\min} f_{s\max}}\right)\right) \\ -\frac{1}{2}\left(\cos\left(2\pi f \frac{f_{s\max} - f_{s\min}}{f_{s\min} f_{s\max}}\right) - \cos\left(2\pi f \frac{f_{s\max} + f_{s\min}}{f_{s\min} f_{s\max}}\right)\right) \end{pmatrix}^{1/2} e^{j\theta} \tag{A.1}$$

where

$$\theta = \tan^{-1}\left(\frac{\sin(2\pi f / f_{s\min}) - \sin(2\pi f / f_{s\max})}{\cos(2\pi f / f_{s\min}) - \cos(2\pi f / f_{s\max})}\right) \tag{A.2}$$

Finally, (A.1) reduces to

$$E\left\{e^{j2\pi f\tau}\right\} = \frac{\sqrt{2} f_{s\min} f_{s\max}}{j2\pi f\left(f_{s\max} - f_{s\min}\right)} \left(1 - \cos\left(2\pi f \frac{f_{s\max} - f_{s\min}}{f_{s\min} f_{s\max}}\right)\right)^{1/2} e^{j\theta} \tag{A.3}$$

Appendix B

Formulation for Section 5.2.1

Formulate our minimizing problem from equation (5.1)

$$F(\tau_1,\tau_2,\cdots,\tau_m)=\frac{{A_0}^2}{\sum_{i=1}^{m}p_i\tau_i\pi^2{f_0}^2}\left(\sum_{i=1}^{m}p_i\sin^2(\pi\alpha_0 f_0\tau_i)+2\,\mathrm{Re}\left[\frac{\left(\sum_{i=1}^{m}p_i\sin(\pi\alpha_0 f_0\tau_i)e^{j\pi f_0\tau_i}\right)^2}{1-\sum_{i=1}^{m}p_i e^{j2\pi f_0\tau_i}}\right]\right)$$

$$=\frac{A_0^2}{\sum_{i=1}^{m}p_i\tau_i\pi^2 f_0^2}\left(\sum_{i=1}^{m}p_i\sin^2(\pi\alpha_0 f_0\tau_i)+2\mathrm{Re}\left[\frac{\left(\sum_{i=1}^{m}p_i\sin(\pi\alpha_0 f_0\tau_i)\cos(\pi f_0\tau_i)+j\sum_{i=1}^{m}p_i\sin(\pi\alpha_0 f_0\tau_i)\sin(\pi f_0\tau_i)\right)^2}{(1-\sum_{i=1}^{m}p_i\cos(2\pi f_0\tau_i))-j\sum_{i=1}^{m}p_i\sin(2\pi f_0\tau_i)}\right]\right)$$

$$=\frac{2A_0^2}{\sum_{i=1}^{m}p_i\tau_i\pi^2{f_0}^2}\left(\begin{array}{r}\left(\sum_{i=1}^{m}{p_i}^2\{\sin(\pi\alpha_0 f_0\tau_i)\cos(\pi f_0\tau_i)\}-\sum_{i=1}^{m}{p_i}^2\{\sin(\pi\alpha_0 f_0\tau_i)\sin(\pi f_0\tau_i)\}\right)\\ \times\left(1-\sum_{i=1}^{m}p_i\{\cos(2\pi f_0\tau_i)\}\right)\\ -2\left(\sum_{i=1}^{m}p_i\{\sin(\pi\alpha_0 f_0\tau_i)\cos(\pi f_0\tau_i)\}\right)\left(\sum_{i=1}^{m}p_i\{\sin(\pi\alpha_0 f_0\tau_i)\sin(\pi f_0\tau_i)\}\right)\\ \times\left(\sum_{i=1}^{m}p_i\{\sin(2\pi f_0\tau_i)\}\right)\end{array}\right)$$

$$/\left[\left(1-\sum_{i=1}^{m}p_i\cos(2\pi f_0\tau_i)\right)^2+\left(\sum_{i=1}^{m}p_i\sin(2\pi f_0\tau_i)\right)^2\right]+\frac{{A_0}^2}{\sum_{i=1}^{m}p_i\tau_i\pi^2{f_0}^2}\sum_{i=1}^{m}p_i\sin^2(\pi\alpha_0 f_0\tau_i)$$

(B.1)

Subject to:

$$\begin{aligned} &\frac{1}{75} \le \tau_1, \tau_2, \cdots, \tau_m \le \frac{1}{55} \\ &p_1, p_2, \cdots, p_m \ge 0 \\ &\sum_{i=1}^{m} p_i = 1 \end{aligned} \tag{B.2}$$

Transforming into an unconstrained minimization problem

Obviously it is a constrained problem to minimize. We first try to transfer it into unconstrained problem then we will use optimization methods to minimize it. We let $\tau_i = \dfrac{\frac{1}{55} + \frac{1}{75} e^{-2x_i}}{1 + e^{-2x_i}}$ $(-\infty \le x_i \le +\infty)$ and $\bar{p}_i^2 = p_i$ then we can get the unconstrained problem as follow:

$$F(x_1, x_2, \cdots, x_m, \lambda) = \frac{2{A_0}^2}{\sum_{i=1}^{m} \bar{p}_i^2 \frac{\frac{1}{55} + \frac{1}{75} e^{-2x_i}}{1 + e^{-2x_i}} \pi^2 {f_0}^2} \times$$

$$\left[\left(\sum_{i=1}^{m} \bar{p}_i^2 \left\{ \sin(\pi \alpha_0 f_0 \frac{\frac{1}{55} + \frac{1}{75} e^{-2x_i}}{1 + e^{-2x_i}}) \cos(\pi f_0 \frac{\frac{1}{55} + \frac{1}{75} e^{-2x_i}}{1 + e^{-2x_i}}) \right\} \right)^2 - \left(1 - \sum_{i=1}^{m} \bar{p}_i^2 \left\{ \cos(2\pi f_0 \frac{\frac{1}{55} + \frac{1}{75} e^{-2x_i}}{1 + e^{-2x_i}}) \right\} \right) \right.$$

$$\left(\sum_{i=1}^{m} \bar{p}_i^2 \left\{ \sin(\pi \alpha_0 f_0 \frac{\frac{1}{55} + \frac{1}{75} e^{-2x_i}}{1 + e^{-2x_i}}) \sin(\pi f_0 \frac{\frac{1}{55} + \frac{1}{75} e^{-2x_i}}{1 + e^{-2x_i}}) \right\} \right)^2$$

$$- 2 \left(\sum_{i=1}^{m} \bar{p}_i^2 \left\{ \sin(\pi \alpha_0 f_0 \frac{\frac{1}{55} + \frac{1}{75} e^{-2x_i}}{1 + e^{-2x_i}}) \cos(\pi f_0 \frac{\frac{1}{55} + \frac{1}{75} e^{-2x_i}}{1 + e^{-2x_i}}) \right\} \right)$$

$$\left. \left(\sum_{i=1}^{m} \bar{p}_i^2 \left\{ \sin(\pi \alpha_0 f_0 \frac{\frac{1}{55} + \frac{1}{75} e^{-2x_i}}{1 + e^{-2x_i}}) \sin(\pi f_0 \frac{\frac{1}{55} + \frac{1}{75} e^{-2x_i}}{1 + e^{-2x_i}}) \right\} \right) \left(\sum_{i=1}^{m} \bar{p}_i^2 \left\{ \sin(2\pi f_0 \frac{\frac{1}{55} + \frac{1}{75} e^{-2x_i}}{1 + e^{-2x_i}}) \right\} \right) \right]$$

$$/\left[\left(1-\sum_{i=1}^{m}\overline{p}_i^2\cos(2\pi f_0\frac{\frac{1}{55}+\frac{1}{75}e^{-2x_i}}{1+e^{-2x_i}})\right)^2+\left(\sum_{i=1}^{m}\overline{p}_i^2\sin(2\pi f_0\frac{\frac{1}{55}+\frac{1}{75}e^{-2x_i}}{1+e^{-2x_i}})\right)^2\right]$$

$$+\frac{{A_0}^2}{\sum_{i=1}^{m}\overline{p}_i^2\frac{\frac{1}{55}+\frac{1}{75}e^{-2x_i}}{1+e^{-2x_i}}}\sum_{i=1}^{n}\overline{p}_i^2\sin^2(\pi\alpha_0 f_0\frac{\frac{1}{55}+\frac{1}{75}e^{-2x_i}}{1+e^{-2x_i}})+\lambda\left(1-\sum_{i=1}^{m}\overline{p}_i^2\right)$$

(B.3)

We assume that the selection probabilities of the switching frequencies and therefore the switching intervals are equally likely. Then under these conditions, we can get the specified objective function

$$F(x_1,x_2,\cdots,x_m)=\frac{2{A_0}^2}{\sum_{i=1}^{m}\frac{1}{m}\tau_i\pi^2{f_0}^2}$$

$$\left(\left(\sum_{i=1}^{m}\frac{1}{m}\left\{\sin(\pi\alpha_0 f_0\frac{\frac{1}{55}+\frac{1}{75}e^{-2x_i}}{1+e^{-2x_i}})\cos(\pi f_0\frac{\frac{1}{55}+\frac{1}{75}e^{-2x_i}}{1+e^{-2x_i}})\right\}-\sum_{i=1}^{m}\frac{1}{m}\left\{\sin(\pi\alpha_0 f_0\frac{\frac{1}{55}+\frac{1}{75}e^{-2x_i}}{1+e^{-2x_i}})\sin(\pi f_0\frac{\frac{1}{55}+\frac{1}{75}e^{-2x_i}}{1+e^{-2x_i}})\right\}\right)\left(1-\sum_{i=1}^{m}\frac{1}{m}\left\{\cos(2\pi f_0\frac{\frac{1}{55}+\frac{1}{75}e^{-2x_i}}{1+e^{-2x_i}})\right\}\right)\right.$$

$$\left.-2\left(\sum_{i=1}^{m}\frac{1}{m}\left\{\sin(\pi\alpha_0 f_0\frac{\frac{1}{55}+\frac{1}{75}e^{-2x_i}}{1+e^{-2x_i}})\cos(\pi f_0\frac{\frac{1}{55}+\frac{1}{75}e^{-2x_i}}{1+e^{-2x_i}})\right\}\right)\right.$$

$$\left.\left(\sum_{i=1}^{m}\frac{1}{m}\left\{\sin(\pi\alpha_0 f_0\frac{\frac{1}{55}+\frac{1}{75}e^{-2x_i}}{1+e^{-2x_i}})\sin(\pi f_0\frac{\frac{1}{55}+\frac{1}{75}e^{-2x_i}}{1+e^{-2x_i}})\right\}\right)\left(\sum_{i=1}^{m}\frac{1}{m}\left\{\sin(2\pi f_0\frac{\frac{1}{55}+\frac{1}{75}e^{-2x_i}}{1+e^{-2x_i}})\right\}\right)\right)$$

$$/\left[\left(1-\sum_{i=1}^{m}\frac{1}{m}\cos(2\pi f_0\frac{\frac{1}{55}+\frac{1}{75}e^{-2x_i}}{1+e^{-2x_i}})\right)^2+\left(\sum_{i=1}^{m}\frac{1}{m}\sin(2\pi f_0\frac{\frac{1}{55}+\frac{1}{75}e^{-2x_i}}{1+e^{-2x_i}})\right)^2\right]$$

$$+\frac{{A_0}^2}{\sum_{i=1}^{m}\frac{1}{m}\frac{\frac{1}{55}+\frac{1}{75}e^{-2x_i}}{1+e^{-2x_i}}\pi^2{f_0}^2}\sum_{i=1}^{m}\frac{1}{m}\sin^2(\pi\alpha_0 f_0\frac{\frac{1}{55}+\frac{1}{75}e^{-2x_i}}{1+e^{-2x_i}})$$

(B.4)

Getting the gradient of the objective function.

Since $\frac{\partial F}{\partial x_i}=\frac{\partial F}{\partial \tau_i}\frac{\partial \tau_i}{\partial x_i}$ so we first derive the expression,

$$\frac{\partial F}{\partial \tau_i}=\frac{-2{A_0}^2\frac{1}{m}\pi^2{f_0}^2}{(\sum_{i=1}^{m}\frac{1}{m}\tau_i\pi^2{f_0}^2)^2}$$

$$\times\left[\begin{array}{l}\left(\left(\sum_{i=1}^{m}\frac{1}{m}^2\{\sin(\pi\alpha_0 f_0\tau_i)\cos(\pi f_0\tau_i)\}-\sum_{i=1}^{m}\frac{1}{m}^2\{\sin(\pi\alpha_0 f_0\tau_i)\sin(\pi f_0\tau_i)\}\right)\right.\\ \qquad\qquad\times\left(1-\sum_{i=1}^{m}\frac{1}{m}\{\cos(2\pi f_0\tau_i)\}\right)\\ -2\left(\sum_{i=1}^{m}\frac{1}{m}\{\sin(\pi\alpha_0 f_0\tau_i)\cos(\pi f_0\tau_i)\}\right)\left(\sum_{i=1}^{m}\frac{1}{m}\{\sin(\pi\alpha_0 f_0\tau_i)\sin(\pi f_0\tau_i)\}\right)\\ \qquad\qquad\left.\times\left(\sum_{i=1}^{m}\frac{1}{m}\{\sin(2\pi f_0\tau_i)\}\right)\right)\\ /\left[\left(1-\sum_{i=1}^{m}\frac{1}{m}\cos(2\pi f_0\tau_i)\right)^2+\left(\sum_{i=1}^{m}\frac{1}{m}\sin(2\pi f_0\tau_i)\right)^2\right]+\frac{1}{2}\sum_{i=1}^{m}\frac{1}{m}\sin^2(\pi\alpha_0 f_0\tau_i)\end{array}\right]$$

$$+\frac{2{A_0}^2}{\sum_{i=1}^{m}\frac{1}{m}\tau_i\pi^2{f_0}^2}\left[\frac{\pi\alpha_0 f_0}{m}\sin(\pi\alpha_0 f_0\tau_i)\cos(\pi\alpha_0 f_0\tau_i)+\frac{VU'-UV'}{V^2}\right]$$

(B.5)

$$V = \left[\left(1 - \sum_{i=1}^{m} \frac{1}{m} \cos(2\pi f_0 \tau_i) \right)^2 + \left(\sum_{i=1}^{m} \frac{1}{m} \sin(2\pi f_0 \tau_i) \right)^2 \right] \tag{B.6}$$

$$U = \begin{pmatrix} \left(\sum_{i=1}^{m} \frac{1}{m}^2 \{\sin(\pi\alpha_0 f_0 \tau_i)\cos(\pi f_0 \tau_i)\} - \sum_{i=1}^{m} \frac{1}{m}^2 \{\sin(\pi\alpha_0 f_0 \tau_i)\sin(\pi f_0 \tau_i)\} \right) \\ \left(1 - \sum_{i=1}^{m} \frac{1}{m} \{\cos(2\pi f_0 \tau_i)\} \right) \\ -2\left(\sum_{i=1}^{m} \frac{1}{m} \{\sin(\pi\alpha_0 f_0 \tau_i)\cos(\pi f_0 \tau_i)\} \right)\left(\sum_{i=1}^{m} \frac{1}{m} \{\sin(\pi\alpha_0 f_0 \tau_i)\sin(\pi f_0 \tau_i)\} \right) \\ \left(\sum_{i=1}^{m} \frac{1}{m} \{\sin(2\pi f_0 \tau_i)\} \right) \end{pmatrix} \tag{B.7}$$

$$U' = \begin{pmatrix} 2\left[\sum_{i=1}^{m} \frac{1}{m} \sin(\pi\alpha_0 f_0 \tau_i)\cos(\pi f_0 \tau_i) \right] \\ \times\left[\frac{\pi\alpha_0 f_0}{m} \cos(\pi\alpha_0 f_0 \tau_i)\cos(\pi f_0 \tau_i) - \frac{\pi f_0}{m} \sin(\pi\alpha_0 f_0 \tau_i)\sin(\pi f_0 \tau_i) \right] \\ -2\left[\sum_{i=1}^{m} \frac{1}{m} \sin(\pi\alpha_0 f_0 \tau_i)\sin(\pi f_0 \tau_i) \right] \\ \times\left[\frac{\pi\alpha_0 f_0}{m} \cos(\pi\alpha_0 f_0 \tau_i)\sin(\pi f_0 \tau_i) + \frac{\pi f_0}{m} \sin(\pi\alpha_0 f_0 \tau_i)\cos(\pi f_0 \tau_i) \right] \end{pmatrix} \times \left(1 - \sum_{i=1}^{m} \frac{1}{m} \{\cos(2\pi f_0 \tau_i)\} \right)$$

$$+ \frac{2\pi f_0}{m} \sin(2\pi f_0 \tau_i) \times \left(\sum_{i=1}^{m} \frac{1}{m}^2 \{\sin(\pi\alpha_0 f_0 \tau_i)\cos(\pi f_0 \tau_i)\} - \sum_{i=1}^{m} \frac{1}{m}^2 \{\sin(\pi\alpha_0 f_0 \tau_i)\sin(\pi f_0 \tau_i)\} \right)$$

$$-2\left(\frac{1}{m} \left[\pi\alpha_0 f_0 \cos(\pi\alpha_0 f_0 \tau_i)\cos(\pi f_0 \tau_i) - \pi f_0 \sin(\pi\alpha_0 f_0 \tau_i)\sin(\pi f_0 \tau_i) \right] \right)$$

$$\times \left(\sum_{i=1}^{m} \frac{1}{m} \{\sin(\pi\alpha_0 f_0 \tau_i)\sin(\pi f_0 \tau_i)\} \right)\left(\sum_{i=1}^{m} \frac{1}{m} \{\sin(2\pi f_0 \tau_i)\} \right)$$

$$
\begin{aligned}
&-2\left(\frac{1}{m}\left\{\pi\alpha_0 f_0 \cos(\pi\alpha_0 f_0 \tau_i)\sin(\pi f_0 \tau_i) + \pi f_0 \sin(\pi\alpha_0 f_0 \tau_i)\cos(\pi f_0 \tau_i)\right\}\right) \\
&\qquad \times \left(\sum_{i=1}^{m}\frac{1}{m}\left\{\sin(\pi\alpha_0 f_0 \tau_i)\cos(\pi f_0 \tau_i)\right\}\right)\left(\sum_{i=1}^{m}\frac{1}{m}\left\{\sin(2\pi f_0 \tau_i)\right\}\right) \\
&-2\left(\sum_{i=1}^{m}\frac{1}{m}\left\{\sin(\pi\alpha_0 f_0 \tau_i)\cos(\pi f_0 \tau_i)\right\}\right)\left(\sum_{i=1}^{m}\frac{1}{m}\left\{\sin(\pi\alpha_0 f_0 \tau_i)\sin(\pi f_0 \tau_i)\right\}\right) \\
&\qquad \left(\frac{2\pi f_0}{m}\cos(2\pi f_0 \tau_i)\right)
\end{aligned}
\tag{B.8}
$$

$$
V' = 2\left(1 - \sum_{i=1}^{m}\frac{1}{m}\cos(2\pi f_0 \tau_i)\right)\left(\frac{2\pi f_0}{m}\sin(2\pi f_0 \tau_i)\right) + 2\left(\sum_{i=1}^{m}\frac{1}{m}\sin(2\pi f_0 \tau_i)\right)\left(\frac{2\pi f_0}{m}\cos(2\pi f_0 \tau_i)\right)
\tag{B.9}
$$

$$
\frac{\partial \tau_i}{\partial x_i} = \frac{\frac{-2}{75}e^{-2x_i}(1+e^{-2x_i}) + 2(\frac{1}{55}+\frac{1}{75}e^{-2x_i})e^{-2x_i}}{(1+e^{-2x_i})^2}
\tag{B.10}
$$

Appendix C

Formulation for Section 5.2.4

First we change this new constrained problem into unconstrained. The transformation is as follows:

The constraint can be written as:

$$\frac{1}{\tau_m} = 62.5 \times m - \left(\frac{1}{\tau_1} + \frac{1}{\tau_2} + \cdots + \frac{1}{\tau_{m-1}} \right) \tag{C.1}$$

Since $\tau_m = \dfrac{\dfrac{1}{55} + \dfrac{1}{75} e^{-2x_m}}{1 + e^{-2x_m}}$ we use it to replace the τ_m of the above equation and get:

$$\frac{1 + e^{-2x_m}}{\dfrac{1}{55} + \dfrac{1}{75} e^{-2x_m}} = 62.5 \times m - \left(\frac{1}{\tau_1} + \frac{1}{\tau_2} + \cdots + \frac{1}{\tau_{m-1}} \right)$$

$$e^{-2x_m} = \frac{\left(62.5 \times m - \left(\dfrac{1}{\tau_1} + \dfrac{1}{\tau_2} + \cdots + \dfrac{1}{\tau_{m-1}} \right) \right) \times \dfrac{1}{55} - 1}{1 - \dfrac{1}{75} \left(62.5 \times m - \left(\dfrac{1}{\tau_1} + \dfrac{1}{\tau_2} + \cdots + \dfrac{1}{\tau_{m-1}} \right) \right)}$$

$$x_m = -\frac{1}{2} \ln \left(\frac{\left(62.5 \times m - \left(\dfrac{1}{\tau_1} + \dfrac{1}{\tau_2} + \cdots + \dfrac{1}{\tau_{m-1}} \right) \right) \times \dfrac{1}{55} - 1}{1 - \dfrac{1}{75} \left(62.5 \times m - \left(\dfrac{1}{\tau_1} + \dfrac{1}{\tau_2} + \cdots + \dfrac{1}{\tau_{m-1}} \right) \right)} \right)$$

We can use this equation to replace the x_m in the objective function. Then we delete the constraint by this way. Now our new objective function is as follows:

$$F(x_1, x_2, \cdots, x_{m-1}) = \frac{2A_0^{\,2}}{\sum_{i=1}^{m} \frac{1}{m} \tau_i \pi^2 f_0^{\,2}}$$

$$\times \left(\left(\sum_{i=1}^{m} \frac{1}{m}^2 \left\{ \sin(\pi\alpha_0 f_0 \frac{\frac{1}{55}+\frac{1}{75}e^{-2x_i}}{1+e^{-2x_i}}) \cos(\pi f_0 \frac{\frac{1}{55}+\frac{1}{75}e^{-2x_i}}{1+e^{-2x_i}}) \right\} \right.\right.$$

$$\left. - \sum_{i=1}^{m} \frac{1}{m}^2 \left\{ \sin(\pi\alpha_0 f_0 \frac{\frac{1}{55}+\frac{1}{75}e^{-2x_i}}{1+e^{-2x_i}}) \sin(\pi f_0 \frac{\frac{1}{55}+\frac{1}{75}e^{-2x_i}}{1+e^{-2x_i}}) \right\} \right) \left(1 - \sum_{i=1}^{m} \frac{1}{m} \left\{ \cos(2\pi f_0 \frac{\frac{1}{55}+\frac{1}{75}e^{-2x_i}}{1+e^{-2x_i}}) \right\} \right)$$

$$\left. - 2 \left(\sum_{i=1}^{m} \frac{1}{m} \left\{ \sin(\pi\alpha_0 f_0 \frac{\frac{1}{55}+\frac{1}{75}e^{-2x_i}}{1+e^{-2x_i}}) \cos(\pi f_0 \frac{\frac{1}{55}+\frac{1}{75}e^{-2x_i}}{1+e^{-2x_i}}) \right\} \right) \right.$$

$$\left. \left(\sum_{i=1}^{m} \frac{1}{m} \left\{ \sin(\pi\alpha_0 f_0 \frac{\frac{1}{55}+\frac{1}{75}e^{-2x_i}}{1+e^{-2x_i}}) \sin(\pi f_0 \frac{\frac{1}{55}+\frac{1}{75}e^{-2x_i}}{1+e^{-2x_i}}) \right\} \right) \times \left(\sum_{i=1}^{m} \frac{1}{m} \left\{ \sin(2\pi f_0 \frac{\frac{1}{55}+\frac{1}{75}e^{-2x_i}}{1+e^{-2x_i}}) \right\} \right) \right)$$

$$/ \left[\left(1 - \sum_{i=1}^{m} \frac{1}{m} \cos(2\pi f_0 \frac{\frac{1}{55}+\frac{1}{75}e^{-2x_i}}{1+e^{-2x_i}}) \right)^2 + \left(\sum_{i=1}^{m} \frac{1}{m} \sin(2\pi f_0 \frac{\frac{1}{55}+\frac{1}{75}e^{-2x_i}}{1+e^{-2x_i}}) \right)^2 \right]$$

$$+ \frac{A_0^{\,2}}{\sum_{i=1}^{m} \frac{1}{m} \frac{\frac{1}{55}+\frac{1}{75}e^{-2x_i}}{1+e^{-2x_i}} \pi^2 f_0^{\,2}} \sum_{i=1}^{m} \frac{1}{m} \sin^2(\pi\alpha_0 f_0 \frac{\frac{1}{55}+\frac{1}{75}e^{-2x_i}}{1+e^{-2x_i}})$$

(C.2)

We notice that in the above equation x_m is not a variable. In fact it is determined by the other x_i. Although the form of the objective function does not change we must get the

new form of the gradient of the objective function, since now x_m is a function of the other x_i.

$$\frac{\partial F}{\partial \tau_i} = \frac{-2A_0^2\left(\frac{1}{m}+\frac{\partial \tau_m}{\partial \tau_i}\right)\pi^2 f_0^2}{(\sum_{i=1}^{m}\frac{1}{m}\tau_i \pi^2 f_0^2)^2}$$

$$\left[\begin{array}{l}\left(\begin{array}{r}\left(\sum_{i=1}^{m}\frac{1}{m}^2\{\sin(\pi\alpha_0 f_0\tau_i)\cos(\pi f_0\tau_i)\}-\sum_{i=1}^{m}\frac{1}{m}^2\{\sin(\pi\alpha_0 f_0\tau_i)\sin(\pi f_0\tau_i)\}\right)\\ \times\left(1-\sum_{i=1}^{m}\frac{1}{m}\{\cos(2\pi f_0\tau_i)\}\right)\\ -2\left(\sum_{i=1}^{m}\frac{1}{m}\{\sin(\pi\alpha_0 f_0\tau_i)\cos(\pi f_0\tau_i)\}\right)\left(\sum_{i=1}^{m}\frac{1}{m}\{\sin(\pi\alpha_0 f_0\tau_i)\sin(\pi f_0\tau_i)\}\right)\\ \times\qquad\left(\sum_{i=1}^{m}\frac{1}{m}\{\sin(2\pi f_0\tau_i)\}\right)\end{array}\right)\\ /\left[\left(1-\sum_{i=1}^{m}\frac{1}{m}\cos(2\pi f_0\tau_i)\right)^2+\left(\sum_{i=1}^{m}\frac{1}{m}\sin(2\pi f_0\tau_i)\right)^2\right]+\frac{1}{2}\sum_{i=1}^{m}\frac{1}{m}\sin^2(\pi\alpha_0 f_0\tau_i)\end{array}\right]$$

$$+\frac{2A_0^2}{\sum_{i=1}^{m}\frac{1}{m}\tau_i\pi^2 f_0^2}\left[\begin{array}{l}\left(\begin{array}{l}\frac{\pi\alpha_0 f_0}{m}\sin(\pi\alpha_0 f_0\tau_i)\cos(\pi\alpha_0 f_0\tau_i)\\ \quad+\frac{\pi\alpha_0 f_0}{m}\sin(\pi\alpha_0 f_0\tau_m)\cos(\pi\alpha_0 f_0\tau_m)\times\frac{\partial\tau_m}{\partial\tau_i}\end{array}\right)\\ \qquad+\frac{VU'-UV'}{V^2}\end{array}\right]$$

(C.3)

$$V=\left[\left(1-\sum_{i=1}^{m}\frac{1}{m}\cos(2\pi f_0\tau_i)\right)^2+\left(\sum_{i=1}^{m}\frac{1}{m}\sin(2\pi f_0\tau_i)\right)^2\right] \tag{C.4}$$

$$U = \begin{pmatrix} \left(\sum_{i=1}^{m} \frac{1}{m}^{2} \{\sin(\pi\alpha_0 f_0 \tau_i)\cos(\pi f_0 \tau_i)\} - \sum_{i=1}^{m} \frac{1}{m}^{2} \{\sin(\pi\alpha_0 f_0 \tau_i)\sin(\pi f_0 \tau_i)\}\right) \\ \left(1 - \sum_{i=1}^{m} \frac{1}{m}\{\cos(2\pi f_0 \tau_i)\}\right) \\ -2\left(\sum_{i=1}^{m} \frac{1}{m}\{\sin(\pi\alpha_0 f_0 \tau_i)\cos(\pi f_0 \tau_i)\}\right)\left(\sum_{i=1}^{m} \frac{1}{m}\{\sin(\pi\alpha_0 f_0 \tau_i)\sin(\pi f_0 \tau_i)\}\right) \\ \left(\sum_{i=1}^{m} \frac{1}{m}\{\sin(2\pi f_0 \tau_i)\}\right) \end{pmatrix} \tag{C.5}$$

$$U' = \begin{pmatrix} 2\left[\sum_{i=1}^{m} \frac{1}{m}\sin(\pi\alpha_0 f_0 \tau_i)\cos(\pi f_0 \tau_i)\right] \\ \times\left[\begin{array}{l} \frac{\pi\alpha_0 f_0}{m}\cos(\pi\alpha_0 f_0 \tau_i)\cos(\pi f_0 \tau_i) - \frac{\pi f_0}{m}\sin(\pi\alpha_0 f_0 \tau_i)\sin(\pi f_0 \tau_i) + \\ \left(\frac{\pi\alpha_0 f_0}{m}\cos(\pi\alpha_0 f_0 \tau_m)\cos(\pi f_0 \tau_m) - \frac{\pi f_0}{m}\sin(\pi\alpha_0 f_0 \tau_m)\sin(\pi f_0 \tau_m)\right)\frac{\partial \tau_m}{\partial \tau_i} \end{array}\right] \\ -2\left[\sum_{i=1}^{m} \frac{1}{m}\sin(\pi\alpha_0 f_0 \tau_i)\sin(\pi f_0 \tau_i)\right] \\ \times\left[\begin{array}{l} \frac{\pi\alpha_0 f_0}{m}\cos(\pi\alpha_0 f_0 \tau_i)\sin(\pi f_0 \tau_i) + \frac{\pi f_0}{m}\sin(\pi\alpha_0 f_0 \tau_i)\cos(\pi f_0 \tau_i) + \\ \frac{\pi\alpha_0 f_0}{m}\cos(\pi\alpha_0 f_0 \tau_m)\sin(\pi f_0 \tau_m) + \frac{\pi f_0}{m}\sin(\pi\alpha_0 f_0 \tau_m)\cos(\pi f_0 \tau_m)\frac{\partial \tau_m}{\partial \tau_i} \end{array}\right] \\ \times\left(1 - \sum_{i=1}^{m} \frac{1}{m}\{\cos(2\pi f_0 \tau_i)\}\right) \\ +\left(\frac{2\pi f_0}{m}\sin(2\pi f_0 \tau_i) + \frac{2\pi f_0}{m}\sin(2\pi f_0 \tau_m)\frac{\partial \tau_m}{\partial \tau_i}\right) \\ \times\left(\sum_{i=1}^{m} \frac{1}{m}^{2} \{\sin(\pi\alpha_0 f_0 \tau_i)\cos(\pi f_0 \tau_i)\} - \sum_{i=1}^{m} \frac{1}{m}^{2} \{\sin(\pi\alpha_0 f_0 \tau_i)\sin(\pi f_0 \tau_i)\}\right) \end{pmatrix}$$

$$-2\left(\begin{array}{c}\frac{1}{m}\left[\pi\alpha_0 f_0\cos(\pi\alpha_0 f_0\tau_i)\cos(\pi f_0\tau_i)-\pi f_0\sin(\pi\alpha_0 f_0\tau_i)\sin(\pi f_0\tau_i)\right]+\\ \left(\frac{1}{m}\left[\pi\alpha_0 f_0\cos(\pi\alpha_0 f_0\tau_m)\cos(\pi f_0\tau_m)-\pi f_0\sin(\pi\alpha_0 f_0\tau_m)\sin(\pi f_0\tau_m)\right]\right)\frac{\partial\tau_m}{\partial\tau_i}\end{array}\right)$$
$$\times\left(\sum_{i=1}^{m}\frac{1}{m}\{\sin(\pi\alpha_0 f_0\tau_i)\sin(\pi f_0\tau_i)\}\right)\left(\sum_{i=1}^{m}\frac{1}{m}\{\sin(2\pi f_0\tau_i)\}\right)$$

$$-2\left(\begin{array}{c}\frac{1}{m}\{\pi\alpha_0 f_0\cos(\pi\alpha_0 f_0\tau_i)\sin(\pi f_0\tau_i)+\pi f_0\sin(\pi\alpha_0 f_0\tau_i)\cos(\pi f_0\tau_i)\}+\\ \left(\frac{1}{m}\{\pi\alpha_0 f_0\cos(\pi\alpha_0 f_0\tau_m)\sin(\pi f_0\tau_m)+\pi f_0\sin(\pi\alpha_0 f_0\tau_m)\cos(\pi f_0\tau_m)\}\right)\frac{\partial\tau_m}{\partial\tau_i}\end{array}\right)$$
$$\times\left(\sum_{i=1}^{m}\frac{1}{m}\{\sin(\pi\alpha_0 f_0\tau_i)\cos(\pi f_0\tau_i)\}\right)\left(\sum_{i=1}^{m}\frac{1}{m}\{\sin(2\pi f_0\tau_i)\}\right)$$

$$-2\left(\sum_{i=1}^{m}\frac{1}{m}\{\sin(\pi\alpha_0 f_0\tau_i)\cos(\pi f_0\tau_i)\}\right)\left(\sum_{i=1}^{m}\frac{1}{m}\{\sin(\pi\alpha_0 f_0\tau_i)\sin(\pi f_0\tau_i)\}\right)$$
$$\left(\begin{array}{c}\frac{2\pi f_0}{m}\cos(2\pi f_0\tau_i)+\\ \left(\frac{2\pi f_0}{m}\cos(2\pi f_0\tau_M)\right)\frac{\partial\tau_m}{\partial\tau_i}\end{array}\right) \tag{C.6}$$

$$V' = 2\left(1-\sum_{i=1}^{m}\frac{1}{m}\cos(2\pi f_0\tau_i)\right)\left(\frac{2\pi f_0}{m}\sin(2\pi f_0\tau_i)+\left(\frac{2\pi f_0}{m}\sin(2\pi f_0\tau_m)\right)\frac{\partial\tau_m}{\partial\tau_i}\right)$$
$$+2\left(\sum_{i=1}^{m}\frac{1}{m}\sin(2\pi f_0\tau_i)\right)\left(\frac{2\pi f_0}{m}\cos(2\pi f_0\tau_i)+\left(\frac{2\pi f_0}{m}\cos(2\pi f_0\tau_m)\right)\frac{\partial\tau_m}{\partial\tau_i}\right) \tag{C.7}$$

$$\frac{\partial\tau_m}{\partial\tau_i} = \frac{-\frac{1}{\tau_i^{\,2}}}{\left(62.5\times m-\left(\frac{1}{\tau_1}+\frac{1}{\tau_2}+\cdots+\frac{1}{\tau_{m-1}}\right)\right)^2} \qquad i=1,2\cdots m-1 \tag{C.8}$$

$$\frac{\partial \tau_i}{\partial x_i} = \frac{\frac{-2}{75} e^{-2x_i}(1+e^{-2x_i}) + 2(\frac{1}{55} + \frac{1}{75} e^{-2x_i}) e^{-2x_i}}{(1+e^{-2x_i})^2} \qquad i = 1, 2 \cdots m-1 \qquad \text{(C.9)}$$

$$\frac{\partial F}{\partial x_i} = \frac{\partial F}{\partial \tau_i} \frac{\partial \tau_i}{\partial x_i} \qquad \text{(C.10)}$$

VITA

Surname: Wang Given Names: Jian

Place of Birth: Qingdao, People's Republic of China

Educational Institutions Attended:

Ocean University of Qingdao	1993 to 1997
University of Victoria	1999 to 2000

Degree Awarded:

B.Sc	Ocean University of Qingdao	1997

Honours and Awards:

Ocean University of Qingdao Fellowship	1994 to 1997
University of Victoria Research Assistantship	1999 to 2000

Publications:

(1) R. L. Kirlin, J. Wang and R. M. Dizaji, "Spectral Analysis and Design for DC/DC Conversion Using Random Switching Rate PWM", SSAP Workshop 2000, Pocono, PA, Aug. 2000.

(2) R. L. Kirlin, J. Wang and R. M. Dizaji, "Spectral Analysis and Design for DC/DC Conversion Using Random Switching Rate PWM", submitted to *IEEE Trans-Power Electronics Systems*, Dec. 1999.

(3) J. Wang, R. L. Kirlin, "A New Method in Analysis and Design of the Power Spectral Density of DC/DC Converters Using Randomized Switching Frequency PWM", submitted to PESC'2001, Vancouver, Canada, Oct. 2000.

(4) J. Wang, R. L. Kirlin, "Design of Local Minimization in the Noise Spectrum of Randomly Switched DC/DC Converters", submitted to ICASSP'2001, USA.

PARTIAL COPYRIGHT LICENSE

I hereby grant the right to lend my thesis to users of the University of Victoria Library, and to make single copies only for such users or in response to a request from the Library of any other university, or similar institution, on its behalf or for one of its users. I further agree that permission for extensive copying of this thesis for scholarly purposes may be granted by me or a member of the University designated by me. It is understood that copying or publication of this thesis for financial gain shall not be allowed without my written permission.

Title of Thesis:

"The Analysis and Design of the Power Spectral Density for DC/DC Converters Using Randomized Switching Frequency Pulse Width Modulation"

Author 

Jian Wang

October, 2000